

**STRUCTURAL AND INITIAL PERMEABILITY
STUDIES OF Y SUBSTITUTED $Mn_{0.5}Zn_{0.5}Fe_{2-x}Y_xO_4$
FERRITES**

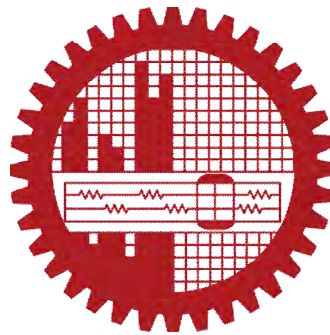
M.Phil. Thesis

(Physics)

Anis Munshi

Roll No.: 0409143023F

Session: April 2009



DEPARTMENT OF PHYSICS

BANGLADESH UNIVERSITY OF ENGINEERING & TECHNOLOGY

DHAKA- 1000, BANGLADESH

**STRUCTURAL AND INITIAL PERMEABILITY STUDIES OF Y
SUBSTITUTED $Mn_{0.5}Zn_{0.5}Fe_{2-x}Y_xO_4$ FERRITES**

*A Dissertation Submitted to the Department Of Physics, Bangladesh University
of Engineering & Technology, Dhaka, in Partial Fulfillment of Requirement for
the Degree of Master of Philosophy in Physics*

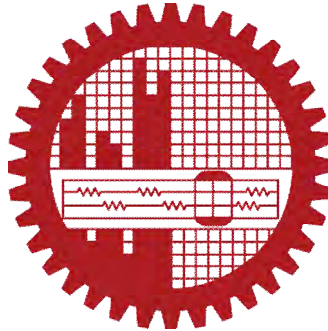
SUBMITTED

By

Anis Munshi

EXAMINATION ROLL NO. : 0409143023F

SESSION : April 2009

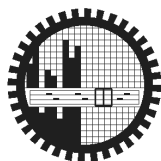


**DEPARTMENT OF PHYSICS
BANGLADESH UNIVERSITY OF ENGINEERING & TECHNOLOGY
DHAKA 1000, BANGLADESH**

CANDIDATE'S DECLARATION

It is hereby declared that this thesis or any part of it has not been submitted elsewhere for the award of any degree or diploma.

Anis Munshi



**BANGLADESH UNIVERSITY OF ENGINEERING &
TECHNOLOGY
DEPARTMENT OF PHYSICS, DHAKA 1000, BANGLADESH**

CERTIFICATION OF THESIS

The thesis titled “**STRUCTURAL AND INITIAL PERMEABILITY STUDIES OF Y SUBSTITUTED $Mn_{0.5}Zn_{0.5}Fe_{2-x}Y_xO_4$ FERRITES**” submitted by **Anis Munshi**, Roll No.: 0409143023F, Session: April 2009, has been accepted as satisfactory in partial fulfillment of the requirement for the degree of **Master of Philosophy** in Physics on 20, August, 2011.

BOARD OF EXAMINERS

1. (_____) Chairman
Dr. A. K. M. Akther Hossain (Supervisor)
Professor, Department of Physics,
BUET, Dhaka-1000, Bangladesh

2. (_____) (Ex-Officio) Member
Head,
Department of Physics,
BUET, Dhaka-1000, Bangladesh

3. (_____) Member
Dr. Md. Abu Hasan Bhuiyan
Professor, Department of Physics,
BUET, Dhaka-1000, Bangladesh

4. (_____) Member
Dr. Md. Forhad Mina,
Associate Professor, Department of Physics,
BUET, Dhaka-1000, Bangladesh

5. (_____) Member
(External)
Dr. Abdul Gafur
Senior Engineer
PP & PDC, BCSIR
Dhaka-1205, Bangladesh

DEDICATED TO
MY
BELLOVED MOTHER

ACKNOWLEDGEMENTS

First of all I express all my admiration and devotion to the almighty Allah-Rabbul Alamin, the most beneficial who has enabled me to perform this research work and to submit this thesis.

I express my profound gratitude to my honourable supervisor Professor Dr. A .K. M. Akther Hossain, Head, Department of Physics, BUET, for his constant direction, constructive criticism and inspiration in pursuing the whole investigation of the present research. Words are always insufficient to express his working capacities and unending enthusiasm for scientific rigorousness for innovative investigations. This always becomes the everlasting source of inspiration for his students.

I like to express my gratitude to, Professor Dr. Md. Abu Hashan Bhuiyan, Professor Dr. Jiban Podder, Professor Dr. Md. Feroz Alam Khan, Professor Dr. Md. Mostak Hossain, Mrs.Fahima Khanam, Dr. Afia Begum, Dr. Md. Forhad Mina, Dr. Md. Rafi Uddin, and all other teachers of the Physics Department, for their co-operation.

I would like to give special thank to authority of DMTBI, PP & PDC, BCSIR, for using their X-ray Diffractometer. I am grateful to Md. Maidul Islam & Mr. Mamun, Scientific Officer of AEC, Bangladesh, for SEM photograph of my sample. I wish to thank specially my senior research worker and PhD students of the department, Md. Hamidur Rahman Khan, Farhad Alam, Md Belal Hossen, Md. Abdur Rahman , Maruf Morshed and others for their cooperation throughout the study. I am also grateful to Nur Hossain Sharifee, Bablu Chandra Das and Md. Towhid Miah for their inspiration and encouragement. I also gratefully acknowledge the wishes of my younger researchers Azizar Rahman ,Arif, and Momin for their constant support .

Ultimately, I would mention a very special gratefulness for the moral support and sustaining inspiration provided by the members of my family. This dissertation would never have been possible without their love and affection.

The Author

Anis Munshi

ABSTRACT

Polycrystalline $Mn_{0.5}Zn_{0.5}Fe_{2-x}Y_xO_4$ ferrites with $x= 0.00, 0.05, 0.10, 0.15, 0.20, 0.25$ and 0.30 were synthesized by the standard solid state reaction technique. Pellet- and toroid -shaped samples were prepared from the ferrite powders and sintered at various temperatures in air for 5 hours. Structural and surface morphology of the ferrites were studied by X-ray diffraction (XRD) method and Scanning Electron Microscopy (SEM), respectively. The magnetic properties of these ferrites were characterized by a high frequency (100 KHz-120 MHz) Impedance Analyzer. The influence of microstructure, various cation distribution and sintering temperature on the complex initial permeability of these samples are discussed. XRD patterns show the formation of spinel crystal structure. Lattice parameters are calculated using the Nelson -Riley function. There is an enhancement of the unit cell dimension depending on Y substitutions in these compositions. This result is explained with the help of ionic radii of substituted cations. The SEM micrographs show that both sintering temperatures and cations substitutions have great influence on the average grain size. As the sintering temperature increases, the bulk density of the samples increases (depending on compositions), and hence the porosity decreases for all compositions. The initial permeability value increases with increasing average grain size of the samples. It is also observed that the real part of initial permeability is found to increase with sintering temperatures for all ferrites because high sintering temperature helps to develop uniform grain. The real part of the initial permeability remains fairly constant in the frequency range up to a critical frequency which is called resonance frequency. The natural resonance frequency of $Mn_{0.5}Zn_{0.5}Fe_{1.9}Y_{0.1}O_4$ is observed to be 2.82 MHz. The relative quality factor is found to be the maximum (3477) for the sample sintered at 1400°C.

CONTENTS

ACKNOWLEDGEMENTS	V
ABSTRACT	VI
CONTENTS	VII
LIST OF FIGURES	X
LIST OF TABLES	XIII
LIST OF SYMBOLS AND ABBREVIATIONS	XIV

CHAPTER 1

INTRODUCTION 1-4

1.1	Introduction	1
1.2	Objectives with specific aims and possible outcome	2
1.3	Outline of the Thesis	2

CHAPTER 2

THEORETICAL BACKGROUND 5-48

2.1	General aspects of magnetism	5
2.1.1	Origin of Magnetism	5
2.1.2	Magnetic moment of atoms	7
2.1.3	Magnetic moment of electrons	8
2.1.4	Magnetic Behavior	10
2.1.5	Hysteresis Loop	14
2.1.6	Magnetic Domains	15
2.1.7	Structure of domain wall	19
2.1.8	Microstructure	20
2.1.9	Theories of initial permeability	22

2.1.10	Mechanisms of Permeability	24
2.1.11	Wall Permeability	25
2.1.12	Rotational Permeability	26
2.2	Soft Magnetic Materials	28
2.2.1	Soft ferrites	29
2.2.2	Cubic ferrites with spinel structure	29
2.2.3	Cation distribution in ferrites	31
2.2.4	Magnetic exchange interaction	32
2.2.5	Superexchange interaction	33
2.2.6	Two sublattices in spinel ferrites	34
2.3	Magnetic Structure of Substituted Ferrites	36
2.3.1	Neel's collinear model of ferrites	36
2.3.2	Non-collinear model	37
2.3.3	Re-entrant spin glass behavior	38
2.3.4	Spin glass behavior	39
2.4	Transport Properties	41
2.4.1	Conduction Mechanism in ferrites	41
2.4.2	Hopping model of electrons	42
2.4.3	Small polaron model Theories of Permeability	42
2.5	Literature Review	43

CHAPTER 3

SAMPLE PREPARATION 49-54

3.1	Composition of the studied ferrite system	49
3.2	Sample preparation	49
3.3	Conventional solid state reaction method	49
3.4	Details of calcining, pressing and sintering	50
3.5	Preparation of the present samples	53

CHAPTER 4

EXPERIMENTAL TECHNIQUES 55-59

4.1	X-ray Diffraction	55
4.2	Study of Microstructure	56
4.3	Complex Permeability Measurement	57
4.3.1	Techniques for the Permeability Measurement	57
4.3.2	Frequency Characteristics of the Present Samples	57

CHAPTER 5

RESULTS AND DISCUSSION 60-86

5	Investigation of polycrystalline $Mn_{0.5}Zn_{0.5}Fe_{2-x}Y_xO_4$	60
5.1	X-ray Diffraction analysis	60
5.2	Lattice parameters	61
5.3	Density and Porosity	63
5.4	Microstructures of $Mn_{0.5}Zn_{0.5}Fe_{2-x}Y_xO_4$	66
5.5	Complex initial Permeability of $Mn_{0.5}Zn_{0.5}Fe_{2-x}Y_xO_4$	75

CHAPTER 6

CONCLUSIONS 87-88

6.1	Conclusions	87
6.2	Suggestion for future work	88

LIST OF FIGURES

		Pages
Figure 2.1	A spin magnetic moment associated with it due to the electron itself spinning like the earth on its own axis.	6
Figure 2.2	Varieties of magnetic orderings (a) paramagnetic, (b) ferromagnetic, (c) ferrimagnetic, (d) antiferromagnetic and (e) superparamagnetic.	11
Figure 2.3	The inverse susceptibility varies with temperature T for (a) paramagnetic, (b) ferromagnetic, (c) ferrimagnetic, (d) antiferromagnetic materials. T_N and T_c are Neel temperature and Curie temperature, respectively.	13
Figure 2.4	Hysteresis loop.	15
Figure 2.5	Illustration of domains in ferromagnetic materials.	16
Figure 2.6	Schematic illustration of the breakup of magnetization into domains (a) single domain, (b) two domains, (c) four domains and (d) closure domains.	18
Figure 2.7	Schematic representation of an 180° domain wall.	19
Figure 2.8	Porosity character: (a) intergranular, (b) intragranular.	21
Figure 2.9	Grain growth (a) discontinuous, (b) duplex (schematic).	22
Figure 2.10	Schematic magnetization curve showing the important parameter: initial permeability, μ_i (the slope of the curve at low fields) and the main magnetization mechanism in each magnetization range.	24
Figure 2.11	Magnetization by wall motion and spin rotation.	26
Figure 2.12	Schematic of two subcells of a unit cell of the spinel structure, showing octahedral and tetrahedral sites.	30
Figure 2.13	Three major types of superexchange interactions in spinel ferrites are as follows: J_{AB} , J_{BB} and J_{AA} . The small empty circle is A site, the small solid circle is B site, and the large empty circle is oxygen ion.	33

Figure 2.14	Schematic representation of ions M and M' and the O^{2-} ion through which the superexchange is made. R and q are the centre to centre distances from m M and M' respectively to O^{2-} and ϕ is the angle between them.	36
Figure 2.15	Examples of (a) an unfrustrated and (b) a frustrated spin configuration.	40
Figure 3.1	Flow chart of the stages in preparation of spinel ferrite.	48
Figure 3.2	Schematic representation of sintering stages: (a) greenbody, (b) initial stage, (c) intermediate stage, and (d) final stage.	50
Figure 3.3.	Sample (a) disk shaped, (b) Toroid shaped.	50
Figure 4.1	Bragg law of diffraction.	52
Figure 4.2	Geometry for the vibration axis, sample position, detection coils and applied magnetic field.	56
Figure 5.1	The X-ray diffraction pattern of polycrystalline $Mn_{0.5}Zn_{0.5}Fe_{2-x}Y_xO_4$	60
Figure 5.2	(a) Variation of lattice parameter 'a' with $F(\theta)$ and (b) variation of lattice constant with Y content x, of polycrystalline $Mn_{0.5}Zn_{0.5}Fe_{2-x}Y_xO_4$ sintered 1200 °C.	61
Figure 5.3	(a) Experimental and theoretical density (ρ_{exp} and ρ_{th}) and (b) Density and porosity of the samples of $Mn_{0.5}Zn_{0.5}Fe_{2-x}Y_xO_4$, sintered at 1350 °C.	63
Figure 5.4	The variation of density and porosity for $Mn_{0.5}Zn_{0.5}Fe_{2-x}Y_xO_4$.	65
Figure 5.5	The Scanning Electron Micrographs (SEM) of $Mn_{0.5}Zn_{0.5}Fe_{2-x}Y_xO_4$ samples sintered at temperature 1200°C for 5 hours in air (magnified 3000×).	67
Figure 5.6	The Scanning Electron Micrographs of $Mn_{0.5}Zn_{0.5}Fe_{2-x}Y_xO_4$ samples sintered at temperature (a) 1200 °C, (b) 1250 °C, and (d) 1300 °C in air (magnified 3000×).	68
Figure 5.7-5.12	Optical Micrograph of various samples of $Mn_{0.5}Zn_{0.5}Fe_{2-x}Y_xO_4$ at various sintering temperature.	69-74

Figure 5.13	(a) The real and (b) imaginary permeability spectra for polycrystalline $Mn_{0.5}Zn_{0.5}Fe_{2-x}Y_xO_4$ samples sintered at 1100 °C for 5 hours.	75
Figure 5.14	(a) The real and (b) imaginary permeability spectra for polycrystalline $Mn_{0.5}Zn_{0.5}Fe_{2-x}Y_xO_4$ samples sintered at 1200 °C for 5 hours.	76
Figure 5.15	(a) The real and (b) imaginary permeability spectra for polycrystalline $Mn_{0.5}Zn_{0.5}Fe_{2-x}Y_xO_4$ samples sintered at 1250 °C for 5 hours.	77
Figure 5.16	The real and imaginary permeability spectra for polycrystalline $Mn_{0.5}Zn_{0.5}Fe_{2-x}Y_xO_4$ samples sintered at various temperatures for 5 hours.	78
Figure 5.17	The variation of μ_i' and ρ_B with T_s for various compositions of $Mn_{0.5}Zn_{0.5}Fe_{2-x}Y_xO_4$.	80
Figure 5.18	The variation of loss factor with frequency for polycrystalline $Mn_{0.5}Zn_{0.5}Fe_{2-x}Y_xO_4$ samples sintered at (a) 1288 °C (b) 1300 °C (c) 1350 °C and (d) 1400 °C temperatures.	81
Figure 5.19	The variations of Loss factor with frequency for $Mn_{0.5}Zn_{0.5}Fe_{2-x}Y_xO_4$ sintered at 1288, 1300, 1350 and 1400 °C.	82
Figure 5.20	The variation of relative quality factors with frequency for polycrystalline $Mn_{0.5}Zn_{0.5}Fe_{2-x}Y_xO_4$ samples sintered at various temperatures.	84
Figure 5.21	Variation of relative quality factor with frequency at different sintering temperature for (a) $Mn_{0.5}Zn_{0.5}Fe_{1.95}Y_{0.05}O_4$ and (b) $Mn_{0.5}Zn_{0.5}Fe_{1.9}Y_{0.1}O_4$	85
Figure 5.22	Variation of maximum Q factor with Y content for polycrystalline $Mn_{0.5}Zn_{0.5}Fe_{2-x}Y_xO_4$ samples sintered at 1400 °C.	85

LIST OF TABLES

	Pages
Table 5.1. The lattice parameter, sintering temperature, T_s , density, porosity, average grain size and natural resonance frequency of the $Mn_{0.5}Zn_{0.5}Fe_{2-x}Y_xO_4$ samples sintered at various temperatures with fixed dwell time 5 h.	62

LIST OF SYMBOLS AND ABBREVIATIONS

Y	Yttrium
B	Magnetic induction
CMR	Colossal magnetoresistance
$F(\theta)$	Nelson-Riley function
f_r	Resonance frequency
g	Landé splitting factor
H_{cr}	Critical field
J	Exchange integral
K	Total anisotropy
K_1	Magnetocrystalline anisotropy constant
L_s	Self-inductance of the sample core
L_o	Inductance of the winding coil without sample
M	Magnetization
M_s	Saturation magnetization
N_A	Avogadro's number
P	Porosity
P_{intra}	Intragranular porosity
P_{inter}	Intergranular porosity
P_e	Eddy-current loss
Q	Relative quality factor
T_c	Curie temperature
T_n	Néel temperature
T_s	Sintering temperature
$\tan\delta$	Loss factor
Z	Complex impedance
α	Restoring force coefficient
β	Viscous damping factor
γ	Domain wall energy
ω	Angular velocity
δ_w	Domain wall thickness
μ_i	Initial permeability
μ'	Real part of complex permeability
μ''	Imaginary part of complex permeability
μ_B	Bohr magneton
χ_{spin}	Intrinsic rotational susceptibility
χ_w	Domain wall susceptibility
ρ_{th} & ρ_B	Theoretical Density & Bulk Density

CHAPTER 1

INTRODUCTION

1.1 Introduction

During the last few years polycrystalline spinel ferrites have drawn a major attention because of their technological importance in magnetic recording, magnetic fluids and catalyst. These types of ferrites are natural super-lattices and have tetrahedral A-site and octahedral B-site in AB_2O_4 crystal structure. This material shows various magnetic properties depending on the cation distribution of the chemical compositions. Various cations can be placed in A-site and B-site to adjust their magnetic properties. Depending on A-site and B-site cations, they can express ferrimagnetic, antiferromagnetic, spin (cluster) glass and paramagnetic behaviors [1, 2]. Spinel ferrites show improved properties by virtue of their unique electronic and crystalline structure which may be used for various applications such as recording heads, inductors, choke coils, transformers, antennas, deflection yokes, electromagnetic interference (EMI) suppressor and power transformer [3-6]. With the rapid development of mobile communication and information technology, electronic components with small size, low cost and high performance are in demand. The small sized surface mounting device (SMD) chip inductors are very attractive due to their performance and reliability in a wide range of applications, such as EMI suppression in universal series bus (USB), low-voltage differential signaling and in other high-speed digital interfaces incorporated in notebooks and personal computers, digital cameras and scanners, etc. [7]. These chip inductors are typically fabricated by coating ferrite and electrical paste alternately and then co-firing. MnZn-ferrites are considered as one of the most important ceramic materials as these have extensive applications in electronic and telecommunication industry. This is due to their excellent properties such as high saturation magnetization, high initial permeability, high resistivity and low losses. The essential feature of these materials is the coexistence of high magnetization and high electric resistivity, which depend on microstructure of the materials. The factors responsible for controlling the microstructure of the material are the method of preparation, conditions during preparation and the dopant used [8-13]. In the present research, structural and magnetic properties of polycrystalline $Mn_{0.5}Zn_{0.5}Fe_{2-x}Y_xO_4$ have been studied.

1.2 Objectives with specific aims and possible outcome:

The main objectives of the present research are as follows:

- Preparation of various $\text{Mn}_{0.5}\text{Zn}_{0.5}\text{Fe}_{2-x}\text{Y}_x\text{O}_4$ ferrite samples of varying Y contents ($x=0, 0.05, 0.10, 0.15, 0.20, 0.25, 0.30$) by the standard solid state reaction technique.
- Study of crystal structure by (X-ray diffraction) and hence determination of density and porosity of various samples.
- Investigation of surface morphology, especially grain size.
- Measurement of initial permeability as a function of frequency (100Hz-120MHz) for all samples having various microstructures.

Possible outcome of the research is as follows:

Due to incorporation of Y cations, spinel lattice may be either compressed or expanded depending on ionic radius and hence there is a change of cation distribution in A- and B-sites of AB_2O_4 spinel structure is expected. The crystal structure is also expected to change for the substitution of Y in $\text{Mn}_{0.5}\text{Zn}_{0.5}\text{Fe}_2\text{O}_4$ ferrites. Due to the structural change, there may be a variation of magnetic interaction between A-site and B-site cations and hence a change of magnetic properties is also expected in $\text{Mn}_{0.5}\text{Zn}_{0.5}\text{Fe}_{2-x}\text{Y}_x\text{O}_4$. The results of the present research will be helpful for practical applications of these ferrites.

1.3 Outline of the Thesis

The summary of the thesis is as follows:

Chapter 1 of this thesis deals with the importance of ferrites and objectives of the present work.

Chapter 2 gives theoretical background as well as crystal structure of the spinel type ferrites and a brief overview of the last research work on Mn-Zn ferrites

Chapter 3 gives the details of the sample preparation

Chapter 4 gives descriptions of different experimental setup that have been used in this research work.

Chapter 5 is devoted to the results of various investigations of the study and a brief discussion.

The conclusions drawn from the overall experimental results and discussion are presented in Chapter 6.

References:

- [1] Peelamedu, R., Grimes, C., Agrawal, D., and Roy, R., "Ultralow dielectric constant nickel-zinc ferrites using microwave sintering," *J. Mater. Res.*, Vol-18(10), pp 2292-2296, 2003.
- [2] Hossain, A.K.M. Akther, Mahmud, S.T., Seki, M., Kawai, T. and Tabata, H., "Structural, Electrical transport and magnetic properties of $Ni_{1-x}Zn_xFe_2O_4$ ", *J. Magn. Magn. Mater.* Vol-312, pp 210-219, 2007.
- [3] Valenzuela, R., "Magnetic Ceramics", Cambridge University Press, Cambridge, 1994.
- [4] Schiessl, W., Potzel, W., Karzel H., Steiner, M. and Kalvius G. M., "Magnetic properties of the $ZnFe_2O_4$ spinel," *Phys. Rev. B*, Vol-53, No. 14, pp 9143-9152, 1996.
- [5] Hossain, A.K.M. Akther, Tabata, H. and Kawai, T., "Magnetoresistive properties of $Zn_{1-x}Co_xFe_2O_4$ ferrites", *J. Magn. Magn. Mater.* Vol- 320, pp 1157, 2008.
- [6] Sousa, M. H., Tourinho, F. A., Depeyrot, J., Da silva, G. J. and Lara, M. C. F., "New Electric Double-Layered Magnetic Fluids Based on Copper, Nickel, and Zinc Ferrite Nanostructures", *J. Phys. Chem.*, Vol- 105, pp 1169, 2001.
- [7] Stojanovic, G., Srdic, V. and Maletin, M. "Electrical properties of yttrium-doped Zn and Ni-Zn ferrites" *Phys. stat. sol. (a)* 205, No. 10, 2464–2468 (2008);
- [8] Znidarsic, M. A. and Zajc, I., "High resistivity grain boundaries in doped MnZn ferrites for high frequency power supplies", *J. Appl. Phys.*, Vol- 82, pp 333, 1997.
- [9] Inaba, H, Abe, T, Kitano, Y, and Shimomura, J., "Mechanism of core loss and the Grain-boundary structure of Niobium-Doped Manganese -Zinc Ferrite", *J. Solid State Chem*, Vol-121, pp 117, 1996.
- [10] Verma, A., Goel, T. C. and Mendiratta, R. G, "Low temperature processing of NiZn ferrite by citrate precursor method and study of properties", *Mater. Sci. Tech.*, Vol- 16, pp 712, 2000.
- [11] M.J. Tsay, M.J. Tung, C.J. Chen and T.Y. Liu, "The Manufacture of High Permeability Mn-Zn Ferrites by Atmospheric Protection", *J. Phys. Ivfrance* 7 (1997), Colloque, SupplCment au Journal de Physique II 1 de mars 1997

Chapter I: General Introduction

- [12] Emad M. M. Ewais, Mahmoud M. Hessien and Abdel-Hady A. El-Geassy, "In-Situ Synthesis of Magnetic Mn-Zn Ferrite Ceramic Object by Solid State Reaction", *J. Aust. Ceram. Soc.* 44 [1] (2008) 57-62.
- [13] Dawoud, H. A. and Shaat, S. K. K., "Initial Permeability and Dc Conductivity of Cu – Zn Ferrite", *the Isla. Unive. J.* (Series of Natural Studies And Engineering), Vol-14, No.1, pp 165-182, 2006.

Chapter 2

Theoretical Background

2.1 General aspects of magnetism

2.1.1 Origin of Magnetism

The origin of magnetism lies in the orbital and spin motions of electrons and how the electrons interact with one another. The best way to introduce the different types of magnetism is to describe how materials respond to magnetic fields. It is just that some materials are much more magnetic than others. The main distinction is that in some materials there is no collective interaction of atomic magnetic moments, whereas in other materials there is a very strong interaction between atomic moments. The magnetic moment of an electron in orbit is given by

$$\mu = \pi r^2 (ev/2\pi r) = evr/2 \quad \dots \quad \dots \quad \dots \quad \dots \quad \dots \quad \dots \quad \dots \quad (2.1)$$

Where r is the radius of orbit, e - charge and v is the velocity

The angular momentum of an electron must be an integral multiple of Planck's const.

$$mvr = nh/2\pi \quad \dots \quad \dots \quad \dots \quad \dots \quad \dots \quad \dots \quad \dots \quad (2.2)$$

Where m is the mass and h is the Planck's const.

If the electron revolves in the first orbit then $n=1$

Therefore orbital magnetic moment of an electron is given by from (2.1) and (2.2)

$$\mu = eh/4\pi m \quad \dots \quad \dots \quad \dots \quad \dots \quad \dots \quad \dots \quad \dots \quad (2.3)$$

This is known as Bohr magneton, the smallest possible orbital magnetic moment.

A simple electromagnet can be produced by wrapping copper wire into the form of a coil and connecting the wire to a battery. A magnetic field is created in the coil but it remains there only while electricity flows through the wire. The field created by the magnet is associated with the motions and interactions of its electrons, the minute charged particles which orbit the nucleus of each atom. Electricity is the movement of electrons, whether in a wire or in an atom, so each atom represents a tiny permanent magnet in its own right. The circulating electron produces its own orbital magnetic moment, measured in

Bohr magnetons (μ_B), and there is also a spin magnetic moment associated with it due to the electron itself spinning, like the earth, on its own axis (illustrated in Figure 2.1). In most materials there is resultant magnetic moment, due to the electrons being grouped in pairs causing the magnetic moment to be cancelled by its neighbor.

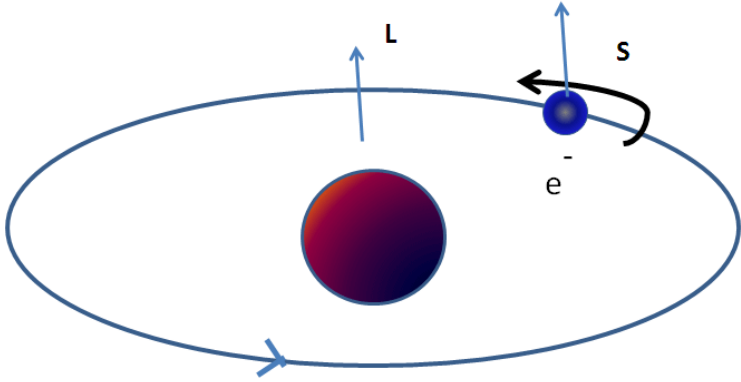


Figure 2.1. A spin magnetic moment associated with it due to the electron itself spinning like the earth on its own axis

In certain magnetic materials the magnetic moments of a large proportion of the electrons align, producing a unified magnetic field. The field produced in the material (or by an electromagnet) has a direction of flow and any magnet will experience a force trying to align it with an externally applied field, the smallest possible magnetic moment due to spin of the electron is $\mu = eh/4\pi m$. According to quantum theory the spin of electrons have only two possibilities $+1/2$ or $-1/2$. Similar to eqn (3) we can write in the form

$$\mu = (e/2m) S \dots \dots \dots (2.4)$$

Where S is the spin quantum number here given by $(1/2) \cdot (h/2\pi)$

In short,

$$\mu = g \cdot (e/2m) \cdot S \quad \dots \quad \dots \quad \dots \quad \dots \quad \dots \quad \dots \quad (2.5)$$

Here g is the term known as g - factor. When $g=2$, the spin contribution arises and when $g=1$ the orbital contribution arises. The mass of the nucleus is so large that the magnetic moment contribution can be neglected compared to the electronic magnetic moment. The gyromagnetic ratio is proportional to the g -factor and ' g ' arises due to the precession of the electrons similar to the precession of a top in a gravitational force. the value of g tells us whether the origin of magnetic moment is spin or orbital motion of electrons.

2.1.2 Magnetic moment of atoms

The strength of a magnetic dipole, called the magnetic dipole moment, may be thought of as a measure of a dipole's ability to turn itself into alignment with a given external magnetic field. In a uniform magnetic field, the magnitude of the dipole moment is proportional to the maximum amount of torque on the dipole, which occurs when the dipole is at right angles to the magnetic field[1].

The magnetic moment or magnetic dipole moment is a measure of the strength of a magnetic source. In the simplest case of a current loop, the magnetic moment is defined as:

$$\mu_m = I \int da \quad \dots \quad \dots \quad \dots \quad \dots \quad \dots \quad \dots \quad (2.6)$$

Where a is the vector area of the current loop, and the current, I is constant. By convention, the direction of the vector area is given by the right hand rule (moving one's right hand in the current direction around the loop, when the palm of the hand is 'touching' the loop's surface, and the straight thumb indicate the direction).

In the more complicated case of a spinning charged solid, the magnetic moment can be found by the following equation:

$$\vec{\mu}_m = \frac{1}{2} \int \vec{r} \times \vec{J} d\tau \quad \dots \quad \dots \quad \dots \quad \dots \quad \dots \quad \dots \quad (2.7)$$

where, $d\tau = r^2 \sin\theta dr d\theta d\phi$, J is the current density.

Magnetic moment can be explained by a bar magnet which has magnetic poles of equal magnitude but opposite polarity. Each pole is the source of magnetic force which weakens with distance. Since magnetic poles come in pairs, their forces interfere

with each other because while one pole pulls, the other repels. This interference is greatest when the poles are close to each other i.e. when the bar magnet is short. The magnetic force produced by a bar magnet, at a given point in space, therefore depends on two factors: on both the strength P of its poles and on the distance d separating them. The force is proportional to the product, $\mu = PR$, where, μ describes the ‘magnetic moment’ or ‘dipole moment’ of the magnet along a distance R and its direction as the angle between R and the axis of the bar magnet. Magnetism can be created by electric current in loops and coils so any current circulating in a planar loop produces a magnetic moment whose magnitude is equal to the product of the current and the area of the loop. When any charged particle is rotating, it behaves like a current loop with a magnetic moment.

The equation for magnetic moment in the current-carrying loop, carrying current I and of area vector a for which the magnitude is given by:

$$\vec{\mu}_m = I\vec{a} \quad \dots \quad \dots \quad \dots \quad \dots \quad \dots \quad \dots \quad (2.8)$$

where, $\vec{\mu}_m$ is the magnetic moment, a vector measured in ampere-square meters, or equivalent joules per tesla, I is the current, a scalar measured in amperes, and \vec{a} is the loop area vector, having as x, y and z coordinates the area in square meters of the projection of the loop into the yz-, zx- and xy-planes.

2.1.3 Magnetic moment of electrons

The electron is a negatively charged particle with angular momentum. A rotating electrically charged body in classical electrodynamics causes a magnetic dipole effect creating magnetic poles of equal magnitude but opposite polarity like a bar magnet. For magnetic dipoles, the dipole moment points from the magnetic south to the magnetic north pole. The electron exists in a magnetic field which exerts a torque opposing its alignment creating a potential energy that depends on its orientation with respect to the field. The magnetic energy of an electron is approximately twice what it should be in classical mechanics. The factor of two multiplying the electron spin angular momentum comes from the fact that it is twice as effective in producing magnetic moment. This factor is called the electronic spin g-factor. The persistent early spectroscopists, such as Alfred Lande, worked out a way to calculate the effect of the

various directions of angular momenta. The resulting geometric factor is called the Lande g -factor.

The intrinsic magnetic moment of a particle with charge q , mass m , and spin s , is

$$\vec{\mu}_m = g \frac{q}{2m} \vec{s} \quad \dots \quad \dots \quad \dots \quad \dots \quad \dots \quad \dots \quad (2.9)$$

where, the dimensionless quantity g is called the g -factor.

The g -factor is an essential value related to the magnetic moment of the subatomic particles and corrects for the precession of the angular momentum. One of the triumphs of the theory of quantum electrodynamics is its accurate prediction of the electron g -factor, which has been experimentally determined to have the value 2.002319. The value of 2 arises from the Dirac equation, a fundamental equation connecting the electron's spin with its electromagnetic properties, and the correction of 0.002319, called the anomalous magnetic dipole moment of the electron, arises from the electron's interaction with virtual photons in quantum electrodynamics. Reduction of the Dirac equation for an electron in a magnetic field to its non-relativistic limit yields the Schrödinger equation with a correction term which takes account of the interaction of the electron's intrinsic magnetic moment with the magnetic field giving the correct energy[2].

The total spin magnetic moment of the electron is

$$\vec{\mu}_s = -g_s \mu_B (\vec{s}/\hbar) \dots \quad \dots \quad \dots \quad \dots \quad \dots \quad \dots \quad \dots \quad (2.10)$$

where $g_s = 2$ in Dirac mechanics, but is slightly larger due to Quantum Electrodynamics effects, μ_B is the Bohr magneton and s is the electron spin. The z component of the electron magnetic moment is

$$\vec{\mu}_z = -g_s \mu_B m_s \dots \quad \dots \quad \dots \quad \dots \quad \dots \quad \dots \quad \dots \quad (2.11)$$

where, m_s is the spin quantum number.

The total magnetic dipole moment due to orbital angular momentum is given by

$$\vec{\mu}_s = -\frac{e}{2m_e} L = -\mu_B \sqrt{l(l+1)} \dots \quad \dots \quad \dots \quad \dots \quad \dots \quad (2.12)$$

where, μ_B is the Bohr magneton.

The z -component of the orbital magnetic dipole moment for an electron with a magnetic quantum number m_l is given by

$$\vec{\mu}_z = -\mu_B m_l \dots \quad \dots \quad \dots \quad \dots \quad \dots \quad \dots \quad \dots \quad (2.13)$$

2.1.4 Magnetic Behaviour

The magnetic properties of a matter are fundamentally the result of the electrons of the atom, which have a magnetic moment by means of the electron motion. There are two types of electronic motion, spin and orbital, and each has a magnetic moment associated with it. Since the response of a material to a magnetic field (H) is characteristic of the magnetic induction or the flux density (B) and the effect that a material has upon the magnetic induction in a magnetic field is represented by the magnetization (M). Thus a universal equation can be established, relating these three magnetic quantities, by

$$B = \mu_0(H+M) \dots \dots \dots \dots \dots \dots (2.14)$$

$$B = \mu H \dots \dots \dots \dots \dots \dots (2.15)$$

where, μ_0 is a universal constant of permeability in a free space and μ is the permeability of a material. In equation (2.14), one can see that μ_0H is the magnetic induction generated by the field alone and μ_0M is the additional magnetic induction contributed by a material. The magnetic susceptibility (χ) is defined as the ratio of magnetization to magnetic field

$$\chi = \frac{M}{H} \dots \dots \dots \dots \dots \dots (2.16)$$

The permeability and susceptibility of a material is correlated with respect to each other by

$$\mu = \mu_0(1+\chi) \dots \dots \dots \dots \dots \dots (2.17)$$

The magnetic behavior of materials can be classified into the following five major groups:

- 1. *Diamagnetism*
- 2. *Paramagnetism*
- 3. *Ferromagnetism*
- 4. *Antiferromagnetism*
- 5. *Ferrimagnetism*

Materials in the first two groups are those that exhibit no collective magnetic interactions and are not magnetically ordered. Materials in the last three groups exhibit long-range magnetic order below a certain critical temperature[1,2]. Ferromagnetic and ferrimagnetic materials are usually what we consider as being magnetic (ie., behaving like iron). The remaining three are so weakly magnetic that they are usually thought of

as “nonmagnetic”. The varieties of magnetic orderings are schematically presented in Fig. 2.2.

A brief description of the above mentioned classes of magnetic materials are described below:

1. Diamagnetism

Diamagnetism is a fundamental property of all matter, although it is usually very weak. It is due to the non-cooperative behavior of orbiting electrons when exposed to an applied magnetic field. Diamagnetic substances are composed of atoms which have no net magnetic moments (i.e., all the orbital shells are filled and there are no unpaired electrons). However, when exposed to a field, a negative magnetization is produced and thus the susceptibility is negative. It obeys Lenz's law. The other characteristic behavior of diamagnetic materials is that the susceptibility is temperature independent. The typical values of susceptibility on the order of 10^{-5} to 10^{-6} . Most of the materials are diamagnetic, including Cu, B, S, N₂ and most organic compounds.

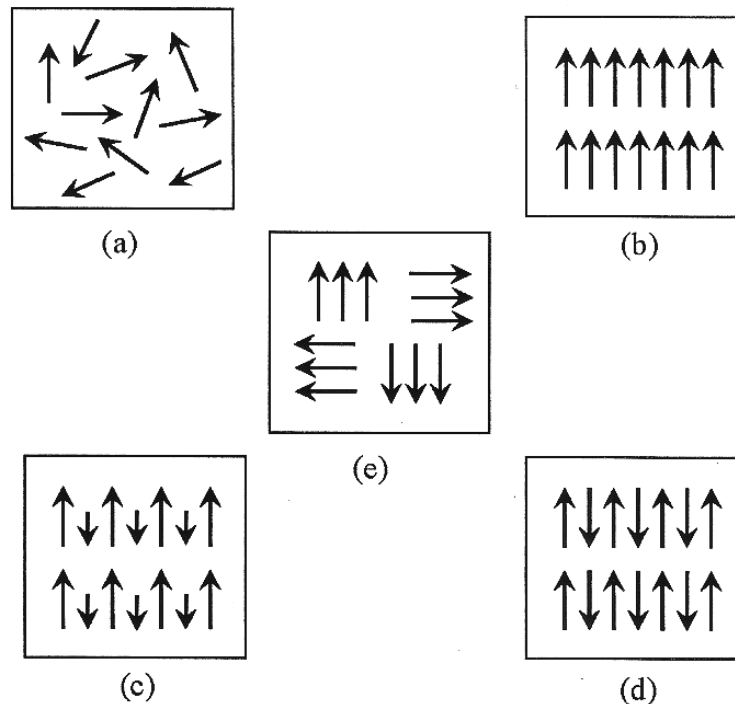


Figure 2.2. Varieties of magnetic orderings (a) paramagnetic, (b) ferromagnetic, (c) ferrimagnetic, (d) antiferromagnetic and (e) superparamagnetic.

2. Paramagnetism

Paramagnetic materials possess a permanent dipole moment due to incomplete cancellation of electron spin and/or orbital magnetic moments (unpaired electrons). In the absence of an applied magnetic field the dipole moments are randomly oriented; therefore the material has no net macroscopic magnetization. When a field is applied these moments tend to align by rotation towards the direction of the applied field and the material acquires a net magnetization [4]. The magnetic moment can be oriented along an applied field to give rise to a positive susceptibility and the values of susceptibility are very small with the order of 10^{-5} to 10^{-3} . O_2 , NO , Mn and Cr are just a few examples of the paramagnetic materials. The susceptibility of a paramagnetic material is inversely dependent on temperature, which is known as Curie law (Figure 2.3a)

$$\chi = \frac{C}{T} \dots \dots \dots \dots \dots \quad (2.18)$$

Where C is the Curie constant.

3. Ferromagnetism

Ferromagnetic material differs from diamagnetic and paramagnetic materials in many different ways. In a ferromagnetic material, the exchange coupling between neighboring moments leads the moments to align parallel with each other. In ferromagnetic materials, this permanent magnetic moment is the result of the cooperative interaction of large numbers of atomic spins in what are called domains regions where all spins are aligned in the same direction. The exchange force is a quantum mechanical phenomenon due to the relative orientation of the spins of two electrons.

Therefore, the ferromagnetic materials generally can acquire a large magnetization even in absence of a magnetic field, since all magnetic moments are easily aligned together. The susceptibility of a ferromagnetic material does not follow the Curie law, but displayed a modified behavior defined by Curie-Weiss law (Figure 2.3b).

$$\chi = \frac{C}{T - \theta} \dots \dots \dots \dots \dots \quad (2.19)$$

C is a constant and θ is called Weiss constant. For ferromagnetic materials, the Weiss - constant is almost identical to the Curie temperature (T_c). At temperature below T_c , the

magnetic moments are ordered whereas above T_c , material loses magnetic ordering and show paramagnetic character. The elements Fe, Ni, and Co and many of their alloys are typical ferromagnetic materials.

Two distinct characteristics of ferromagnetic materials are:

- Spontaneous magnetization and
- The existence of magnetic ordering temperature (Curie temperature)

The spontaneous magnetization is the net magnetization that exists inside a uniformly magnetized microscopic volume in the absence of a field. The magnitude of this magnetization, $0K$, is dependent on the spin magnetic moments of electrons. The saturation magnetization is the maximum induced magnetic moment that can be obtained in a magnetic field (H_{sat}); beyond this field no further increase in magnetization occurs. Saturation magnetization is an intrinsic property, independent of particle size but dependent on temperature.

Even though electronic exchange forces in ferromagnets are very large, thermal energy eventually overcomes the exchange and produces a randomizing effect. This occurs at a particular temperature called the Curie temperature (T_c). Below the Curie temperature, the ferromagnet is ordered and above it, disordered. The saturation magnetization goes to zero at the Curie temperature. The Curie temperature is also an intrinsic property.

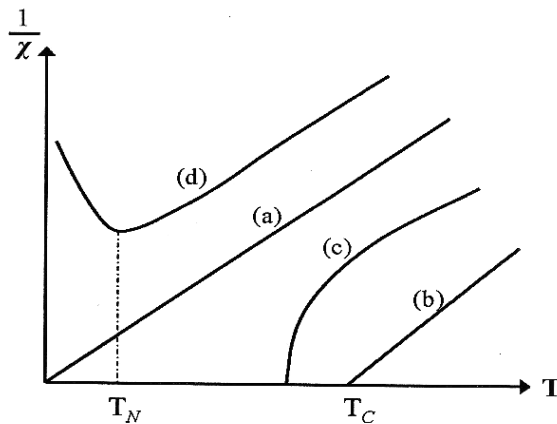


Figure 2.3. The inverse susceptibility varies with temperature T for (a) paramagnetic, (b) ferromagnetic, (c) ferrimagnetic, (d) antiferromagnetic materials. T_N and T_c are Néel temperature and Curie temperature, respectively.

4. Antiferromagnetism

Antiferromagnetic material aligns the magnetic moments in a way that all moments are anti-parallel to each other, the net moment is zero. The anti-ferromagnetic susceptibility is followed the Curie-Weiss law with a negative θ as in equation (2.14). The inverse susceptibility as a function of temperature is shown in Fig. 2.3(d). Common examples of materials with antiferromagnetic ordering include *MnO*, *FeO*, *CoO* and *NiO*.

5. Ferrimagnetism

Ferrimagnetic material has the same anti-parallel alignment of magnetic moments as an antiferromagnetic material does. However, the magnitude of magnetic moment in one direction differs from that of the opposite direction. As a result, a net magnetic moment remains in the absence of external magnetic field. The behavior of susceptibility of a ferrimagnetic material also obeys Curie-Weiss law and has a negative θ as well in Fig. 2.3(c). In ionic compounds, such as oxides, more complex forms of magnetic ordering can occur as a result of the crystal structure. The magnetic structure is composed of two magnetic sublattices (called *A* and *B*) separated by oxygens. The exchange interactions are mediated by the oxygen anions. When this happens, the interactions are called indirect or superexchange interactions. The strongest superexchange interactions result in an antiparallel alignment of spins between the *A* and *B* sublattice. In ferrimagnets, the magnetic moments of the *A* and *B* sublattices are not equal and result in a net magnetic moment. Ferrimagnetism is therefore similar to ferromagnetism. It exhibits all the hallmarks of ferromagnetic behavior like spontaneous magnetization, Curie temperature, hysteresis, and remanence. However, ferro- and ferrimagnets have very different magnetic ordering.

2.1.5 Hysteresis Loop

In addition to the Curie temperature and saturation magnetization, ferromagnets and ferrimagnets can retain a memory of an applied field once it is removed. This behavior is called hysteresis and a plot of the variation of magnetization with magnetic field is called a hysteresis loop.

Another hysteresis property is the coercivity of remanence (H_r) as in Fig. 2.4. This is the reverse field which, when applied and then removed, reduces the saturation

remanence to zero is always larger than the coercive force. The initial susceptibility (χ_0) is the magnetization in low fields, on the order of the earth's field (50-100 μT). The various hysteresis parameters are not solely intrinsic properties but are dependent on grain size, domain state, stresses, and temperature. Because hysteresis parameters are dependent on grain size, they are useful for magnetic grain sizing of natural samples.

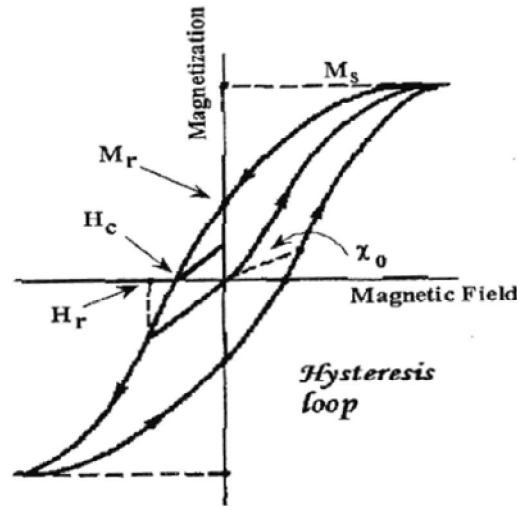


Figure 2.4. Hysteresis loop

2.1.6 Magnetic Domains

In 1907 Weiss proposed that a magnetic material consists of physically distinct regions called domains and each of which was magnetically saturated in different directions (the magnetic moments are oriented in a fixed direction) as shown schematically in Fig. 2.5. Even each domain is fully magnetized but the material as a whole may have zero magnetization. The external applied field aligns the domains, so there is net moment. At low fields this alignment occurs through the growth of some domains at the cost of less favorably oriented ones and the intensity of the magnetization increases rapidly. Growth of domains stops as the saturation region is approached and rotation of unfavorably aligned domain occurs. Domain rotation requires more energy than domain growth. In a ferromagnetic domain, there is parallel alignment of the atomic moments. In a ferrite domain, the net moments of the anti ferromagnetic interactions are spontaneously oriented parallel to each other. Domains typically contain from 10^{12} to 10^{15} atoms and are separated by domain boundaries or walls called Bloch walls. The

formation of domains allows a ferro or ferri-material to minimize its total magnetic energy.

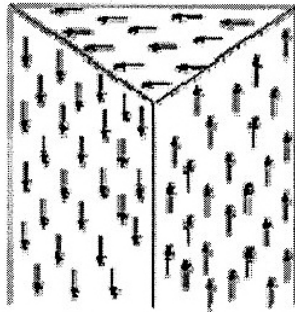


Figure 2.5. Illustration of domains in ferromagnetic materials

The magnetic energy is composed of several types of energy [5, 6]:

i) Magnetostatic or demagnetization energy: The magnetized material behaves like a magnet, with a surrounding magnetic field. This field acts to magnetize the material in the direction opposite from its own magnetization, causing a magnetostatic energy which depends on the shape of the material. This magnetostatic energy can be reduced by reducing the net external field through the formation of domains inside the material.

ii) Magnetocrystalline anisotropy energy: In some materials the domain magnetization tends to align in a particular crystal direction (the so-called easy axis). The material is easiest to magnetize to saturation or demagnetize from saturation if the field is applied along an easy axis. The energy difference between aligning the domain in the easy and another direction (hard direction) is called magnetocrystalline anisotropy energy. Anisotropy energy is the energy needed to rotate the moment from the easy direction to a hard direction. For materials with cubic crystalline structure (such as ferrites), the energy is expressed in terms of anisotropy constants and the direction to which the magnetization rotates.

$$E_k = K_1 \sin^2 \theta + K_2 \sin^4 \theta \dots \quad (\text{hexagonal structure})$$

$$E_k = K_1 (\alpha_1^2 \alpha_2^2 + \alpha_2^2 \alpha_3^2 + \alpha_3^2 \alpha_1^2) + K_2 (\alpha_1^2 \alpha_2^2 \alpha_3^2 + \dots) \quad (\text{cubic Structure})$$

where, K is the anisotropy constant, θ is the angle between the easy axis and the direction of magnetization, and α 's are the direction cosines, which are the ratios of the individual components of the magnetization projected on each axis divided by the

magnitude of the magnetization. A crystal is higher in anisotropy energy when the magnetization points in the hard direction rather than along the easy direction. The formation of domains permits the magnetization to point along the easy axis, resulting in a decrease in the net anisotropy energy.

c) *Magnetostrictive energy*: In a magnetic field, the material may change its dimensions on the order of several parts per million. This change in dimension results in what is called magnetostrictive energy, which is lowered by a reduction in the size of the domains, requiring the formation of more domains.

d) *Domain wall energy*: This is energy resulting from the increase or decrease in the width of the walls due to the growth/shrinkage of domains.

The magnetization in a domain changes by two mechanisms: rotation of the magnetic dipoles toward the direction of the applied field and change in the domain volume. In the first case, a certain amount of anisotropy energy is needed to rotate the magnetization in a crystal from the easy to another axis. In the second mechanism, the volume of the domain changes, changing its contribution to the bulk magnetization, while the magnetization direction is unchanged. The change in the magnetization intensity of a domain depends on how close its direction is to the direction of the applied field. If the magnetization direction is close, the intensity in the domain increases, whereas if it is far, the intensity decreases.

The domain volume changes due to motion of the domain wall. This movement is originated by a torque that rotates the moments of the domain in line with the field, moving the center of the wall toward the domain opposed to the field. Consequently, the volume of the domains whose direction is favorable is increased whereas the domains with unfavorable direction decrease in volume [5]. In order to explain the fact that ferromagnetic materials with spontaneous magnetization could exist in the demagnetized state Weiss proposed the concept of magnetic domains. The magnetization within the domain is saturated and will always lie in the easy direction of magnetization when there is no externally applied field. The direction of the domain alignment across a large volume of material is more or less random and hence the magnetization of a specimen can be zero.

Magnetic domains exist in order to reduce the energy of the system. A uniformly magnetized specimen as shown in Fig. 2.6 (a) has a large magnetostatic energy

associated with it. This is the result of the presence of magnetic free poles at the surface of the specimen generating a demagnetizing field, H_d . From the convention adopted for the definition of the magnetic moment for a magnetic dipole the magnetization within the specimen points from the South Pole to the North Pole, while the direction of the magnetic field points from north to south. Therefore, the demagnetizing field is in opposition to the magnetization of the specimen. The magnitude of H_d is dependent on the geometry and magnetization of the specimen. In general if the sample has a high length to diameter ratio (and is magnetized in the long axis) then the demagnetizing field and the magnetostatic energy will be low.

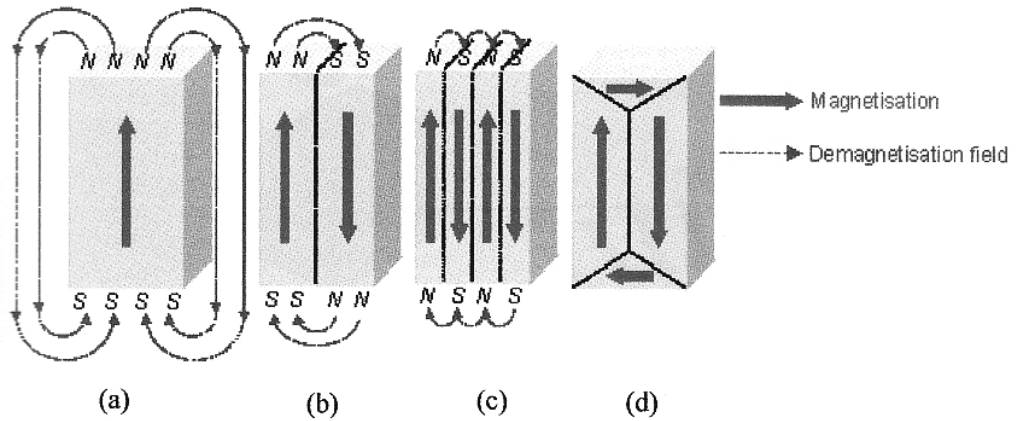


Figure 2.6. Schematic illustration of the break up of 'magnetization into domains (a) single domain, (b) two domains, (c) four domains and (d) closure domains.

The break up of the magnetization into two domains as illustrated in figure 2.6(b) reduces the magnetostatic energy by half. In fact if the magnet breaks down into N domains then the magnetostatic energy is reduced by a factor of $1/N$, hence figure 2.6(c) has a quarter of the magnetostatic energy of Fig. 2.6(a). Figure 2.6(d) shows a closure domain structure where the, magnetostatic energy is zero, this is only possible for materials that do not have a strong uniaxial anisotropy, and the neighbouring domains do not have to be at 180° to each other.

2.1.7 Structure of domain wall

The introduction of a domain raises the overall energy of the system, therefore the division into domains only continues while the reduction in magnetostatic energy is greater than the energy required to form the domain wall. The energy associated with a domain wall is proportional to its area. The schematic representation of the domain wall, shown in Fig. 2.7, illustrates that the dipole moments of the atoms within the wall are not pointing in the easy direction of magnetization and hence are in a higher energy state. In addition, the atomic dipoles within the wall are not at 180° to each other and so the exchange energy is also raised within the wall. Therefore, the domain wall energy is an intrinsic property of a material depending on the degree of magnetocrystalline anisotropy and the strength of the exchange interaction between neighbouring atoms. The thickness of the wall will also vary in relation to these parameters, as strong magnetocrystalline anisotropy will favor a narrow wall, whereas a strong exchange interaction will favor a wider wall.

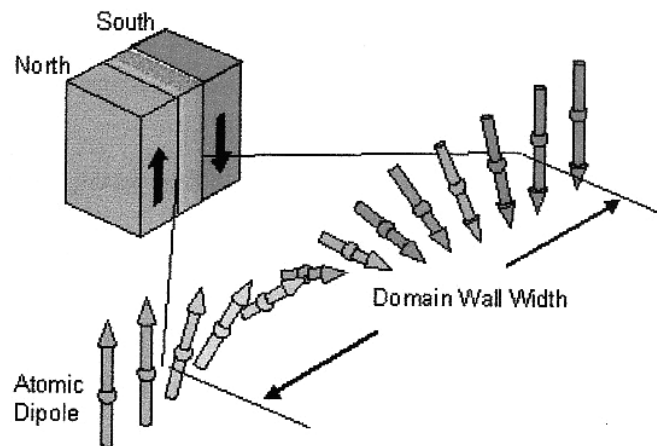


Figure 2.7. Schematic representation of a 180° domain wall

A minimum energy can therefore be achieved with a specific number of domains within a specimen. This number of domains will depend on the size and shape of the sample (which will affect the magnetostatic energy) and the intrinsic magnetic properties of the material (which will affect the magnetostatic energy and the domain wall energy).

Ferromagnetic materials get their magnetic properties not only because their atoms carry a magnetic moment but also because the material is made up of small regions known as magnetic domains. In each domain, all of the atomic dipoles are coupled together in a preferential direction. During solidification, a trillion or more atom moments are aligned parallel so that the magnetic force within the domain is strong in one direction. Ferromagnetic materials are said to be characterized by “spontaneous magnetization” since they obtain saturation magnetization in each of the domains without an external magnetic field being applied. Even though the domains are magnetically saturated, the bulk material may not show any signs of magnetism because the domains develop themselves and are randomly oriented relative to each other.

Ferromagnetic materials become magnetized when the magnetic domains within the material are aligned. This can be done by placing the material in a strong external magnetic field or by passing electrical current through the material. Some or all of the domains can become aligned. The more domains that are aligned, the stronger the magnetic field in the material. When all of the domains are aligned, the material is said to be magnetically saturated. When a material is magnetically saturated, no additional amount of external magnetization force will cause an increase in its internal level of magnetization. In an unmagnetized sample of material, the domains point in random directions, or form closed loops, so that there is no overall magnetization of the sample. In a magnetized sample, the domains are aligned so that their magnetic effects combine to produce a strong overall magnetism.

2.1.8 Microstructure

A polycrystal is much more than many tiny crystals bonded together. The interfaces between the crystals, or the grain boundaries which separate and bond the grains, are complex and interactive interfaces. The whole set of a given material’s properties (mechanical, chemical and especially electrical and magnetic) depend strongly on the nature of the microstructure.

In the simplest case, the grain boundary is the region, which accommodates the difference in crystallographic orientation between the neighbouring grains. For certain simple arrangements, the grain boundary is made of an array of dislocations whose number and spacing depends on the angular deviation between the grains. The ionic

nature of ferrites leads to dislocation patterns considerably more complex than in metals, since electrostatic energy accounts for a significant fraction of the total boundary energy [2].

For low-loss ferrite, Ghate [3] states that the grain boundaries influence properties by

- 1) creating a high resistivity intergranular layer,
- 2) acting as a sink for impurities which may act as a sintering aid and grain growth modifiers,
- 3) providing a path for oxygen diffusion, which may modify the oxidation state of cations near the boundaries.

In addition to grain boundaries, ceramic imperfections can impede domain wall motion and thus reduce the magnetic property. Among these are pores, cracks, inclusions, second phases, as well as residual strains. Imperfections also act as energy wells that pin the domain walls and require higher activation energy to detach. Stresses are microstructural imperfections that can result from impurities or processing problems such as too rapid a cool. They affect the domain dynamics and are responsible for a much greater share of the degradation of properties than would expect [3].

Grain growth kinetics depends strongly on the impurity content. A minor dopant can drastically change the nature and concentration of defects in the matrix, affecting grain boundary motion, pore mobility and pore removal [2]. The effect of a given dopant depends on its valence and solubility with respect to host material. If it is not soluble at the sintering temperature, the dopant becomes a second phase which usually segregates to the grain boundary.

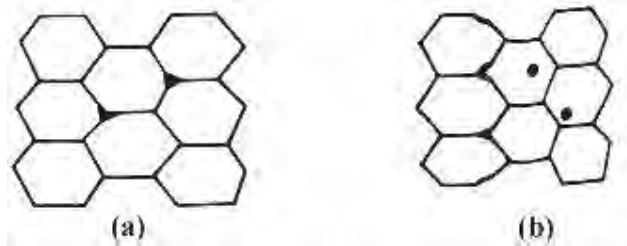


Figure 2.8. Porosity character: (a) intergranular, (b) intragranular.

amorphous materials containing a large number of randomly oriented magnetic atoms the permeability will be scalar. As we have

$$B = \mu_0(H + M) \quad \dots \quad \dots \quad \dots \quad \dots \quad \dots \quad (2.21)$$

and susceptibility,

$$\chi = \frac{dM}{dH} = \frac{d}{dH} \left(\frac{B}{\mu_0} - H \right) = \frac{1}{\mu_0} (\mu - 1) \quad \dots \quad \dots \quad \dots \quad (2.22)$$

The magnetic energy density

$$E = \frac{1}{\mu_0} \int H dB \quad \dots \quad \dots \quad \dots \quad \dots \quad \dots \quad (2.23)$$

For time harmonic fields $H = H_0 \sin \omega t$, the dissipation can be described by a phase difference δ between H and B . In the case of permeability, defined as the proportional constant between the magnetic field induction B and applied intensity H ;

$$B = \mu H \quad \dots \quad \dots \quad \dots \quad \dots \quad \dots \quad (2.24)$$

If a magnetic material is subjected to an ac magnetic field as we get,

$$B = B_0 e^{i\omega t} \quad \dots \quad \dots \quad \dots \quad \dots \quad \dots \quad (2.25)$$

Then it is observed that the magnetic flux density B experiences a delay. This is caused due to the presence of various losses and is thus expressed as,

$$B = B_0 e^{i(\omega t - \delta)} \quad \dots \quad \dots \quad \dots \quad \dots \quad \dots \quad (2.26)$$

where δ is the phase angle and marks the delay of B with respect to H , the permeability is then given by

$$\mu = \frac{B}{H} = \frac{B_0 e^{i(\omega t - \delta)}}{H_0 e^{i\omega t}} = \frac{B_0 e^{-i\delta}}{H_0} = \frac{B_0}{H_0} \cos \delta - i \frac{B_0}{H_0} \sin \delta = \mu' - i\mu'' \quad (2.27)$$

Where $\mu' = \frac{B_0}{H_0} \cos \delta \quad \dots \quad \dots \quad \dots \quad \dots \quad \dots \quad (2.28)$

And $\mu'' = \frac{B_0}{H_0} \sin \delta \quad \dots \quad \dots \quad \dots \quad \dots \quad \dots \quad (2.29)$

The real part μ' of complex permeability μ as expressed in equation (2.28) represents the component of induction B , which is in phase with H , so it corresponds to the normal permeability. If there are no losses, we should have $\mu = \mu'$. The imaginary part μ'' corresponds to that part of B , which is delayed by phase δ from H . The presence of such a component requires a supply of energy to maintain the alternation magnetization,

regardless of the origin of delay. It is useful to introduce the loss factor or loss tangent ($\tan\delta$). The ratio of μ'' to μ' , as is evident from equation gives.

$$\frac{\mu''}{\mu'} = \frac{\frac{B_0}{H_0} \sin \delta}{\frac{B_0}{H_0} \cos \delta} = \tan \delta \dots \dots \dots \dots \dots \dots (2.30)$$

This $\tan\delta$ is called the loss factor. The Q-factor or quality factor is defined as the reciprocal of this loss factor i.e.

$$\text{Quality factor} = \frac{1}{\tan \delta} \dots \dots \dots \dots \dots \dots (2.31)$$

And the relative quality factor, $Q = \frac{\mu'}{\tan \delta}$

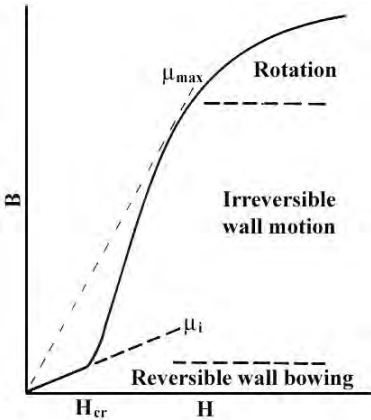


Figure 2.10. Schematic magnetization curve showing the important parameter: initial permeability, μ_i (the slope of the curve at low fields) and the main magnetization mechanism in each magnetization range.

The behavior of μ' and μ'' versus frequency is called the complex permeability spectrum. The initial permeability of a ferromagnetic substance is the combined effect of the wall permeability and rotational permeability mechanism.

2.1.10 Mechanisms of Permeability

The mechanisms can be explained as follows: A demagnetized magnetic material is divided into number of Weiss domains separated by Bloch walls. In each domain all the magnetic moments are oriented in parallel and the magnetization has its saturation

value M_s . In the walls the magnetization direction changes gradually from the direction of magnetization in one domain to that in the next. The equilibrium positions of the walls result from the interactions with the magnetization in neighboring domains and from the influence of pores; crystal boundaries and chemical inhomogeneities which tend to favour certain wall positions.

2.1.11 Wall Permeability

The mechanism of wall permeability arises from the displacement of the domain walls in small fields. Lets us consider a piece of material in the demagnetized state, divided into Weiss domains with equal thickness L by means of 180° Bloch walls (as in the Fig. 2.11). The walls are parallel to the YZ plane. The magnetization M_s in the domains is oriented alternately in the $+Z$ or $-Z$ direction. When a field H with a component in the $+Z$ direction is applied, the magnetization in this direction will be favoured. A displacement dx of the walls in the direction shown by the dotted lines will decrease the energy density by an amount [47, 48]:

$$\frac{2M_s H_z dx}{L}$$

This can be described as a pressure $M_s H_z$ exerted on each wall. The pressure will be counteracted by restoring forces which for small deviations may assume to be kdx per unit wall surface. The new equilibrium position is then given by

$$d = \frac{M_s H_z dx}{L}$$

From the change in the magnetization

$$\Delta M = \frac{2M_s d}{L},$$

the wall susceptibility χ_w may be calculated. Let H makes the angle θ with Z direction.

The magnetization in the θ direction becomes

$$(\Delta M)_\theta = \frac{2M_s d}{L} \cos\theta, \text{ And with } H_z = H \cos\theta \text{ and } d = \frac{2M_s H_z}{K}$$

we obtain

$$\chi_w = \frac{(\Delta M)_\theta}{H} = \frac{4M_s^2 \cos^2 \theta}{KL} \dots \dots \dots (2.32)$$

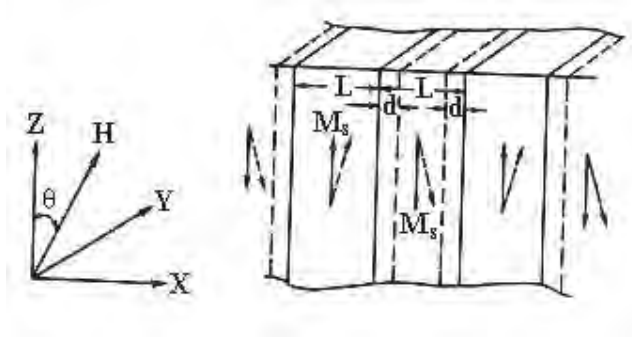


Figure 2.11. Magnetization by wall motion and spin rotation.

2.1.12 Rotational Permeability

The rotational permeability mechanism arises from rotation of the magnetization in each domain. The direction of M can be found by minimizing the magnetic energy E as a function of the orientation. Major contribution to E comes from the crystal anisotropy energy. Other contributions may be due to the stress and shape anisotropy. The stress may influence the magnetic energy via the magnetostriction. The shape anisotropy is caused by the boundaries of the sample as well as by pores, nonmagnetic inclusions and inhomogeneities. For small angular deviations, α_x and α_y may be written as

$$\alpha_x = \frac{M_x}{M_s} \text{ and } \alpha_y = \frac{M_y}{M_s}$$

For equilibrium z-direction, E may be expressed as [47, 48]

$$E = E_0 + \frac{1}{2}\alpha_x^2 E_{xx} + \frac{1}{2}\alpha_y^2 E_{yy}$$

where it is assumed that x and y are the principal axes of the energy minimum. Instead of E_{xx} & E_{yy} , the anisotropy field H_x^A and H_y^A are often introduced. Their magnitude is given by

$$H_x^A = \frac{E_{xx}}{2M_s} \text{ and } H_y^A = \frac{E_{yy}}{2M_s},$$

H_x^A and H_y^A represent the stiffness with which the magnetization is bound to the equilibrium direction for deviations in the x and y direction, respectively. The rotational susceptibilities $\chi_{r,x}$ and $\chi_{r,y}$ for fields applied along x and y directions, respectively are

$$\chi_{r,x} = \frac{M_s}{H_x^A} \text{ and } \chi_{r,y} = \frac{M_s}{H_y^A}.$$

For cubic materials it is often found that H_x^A and H_y^A are equal. For $H_x^A = H_y^A = H^A$ and a field H which makes an angle θ with the Z direction (as shown in Fig. 2.16) the rotational susceptibility, $\chi_{r,c}$ in one crystallite becomes

$$\chi_{r,c} = \frac{M_s}{H^A} \sin^2 \theta \quad \dots \quad \dots \quad \dots \quad \dots \quad \dots \quad (2.33)$$

A polycrystalline material consisting of a large number of randomly oriented grains of different shapes, with each grain divided into domains in a certain way. The rotational susceptibility χ_r of the material has to be obtained as a weighted average of $\chi_{r,c}$ of each crystallite, where the mutual influence of neighbouring crystallites has to be taken into account. If the crystal anisotropy dominates other anisotropies, then H^A will be constant throughout the material, so only the factor $\sin^2 \theta$ (equation 2.33) has to be averaged. Snoek [9] assuming a linear averaging of $\chi_{r,c}$ and found

$$\chi_r = \frac{2M_s}{3H^A}$$

The total internal susceptibility

$$\chi = \chi_w + \chi_r = \frac{4M_s^2 \cos^2 \theta}{KL} + \frac{2M_s}{3H^A} \quad (2.34)$$

If the shape and stress anisotropies cannot be neglected, H^A will be larger. Any estimate of χ_r will then be rather uncertain as long as the domain structure, and the pore distribution in the material are not known. A similar estimate of χ_w would require knowledge of the stiffness parameter K and the domain width L . These parameters are influenced by such factors as imperfection, porosity and crystallite shape and distribution which are essentially unknown.

2.2 Soft Magnetic Materials

The wide variety of magnetic materials can be divided into two groups, the magnetically soft and the magnetically hard. Soft magnetic materials are those materials that are easily magnetised and demagnetised. Soft magnetic materials have low magnetocrystalline anisotropy resulting in reduced coercivity and high permeability. They typically have intrinsic coercivity less than 1000 Am^{-1} . They are used primarily to enhance and/or channel the flux produced by an electric current. The main parameter, often used as a figure of merit for soft magnetic materials, is the high relative permeability μ_r (where $\mu_r = B/\mu_0 H$), which is a measure of how readily the material responds to the applied magnetic field. The other main parameters of interest are the coercivity, the saturation magnetisation and the electrical conductivity.

The types of applications for soft magnetic materials fall into two main categories: AC and DC. In DC applications the material is magnetised in order to perform an operation and then demagnetised at the conclusion of the operation, e.g. an electromagnet on a crane at a scrap yard still be switched on to attract the scrap steel and then switched off to drop the steel. In AC applications the material will be continuously cycled from being magnetised in one direction to the other, throughout the period of operation, e.g. a power supply transformer. A high permeability will be desirable for each type of application but the significance of the other properties varies.

For DC applications the main consideration for material's election is most likely to be the permeability. This would be the case, for example, in shielding applications where the flux must be channeled through the material. Where the material is used to generate a magnetic field or to create a force then the saturation magnetisation may also be significant. For AC applications the important consideration is how much energy is lost in the system as the material is cycled around its hysteresis loop. The energy loss can originate from three different sources: (1) hysteresis loss, which is related to the area contained within the hysteresis loop; (2) eddy current loss, which is related to the generation of electric currents in the magnetic material and the associated resistive losses and (3) anomalous loss, which is related to the movement of domain walls within the material. Hysteresis losses can be reduced by the reduction of the intrinsic coercivity, with a consequent reduction in the area contained within the hysteresis loop. Eddy current losses can be reduced by decreasing the electrical conductivity of the material

and by laminating the material, which has an influence on overall conductivity and is important because of skin effects at higher frequency. Finally, the anomalous losses can be reduced by having a completely homogeneous material, within which there will be no hindrance to the motion of domain walls.

2.2.1 Soft ferrites

At high frequency metallic soft magnetic materials simply cannot be used due to the eddy current losses. Therefore, soft ferrites, which are ceramic insulators, become the most desirable material. These materials are ferrimagnetic with a cubic crystal structure and the general composition $MO.Fe_2O_3$, where M is a transition metal such as nickel, manganese, magnesium or zinc[2]. The magnetically soft ferrites first came into commercial production in 1948.

MnZn ferrite, sold commercially as ferroxcube, can be used at frequencies up to 10 MHz, for example in telephone signal transmitters and receivers and in switch mode power supplies (also referred to as DC-DC converters). For these type of application the driving force to increase frequency is to allow miniaturisation.

Additionally, part of the family of soft ferrites, are the microwave ferrites, e.g. yttrium iron garnet. These ferrites are used in the frequency range from 100 MHz to 500 GHz, for waveguides for electromagnetic radiation and in microwave devices such as phase shifters.

2.2.2 Cubic ferrites with spinel structure

The cubic ferrite has the general formula $MO.Fe_2O_3$ where M is one of the divalent cations of the transition elements such as *Mn, Ni, Mg, Zn, Cd, Cu, Co* etc. A combination of these ions is also possible and it can be named as solid solution of two ferrites or mixed spinel ferrites. Generally, M represents a combination of ions which has an average valency of two. The trivalent iron ion in $MO.Fe_2O_3$ can partially be replaced by another trivalent ion such as Al^{3+} or Cr^{3+} giving rise to mixed crystals. The structure of ferrite is derived from the $MgAl_2O_4$ determined by Bragg [7]. These ferrites crystallize in the FCC spinel structure. The spinel lattice is composed of a close-packed oxygen arrangement in which 32 oxygen ions form the unit cell (the smallest repeating unit in the crystal network). These anions are packed in a face centered cubic (FCC)

arrangement leaving two kinds of spaces between anions: tetrahedrally coordinated sites (A), surrounded by four nearest oxygen atoms, and octahedrally coordinated sites (B), surrounded by six nearest neighbor oxygen atoms. These are illustrated in Fig. 2.12. In total, there are 64 tetrahedral sites and 32 octahedral sites in the unit cell, of which only 8 tetrahedral sites and 16 octahedral sites are occupied, resulting in a structure that is electrically neutral [2, 5].

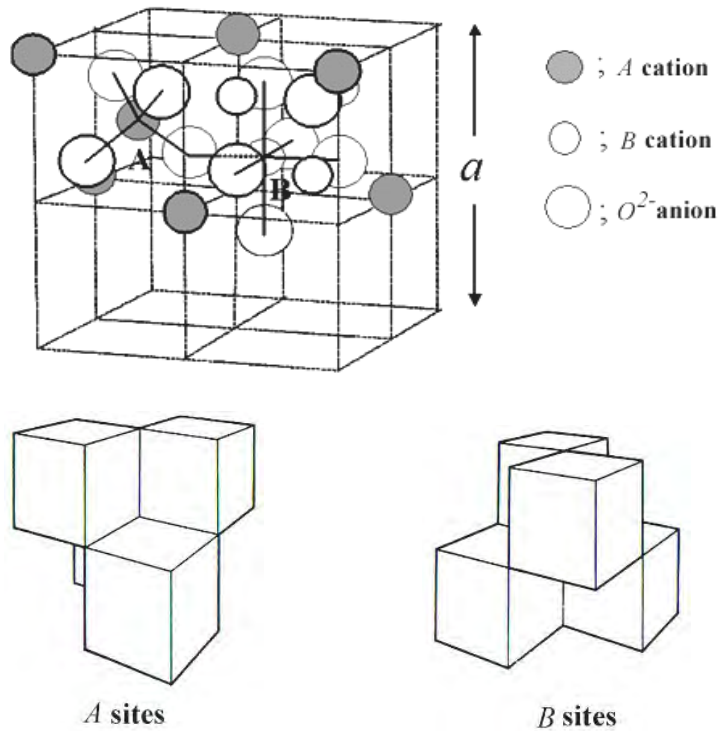


Figure 2.12. Schematic of two subcells of a unit cell of the spinel structure, showing octahedral and tetrahedral sites.

The localization of ions either in the A or B sites depends fundamentally on the ion and lattice sizes. Also it has been observed to depend on the temperature and the orbital preference for specific coordination. In general, divalent ions are larger than trivalent ions. This is because trivalent ion nuclei produce greater electrostatic attraction, hence their electron orbits contract.

The octahedral sites are larger than the tetrahedral sites, thus, the divalent ions are

localized in the octahedral sites whereas trivalent ions are in the tetrahedral sites [5].

According to the site occupancy of the metal ions, the spinel ferrites are classified as:

(a) Normal spinel: where the tetrahedral A-sites are occupied by divalent metal ions and trivalent ions occupy B sites. A majority of these ferrites present paramagnetic behavior,

(b) Inverse spinel: where all the divalent ions are present in the octahedral site while trivalent ions are located on both A and B sites. The spin moments of the trivalent ions in an inverse spinel] are canceled (direction of moment on A sites is opposed to B sites) whereas the spin moments of the divalent ions are aligned, resulting in a net magnetic moment [6] and

(c) Mixed spinel; where divalent ions are present both in tetrahedral and octahedral sites.

The cubic ferrite is easily magnetized and demagnetized; it has high permeability and saturation magnetization, low electrical conductivity, and the anisotropy energy is dominated by the anisotropy constant K_1 . If K_1 , is greater than zero, the easy direction is the cube edge direction (100) whereas if K_1 , is less than zero, the body direction is preferred (111). For most ferrites the value of K , is negative, with the exception of cobalt ferrite [5].

2.2.3 Cation distribution in ferrites

The cation distribution in the spinel ferrite $Me^{2+}Fe^{3+}O_4$ can be as follows [5]:

- Normal spinel ferrite

The Me^{2+} cations are in tetrahedral positions, while the two Fe^{3+} cations are in octahedral sites which is represented as $(Me^{2+})_A[Fe^{3+}]_BO_4$

- Inverse spinel ferrite

In this case the Me^{2+} cation and one of the Fe^{3+} cations are in octahedral positions while the second Me^{3+} cation occupies tetrahedral sites. The arrangement is as $(Fe^{3+})_A[Me^{2+}Fe^{3+}]_BO_4$.

- Mixed spinel ferrite

The arrangement of the form $(Me_{1-\delta}^{2+}Fe_{1-\delta}^{3+})[Me_{1-x}^{2+}Fe_{1+x}^{3+}]O_4$ is often referred as mixed spinel, where δ is called the inversion parameter. $\delta = 0$ for completely normal and $\delta = 1$ for completely iverse spinels $0 < \delta < 1$ for mixed spinels.

The factors affecting the cation distribution over A and B sites are as follows [5]

- The size of the cations
- The electronic configurations of the cations
- The electronic energy
- The saturation magnetization of the lattice

Smaller cations (trivalent) prefer to occupy the A-sites. The cations have special preference for A and B sites and the preference depends on the following factors:

- Ionic radius
- Size of interstices
- Sintering temperature
- Orbital preference for the specific coordination

Zn^{2+} , Cd^{2+} , Ga^{2+} , In^{3+} , Ge^{2+} etc. have strong preference for A-sites while Ni^{2+} , Cr^{3+} , Ti^{4+} , Sn^{4+} etc. have the preference for B-sites. Mg^{2+} , Fe^{3+} , Al^{3+} , Mn^{2+} , Cu^{2+} , Co^{2+} are distributed among A and B-sites. Moreover, the electrostatic energy also affects the cation distribution in the spinet lattice.

2.2.4 Magnetic exchange interaction

The exchange energy between the two atoms having spins S_i and S_j can be expressed universally in terms of Heigenburg Hamiltonian [8]

$$H = - \sum J_{ij} S_i S_j \quad \dots \quad \dots \quad \dots \quad \dots \quad \dots \quad (2.35)$$

where, J_{ij} the exchange integral represents the strength of the exchange coupling between the spin angular momentum i and j . It is well known that the favored situation is the one with the lowest energy and there are two ways in which the wave functions can combine for lowering the energy by H . These are:

If J_{ij} is positive, the parallel spin configuration will minimize the system total energy and all spins aligned to each other in the ground state. This is the case leading to ferromagnetic ordering.

If J_{ij} is negative, J_{ij} favors the antiparallel alignment of spins and consequently gives rise to antiferromagnetic ordering.

2.2.5 Superexchange interaction

The magnetic interaction in magnetic oxide (ferrites) cannot be explained on the basis of direct exchange interaction because of the following facts:

- The magnetic ions are located too far apart from each other shielded by the nonmagnetic anion (oxygen). This is because these are not band type semiconductor [10]. The non-magnetic anion is situated in the line joining magnetic cations.
- Superexchange interactions appear, i.e., indirect exchange via anion p-orbitals that may be strong enough to order the magnetic moments.

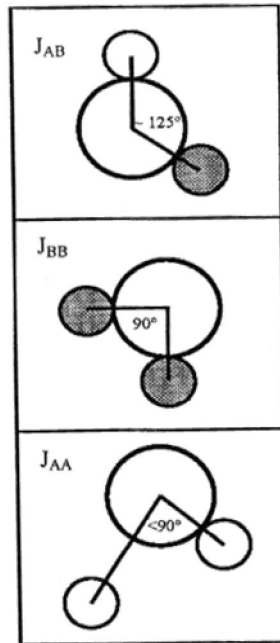


Figure 2.13. Three major types of superexchange interactions in spinel ferrites are as follows: J_{AB} , J_{BB} and J_{AA} . The small empty circle is A site, the small solid circle is B site, and the large empty circle is oxygen anion

Ferrimagnetic oxides are one kind of magnetic systems in which there exist at least two mequivalent sublattices for the magnetic ions. The antiparallel alignment between these sublattices (ferrimagnetic ordering) may occur provided the inter-sublattice exchange interactions are anti ferromagnetic (AF) and some requirements

concerning the signs and strengths of the intra-sublattice interactions are fulfilled. Since usually in ferrimagnetic oxides the magnetic cations are surrounded by bigger oxygen anions (almost excluding the direct overlap between cation orbitals) magnetic interactions occur via indirect superexchange mediated by the p oxygen orbitals. It is well-known that the sign of these superexchange interactions depends both on the electronic structure of the cations and their geometrical arrangement [11]. In most of ferrimagnetic oxides, the crystallographic and electronic structure give rise to antiferromagnetic inter and intra-sublattice competing interactions. The magnitude of negative exchange energies between two magnetic ions M and M' depends upon the distances from these ions to the oxygen ion O²⁻, via which the superexchange takes place, and on the angle M-O²⁻-M' (φ). According to the superexchange theory, the angle $\varphi=180^\circ$ gives rise to the greatest exchange energy, and this energy decreases very rapidly as the distance between the ions increases. If A and B are the tetrahedral and octahedral ions respectively in a spinel structure, the A-B interaction is the greatest and A-A exchange interaction is the weakest [8].

2.2.6 Two sublattices in spinel ferrites

The term 'magnetic sublattice' is widely used in the study of magnetic structures of the whole spectrum of magnetic materials [12]. In the case of ferromagnetic materials, the 'magnetic sublattice' is exactly the same as the crystal structure and no problem arises. In the case of antiferromagnetics, the importance of the direction of the magnetic moments is evident and makes clear the existence of two magnetic sublattices, as for example, in *MnO*. The difference between the two magnetic sublattices is the direction of their magnetic moment. However, ferrimagnetic materials are considerably more complex and the application of the molecular field theory to spinels has pointed to the problem of a clear definition of the concept of magnetic sublattices. In spinel ferrites the metal ions are separated by the oxygen ions and the exchange energy between spins of neighbouring metal ions is found to be negative, that is, antiferromagnetic. This is explained in terms of superexchange interaction of the metal ions via the intermediate oxygen ions [13]. There are a few points to line out about the interaction between two ions in tetrahedral (A) sites:

- The distance between two A ions ($\sim 3.5 \text{ \AA}$) is very large compared with their

ionic radius (0.67 Å for Fe^{3+}),

- The angle A-O²⁻-A ($\varphi=79^\circ38'$) is unfavorable for superexchange interaction [8], and
- The distance from one A ion to O²⁻ is not the same as the distance from the other A ion to O²⁻ as there is only one A nearest neighbour to an oxygen ion (in figure 2.10, M and M' are A ions, $r = 3.3 \text{ \AA}$ and $q = 1.7 \text{ \AA}$) [8]. As a result, two nearest A ions are connected via two oxygen ions.

These considerations led us to the conclusion that superexchange interaction between A ions is very unlikely. This conclusion together with the observation that direct exchange is also unlikely in this case [8] support the assumption that $J_{AA} = 0$ in the spinet ferrites. According to Néel's theory, the total magnetization of a ferrite divided into two sublattices A and B is:

$$M_T(T) = M_B(T) - M_A(T) \quad \dots \quad \dots \quad \dots \quad \dots \quad (2.36)$$

where, T is the temperature, $M_B(T)$ and $M_A(T)$ are A and B sublattice magnetizations. Both $M_B(T)$ and $M_A(T)$ are given in terms of the Brillouin function $B_{si}(x_i)$;

$$M_B(T) = M_B(T=0) B_{sB}(x_s) \quad \dots \quad \dots \quad \dots \quad \dots \quad (2.37)$$

$$M_A(T) = M_A(T=0) \quad \dots \quad \dots \quad \dots \quad \dots \quad (2.38)$$

with

$$\chi_B = \frac{\mu_B g_A S_A}{k_B T} M_B N_{AB} \quad \dots \quad \dots \quad \dots \quad \dots \quad (2.39)$$

$$\chi_B = \frac{\mu_B g_B S_B}{k_B T} (M_B N_{BB} + M_A N_{AB}) \quad \dots \quad \dots \quad \dots \quad \dots \quad (2.40)$$

The molecular field coefficients N_{ij} , are related to the exchange constants J_{ij} by the following expression:

$$J_{ij} = \frac{n_j g_i g_j \mu_B^2}{2z_{ij}} N_{ij} \quad \dots \quad \dots \quad \dots \quad \dots \quad (2.41)$$

with r_{ij} the number of magnetic ions per mole in the j th sublattice, g the Lande factor, μ_B is the Bohr magneton and z_{ij} the number of nearest neighbours on the j^{th} sublattice that interact with the i^{th} ion.

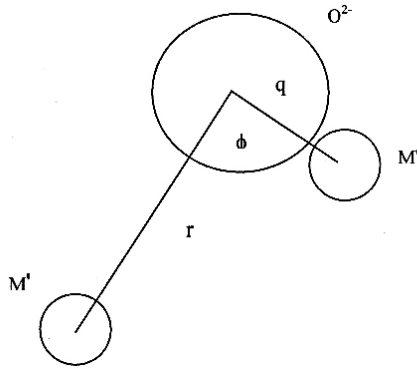


Figure 2.14. Schematic representation of ions M and M' and the O^{2-} ion through which the superexchange is made. R and q are the centre to centre distances from m M and M' respectively to O^{2-} and ϕ is the angle between them.

According to Néel's theory and using $J_{AA} = 0$, equating the inverse susceptibility $1/\chi = 0$ at $T = T_c$ we obtain for the coefficients of the molecular field theory N_{AB} and N_{BB} of the following expression:

$$N_{BB} = \frac{T_c}{C_B} - \frac{C_A N_{AB}^2}{T_c} \dots \dots \dots \dots \dots \quad (2.42)$$

where, C_A and C_B are the Curie constants for each sublattice. Equations (2.36) and (2.42) constitute a set of equations with two unknown, N_{AB} and N_{BB} , provided that M_A and M_B are a known function of T .

2.3 Magnetic Structure of Substituted Ferrites

2.3.1 Néel's collinear model of ferrites

Soft ferrites belong to the cubic spinel structure. According to Néel's theory, the magnetic ions are assumed to be distributed among the tetrahedral A and octahedral B-sites of the spinel structure. The magnetic structure of such crystals essentially depends upon the type of magnetic ions residing on the A and B sites and the relative strengths of the inter- (J_{AB}) and intra-sublattice exchange interactions (J_{AA} , J_{BB}). Negative exchange interactions exist between A–A, A–B and B–B ions. When A–B antiferromagnetic interaction is the dominant one, A and B sublattices will be magnetized in opposite direction below a transition temperature. When the A–A (or B–B) interaction is dominant, Néel found that the above transition will not take place and he concluded that

the substance remains paramagnetic down to the lower temperature. But this conclusion was not correct, as in the presence of strong interactions, some kind of ordering may be expected to occur at low temperature as claimed by Yafet and Kittel [14].

2.3.2 Non-collinear model

In general, all the interactions are negative (antiferromagnetic) with $|J_{AB}| \gg |J_{BB}| \gg |J_{AA}|$. In such situation, collinear or Néel type of ordering is obtained. Yafet and Kittel theoretically considered the stability of the ground state of magnetic ordering, taking all the three exchange interactions into account and concluded that beyond a certain value of J_{BB}/J_{AB} , the stable structure was a non-collinear triangular configuration of moment wherein the B-site moments are oppositely canted relative to the A-site moments. Later on Leyons et. al. [15] extending these theoretical considerations showed that for normal spinel the lowest energy correspond to conical spinel structure for the value of $3J_{BB}S_B/2J_{AB}S_A$ greater than unity. Initially one can understand why the collinear Néel structure gets perturbed when J_{BB}/J_{AB} increases. Since all these three exchange interactions are negative (favoring anti ferromagnetic alignment of moments) the inter- and intra-sublattice exchange interaction compete with each other in aligning the moment direction in the sublattice. This is one of the origins of topological frustration in the spinel lattice. By selective magnetic directions of say A - sublattice one can effectively decrease the influence of J_{AB} vis-a-vis J_{BB} and thus perturb the Néel ordering. The first neutron diffraction study of such system i.e., $Zn_xNi_{1-x}Fe_2O_4$ was done at Trombay [16] and it was shown to have the Y-K type of magnetic ordering followed by Néel ordering before passing on to the paramagnetic phase [17].

It was found that ferrites which have been substituted sufficiently with non-magnetic atoms showed significant departure from Néel collinear model. These theoretical models have been used to explain these departures:

- A paramagnetic centre model in which a number of magnetic nearest neighbours determines whether a magnetic ion remains paramagnetic or contributes to the magnetization
- A uniform spin canting relative to the average magnetization and
- A localized canting where the canting angle of a magnetic ion spin depends on the local magnetic environment.

The discrepancy in the Néel's theory was resolved by Yafet and Kittel [14] and they formulated the non-collinear model of ferrimagnetism. They concluded that the ground state at 0K might have one of the following configurations:

- Have an antiparallel arrangement of the spins on two sites
- Consists of triangular arrangements of the spins on the sublattices
- An antiferromagnetic in each of the sites separately.

2.3.3 Re-entrant spin glass behaviour

When a piece of material is cooled down its constituent atoms or molecules become more and more ordered. Some systems, however, seem to become disordered again when the temperature continues to decrease. Such a behavior is commonly referred to as reentrant transition, because the system reenters a disordered phase when lowering the temperature. When such a system is cooled from a high temperature, it first exhibits a transition from paramagnetic (PM) to a ferromagnetic (FM) phase. Upon further lowering the temperature, the spins are progressively frozen below a freezing temperature T_f . The low temperature spin frozen state is called a reentrant spin glass (SG) or mixed state, in which ferromagnetic order is argued to coexist with spin-glass order [18,19]. If the cooling proceeds, a transition to a RSG phase occurs. For comparison, in a diluted spin glass, spins freeze directly from a paramagnetic state. This contradictory behavior was first seen in binary liquid mixtures [20]. After that it has been observed and investigated in a variety of different physical systems, e.g., magnets [21], superconductors [22], and liquid crystals [23]. When there is a majority of the ferromagnetic interactions and a minority of the anti ferromagnetic interactions to create substantial spin frustration effect, the situation may drastically change. Such random spin systems are called a reentrant ferronagnet. The system exhibits two phase transitions at T_{RSG} and T_c ($T_c > T_{RSG}$): the reentrant spin glass (RSG) phase below T_{RSG} and the ferromagnetic (FM) phase between T_{RSG} and T_c . In a reentrant spin glass, the fact that the FM state occurs at higher temperatures than the SG state suggests larger entropy for the FM state than for the SG state [24].

The usual mechanism for reentrance is the existence of interactions that are capable of lowering the entropy in some hudder way while at the same time reducing the energy of the system. Reentrant behaviour in random ferromagnets has been observed in

many systems. Neutron scattering on $Eu_xSr_{1-x}S$ [25] has indicated that the long range order disappears at temperatures below the reentrant irreversibilities. This suggests a transition to a low temperature reentrant phase. This phase should be characterized by lack of long range ferromagnetic order and a diverging spin glass correlation length.

2.3.4 Spin glass behaviour

The introduction of randomness and disorder may dramatically change the physical properties of a magnetic material. Spin glasses (SG's) are disordered magnetic systems with competing ferromagnetic and antiferromagnetic interactions. The combination of randomness with these competing interactions causes "spin frustration". Below a SG freezing temperature T_g , a highly irreversible metastable frozen state occurs without any usual long-range spatial spin order [24, 26, 27]. Spin glass was first observed by Canella and Mydosh [24] in 1972 by observing a peak in the ac susceptibility, and predicted the existence of a phase transition to a low temperature spin glass phase.

A spin glass is a magnetic material in which the exchange interaction, J_{ij} , between atomic Spins S_j , is a random variable. A positive sign favors an antiparallel alignment of a spin pair, while a negative sign favors an antiparallel alignment. A consequence of such random exchange Interactions between the moments is a frustrated system, i.e., for a representative spin there is no obvious direction relative to its neighbours to align

$$H = - \sum J_{ij} S_i S_j \dots \dots \dots \dots \dots \quad (2.43)$$

If $J_{ij} = J > 0$, parallel orientation of the spins is favoured and at low temperatures all spins will be aligned ferromagnetically. Such a system has two phases. At temperature high compared to J , the entropy dominates the energy and the spins fluctuate almost independently. In this paramagnetic phase, the expectation value of a spin is $\langle S_i \rangle$ ($\langle \rangle$ denotes the time average over long times). At temperature low compared to J , the energy dominates the entropy and the spins of the system are predominantly aligned in the same direction, i.e. $\langle S_i \rangle \neq 0$. This phase is called ferromagnetic. A transition between the two phases occurs at a finite critical temperature, T_c . An order parameter is associated to the transition, with the property that it is zero above and non-zero below the phase transition. For $J_{ij} = J < 0$, the low temperature phase is antiferromagnetic with the spins aligned anti-parallel. If $J_{ij} = 0$, the Hamiltonian describes a system being

paramagnetic at all temperatures.

If positive and negative interactions are mixed the situation becomes more complicated. Then there is a possibility that not all of the exchange interactions can be satisfied simultaneously. This property is called frustration [28]. An example of frustration is given in Fig. 2.15. Here the frustration arises due to bond disorder, but it may also arise from randomness in spin positions (site disorder). If only a small fraction of the interactions are of opposite sign the ground state will still be ferromagnetic or antiferromagnetic, with only a small fraction of the spins misaligned. If the density of positive and negative interactions is comparable, the system will be strongly frustrated. Such systems are called spin glasses (SG).

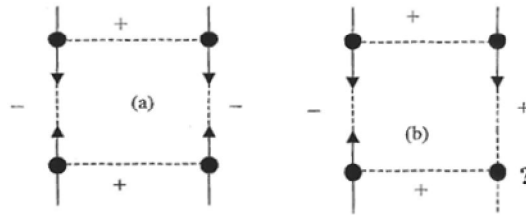


Figure 2.15. Examples of (a) an unfrustrated and (b) a frustrated spin configuration.

Edwards and Anderson [29] proposed the following Hamiltonian to describe a spin-glass

$$H = -\sum_{ij} J_{ij} S_i S_j + H \sum_i S_i \quad \dots \quad \dots \quad \dots \quad \dots \quad \dots \quad (2.44)$$

where, H is an applied magnetic field. The interactions are random and symmetrically disordered around zero, i.e. $[J_{ij}] = 0$ and $[J_{ij}^2] = j^2$. The order parameter is not the same as in the other models since the magnetization is zero without an external field. Edwards and Anderson [29] proposed the order parameter $q = [\langle S_i \rangle]$.

Ferrites represent the most important and interesting class of magnetic oxides where magnetic disorder and exchange frustration, introduced by size mismatch of cations and competition between superexchange interactions amongst A and B site moments, gives rise to various kind of magnetic order [30].

In recent years, aging dynamics, of SG systems has been extensively studied theoretically [31, 32] and experimentally [33-37] The low temperature SG phase below a SG freezing temperature T_g exhibits intriguing non-equilibrium dynamics which is characterized by the chaotic nature and ageing behavior. The zero-field SG never

reaches equilibrium. The non-equilibrium character can be experimentally observed from an age-dependence of the magnetic response. When the SG system is quenched from a high temperature above the SG transition temperature T_g to a low temperature T below T_g (this process is called the zero-field cooled (ZFC) aging protocol), the initial state is not thermodynamically stable and relaxes to more stable state. The aging behaviors depend strongly on their thermal history within the SG phase. The rejuvenation (chaos) and memory effects are also significant features of the aging dynamics. These effects are typically measured from the low frequency AC magnetic susceptibility. The SG phase is also susceptible to any perturbation in the form of temperature or field changes, which consequently, if large enough, effectively reinitializes the ageing process (temperature chaos). Both aging behavior and chaotic nature of the low temperature SG phase have been viewed first as additional difficulty in the understanding of SG's. However, it proved to be a key feature of the SG behavior, offering the unique opportunity to explore the nature of the SG phase.

2.4 Transport Properties

2.4.1 Conduction Mechanism in ferrites

Ferrites are ferromagnetic semiconductors that could be used in electronic devices. The increasing demand for low loss ferrites resulted in detailed investigations on conductivity and on the influence of various substitutions on the electrical conductivity, thermoelectric power, etc. The conduction mechanism in ferrites is quite different from that in semiconductors. In ferrites, the temperature dependence of mobility affects the conductivity and the carrier concentration is almost unaffected by temperature variation. In semiconductors, the band type conduction occurs, where in ferrites, the cations are surrounded by closed pack oxygen anions and as a first approximation can well be treated as isolated from each other. There will be a little direct overlap of the anion charge clouds or orbital. In other words, the electrons associated with particular ion will largely remain isolated and hence a localized electron model is more appropriate than a collective electron (band) model. This accounts for the insulating nature of ferrites. These factors led to the hopping electron model [38]. An appreciable conductivity in these ferrites is found to be due to the presence of iron ions with different valence states at crystallographically different equivalent lattice sites

[39]. Conduction is due to exchange of 3d electron, localized at the metal ions, from Fe^{3+} to Fe^{2+} . Various models have been suggested to account for the electrical properties. These are as follows

- Hopping model of electrons
- Small polaron model

2.4.2 Hopping model of electrons

In ferrites, there is a possibility in exchanging valency of a considerable fraction of metal ions and especially that of iron. The temperature dependence of conductivity arises only due to mobility and not due to the number of charge carriers in the sample. It is noted that for hopping conduction mechanism;

- The mobility has a minimum value much lower than the limiting value (0.1 cm/VS) taken as minimum for band conduction [40].
- The independence of Seebeck coefficient on temperature is due to the fact that in hopping model the number of charge carriers is fixed.
- Thermally activated process with activation energy E_a called hopping activation energy.
- Occurrence of $n-p$ transitions with charge carriers in the Fe^{2+} or oxygen concentration in the system.

2.4.3 Small polaron model

A small polaron is a defect occurred when an electronic carrier becomes trapped at a given site as a consequence of the displacement of adjacent atoms or ions. The entire defect then migrates by an activated hopping mechanism. Small polaron formation can take place in materials whose conduction electrons belong to incomplete inner (d or f) shells which due to small electron overlap, tend to form extremely narrow bands [41, 42]. The migration of small polaron requires the hopping of both the electron and the polarized atomic configuration from one site to an adjacent site. The small polaron model also explains the low mobility, temperature independence of the Seebeck coefficient and thermally activated hopping.

2.5 Literature Review

Double oxides of iron and other metals are important members of ferrimagnetic system commonly known as ferrites. The outstanding properties of ferrites are their complex magnetic structure, which can be varied to tailor their magnetic properties for various high frequency applications. In this chapter we describe a brief overview of the ferrites. The basic issue of ferrimagnetisms, crystal structure of the spinel ferrites and effect of non-magnetic Y substitution of Mn-Zn spinel ferrites are discussed.

Overview of the materials

Ferrites commonly expressed by the general chemical formula $MeO.Fe_2O_3$, where Me represents divalent metals, first commanded the public attention when Hilpert (1909) focused on the usefulness of ferrites at high frequency [3]. A systematic investigation was launched by Snoek (1936) at Philips Research Laboratory [2]. At the same time Takai (1937) in Japan was seriously engaged in the research work on the same materials [3]. Snoek's extensive works on ferrites unveiled many mysteries regarding magnetic properties of ferrites. He was particularly looking for high permeability materials of cubic structure. This particular structure for symmetry reasons supports low crystalline anisotropy. He found suitable materials in the form of mixed spinels of the type $MeZnFe_2O_4$, where Me stands for metals like Zn , Mg , Ni , Co or Mn , for which permeability were found to be up to 4000 [2-3]. Many Researchers studied Mn-Zn ferrites [43-44] and found the strong effect on their properties of composition, reactants, forming techniques and conditions of sintering for Mn-Zn ferrite. M.J. Tsay et.al. [43] studied of High Permeability of Mn-Zn. It is successful to manufacture homogeneous and high permeability of Mn-Zn ferrites both increasing the quality of products and decreasing the operating costs. Emad M. M. Ewais et. al.[44] observed Synthesis of Magnetic Mn-Zn Ferrite Ceramic. In this work, in-situ MnZn-ferrite ceramic ($Mn_{0.8}Zn_{0.2}Fe_2O_4$) was fabricated by the compaction of pure oxides of Mn, Zn and Fe. The properties in terms of densification pore size distribution, microstructure, cold crushing strength and magnetic measurements of Mn Zn-ferrite compact associated with

firing temperature were examined. On the other hand, the results of the formation and magnetic properties of the $\text{Mn}_{0.8}\text{Zn}_{0.2}\text{Fe}_2\text{O}_4$ prepared through compacts were compared with the powder prepared through conventional ceramic processes. The obtained results were rationalized based on the microstructure feature, porosity measurements and pore size analysis. Successful fabrication of dense MnZn ferrite which has high crushing strength and magnetic properties at 1150°C was processed. Syue et al. [45] studied on Magnetic and electrical properties of Mn–Zn ferrites. In this study, we have demonstrated a novel combustion route without subsequent heat treatment to synthesize nanocrystalline ferrite of $\text{Mn}_{1-x}\text{Zn}_x\text{Fe}_2\text{O}_4$. As-synthesized Mn–Zn ferrites have shown highly pure phase and superior electromagnetic properties compared to conventional combustion methods and solid-state reactions. The results imply that the relatively efficient and economical combustion route is a potential green process for industrial synthesis of Mn–Zn ferrites in electromagnetic devices applications. Amarendra K. Singh et.al. [46] studied on Ni-substituted Mn–Zn ferrites. Substitution of Mn by Ni in Mn–Ni–Zn ferrites increases the resistivity by two orders of magnitude. Space charge polarization is the primary contributing factor to the dielectric relaxation intensity. The values of relative loss factor are also significantly lower as compared to those reported for other ferrites. Spin canting effects are observed in samples with lower nickel content. The samples show almost rectangular B–H curves and reasonably low coercivity. Goran Stojanovic et.al. [47] studied Electrical properties of yttrium-doped Zn and Ni–Zn ferrites. This paper demonstrates that the lowtemperature chemical co-precipitation method can be applied for successful preparation of yttrium-doped Zn and Ni–Zn ferrites for high-frequency applications. The electrical parameters (real and imaginary part of permittivity, dielectric loss factor and resistivity) of uniaxially pressed samples were evaluated through impedance analyzer measurements and studied as a function of frequency. High electrical resistivity and low dielectric loss are a result of appropriate control of chemical composition and nanostructure of the ferrites. Nanostructured samples can be used as various technological applications in electronics and telecommunications fields. The presented results would be very useful for selection of an appropriate ferrite material for the desired operating frequency. M. Ishaque et.al. [48] reported Structural, electrical and dielectric properties of yttrium substituted nickel ferrites. The lattice constant slightly increases with increase in Y^{3+} content. The grain

size decreases with the increase of Y^{3+} contents due to hindrance of grain boundary mobility. FTIR spectra show that the substitution of Y^{3+} ions broadened the n^2 band and also shifts the band towards higher frequency side. The broadening of n^2 band suggested the occupation of Y^{3+} ions on octahedral B-site. The dielectric loss decreases and resistivity increases with the increase of yttrium concentration drastically from 106 to 1080 cm which make them suitable candidate for high frequency applications. This study shows that the substitution of yttrium in Ni ferrites improves the structural and transport properties. The complex permeability of the sintering ferrites is described as the summation of the spin rotational contribution and domain wall motion component. M.A. Ahmed et.al[49] studied on Influence of yttrium ions on the magnetic properties of Ni–Zn ferrites. It showed an increase in the Curie temperature with increasing Y^{3+} ions in the ferrite as a result of increasing the ferrimagnetic region on the expense of the paramagnetic region. In case of additive samples, the general trend is the decrease in the Curie temperature with increasing Yttrium content. The Curie temperature varies with the number of nonmagnetic trivalent ions per molecule in a manner that bears no simple relationship with the distance between magnetic ions. This result agrees well with our expectation about introducing of Y^{3+} in the spinel lattice at low concentration. Besides these many researchers substitute various material in Mn-Zn ferrites and Y is substituted in various ferrites in order to investigate various properties. But No work has been done on Y substitute Mn–Zn ferrite.

References:

- [1] Cullity, B. D., Introduction to Magnetic Materials, Addison-Wisley Publishing Company, Inc., California, 1972.
- [2] Valenzuela, R., Magnetic Ceramics, Cambridge University Press, Cambridge, 1994.
- [3] Goldman, A., Handbook of Modern Ferromagnetic Materials, Kulwer Acad. Pub, Boston, U.S.A 1999.
- [4] Callister, W., “Materials Science and Engineering an introduction”, Sixth ed. New York: JoHn Wiley & Sons, Inc, 2003.
- [5] Goldman, A., “Modern Ferrite Technology”, New York, 1990.
- [6] Spaldin, N., “Magnetic materials: Fundamentals and device applications”, Cambridge: Cambridge University press, 2003.
- [7] Bragg, W. H., “The structure of magnetite and the spinets”, Nature, Vol-95, pp 561, 1915.
- [8] Smit and Wijn, W. J. P., Ferrites, Philips Technical Library Wiley, New York, 1959.
- [9] Snoek, J. L., “Dispersion and absorptions in magnetic ferrites at frequencies above Mc/s”,

Physica, Vol- 14, pp 207, 1948

- [10] Viswanathan, B., Murthy, VRK, "Ferrite Materials Science and Technology", Springer Verlag, noarosa Publishing House, New Delhi, pp 143, 1990.
- [11] Krupicka, S., and Novak, P., "Oxide spinets. In E. P. Wohlfarth, editor", Ferromagnetic Materials, Vol- 3, chapter 4, pp 189-304, 1982.
- [12] Fuentes, V., Aburto, S., and Valenzuela, R., "Magnetic sublattices in nickel ferrite", J.Mag. Mag. Mater., Vol- 69, No. 3, pp 233-236, 1987.
- [13] P. W. Anderson, in Magnetism, Vol-1, Eds, G. T. Rado and H. Suhl, Academic Press, New York, 1963.
- [14] Yafet, Y., and Kittel, C., "Antiferromagnetic arrangements in ferrites", Phys. Rev., Vol- 87, pp 290, 1952.
- [15] Leyons, D. H., Keplan, T. A., Dwight, K. and Menyuk, N., "Classical theory of the ground spin-state in cubic spinets", Phys. Rev., Vol- 126, pp 540, 1962.
- [16] Murthy, N. S. S., Natera, M. G., Youstif, S. I., Begum, R. J. and Srivatava, C. M., "YafetKittel angles in Zinc-Nickel ferrites", Phys. Rev., Vol- 181, No. 2, pp 969, 1969.
- [17] Nogues, M., Dorman, J.L., Teillet, T. and Villers, G., "Randomly canted structures in the ferrite $Zn_xMg_{1-x}Fe_2O_4$ ", J. Mag.Mag. Mater., Vol-415, pp 104-107, 1992.
- [18] Gabay, M. and Toulouse, G., "Coexistence of spin-glass and ferromagnetic orderings", Phys.Rev. Lett., Vol- 47, pp 201, 1981.
- [19] Moore, M. A., and Brag, A. J., "Critical behaviour at the spin glass transition in a magnetic field", J.Phys. C, Vol- 15, No. 10, pp L301, 1982.
- [20] B. C. McEwan, "Studies in mutual solubility. Part 11. The mutual solubility of glycerol and alcohols, aldehydes, phenols, and their derivatives", J.Chem. Soc., Vol- 123, pp 2284, 1923.
- [21] K. Binder and A. P. Young, "Spin glasses: Experimental facts, theoretical concepts, and open questions", Rev.Mod. Phys., Vol- 58, pp 801, 1986.
- [22] Fischer, O., and Maple, M. B., "Superconductivity in Ternary Compounds I+H", (Springer-Verlag), 1982.
- [23] Cladis, P. E., "New liquid-crystal phase diagram", Phys. Rev. Lett., Vol- 35, pp 48, 1975.
- [24] Mydosh, J.A., "Spin Glasses-An Experimental Introduction", Taylor and Francis, London, 1993.
- [25] Shapiro, S. M., Aeppli, G., Maletta, H., Motoya, K., "Neutron scattering studies of magnetic correlations in reentrant spin glasses", Ph vsica B+C, Vol- 137, pp 96, 1986.
- [26] Mezard, M., Parisi, G., and Virasoro, M.A., Spin Glass Theory and Beyond World Scientific, Singapore, 1987
- [27] Fisher, K.H., and Hertz, J.A., Spin Glasses, Cambridge University Press, 1991
- [28] Mattsson, J., "Dynamics of random magnets", PhD thesis, Uppsala University, Sweden, 1994.
- [29] Edwards, S., and Anderson, P., "Theory of spin glasses", J.Phys. F., Vol- 5, pp 965, 1975.
- [30] Belayachi, A., Dormann, J.L., Nogues, M., "Critical analysis of magnetically semi-disordered systems: critical exponents at various transitions", J.Phys. Condens.Matt., Vol- 10, pp 1599,

- 1995.
- [31] Bernardi, L.W., Yoshino, H., Hukushima, K., Takayama, H., Tobo, A., and Ito, A., "Aging of the zero-field-cooled magnetization in Ising spin glasses: experiment and numerical simulation", *Phys. Rev. Lett.*, Vol- 86, pp 720, 2001.
- [32] Yoshino, H., Lemaitre, A., and Bouchaud, J.P., "Multiple domain growth and memory in the droplet model for spin-glasses.", *The European Physical Journal B (EPJ B)*, Vol- 20, pp 367, 2001
- [33] Djurberg, C., Jonason, K., and Nordblad, P., "Magnetic relaxation phenomena in a CuMn spin glass", *The European Physical Journal B (EPJ B)*, Vol-10, pp 15, 1999.
- [34] Jonsson, T., Jonason, K., Jonsson, P., and Nordblad, P., "Nonequilibrium dynamics in a three-dimensional spin glass", *Phys. Rev. B*, Vol- 59, pp 8770, 1999
- [35] Jonason, K., Nordblad, P., Vincent, E., Hanimann, J., and Bouchaud, J.P., "Memory interference effects in spin glasses", *The European Physical Journal B (EPJ B)*, Vol- 13, pp 99, 2000.
- [36] Dupuis, V., Vincent, E., Bouchaud, J.P., Hammann, J., Ito, A., and Katori, H. A., "Aging, rejuvenation, and memory effects in Ising and Heisenberg spin glasses", *Phys. Rev. B.*, Vol- 64, pp 174-204, 2001.
- [37] Nordblad, P., "Spin glasses: model systems for non-equilibrium dynamics", *J.Phys: Condens. Matt*, Vol- 16, pp 5715, 2004.
- [38] Samokhvalov, A. A. and Rustamov, A. G., *Soviet Physics - Solid State*, Vol- 6, pp 749, 1964.
- [39] Bossmann, A. J. and Crevecoeur, C., "Mechanism of the electrical conduction in Li-doped NiO", *Physics Review*, Vol- 144, pp 763, 1966.
- [40] Jonker, G.H., Santen, J.H.V., "Magnetic compounds with perovskite structure III. ferromagnetic compounds of cobalt", *Physica*, Vol- 19, pp 120, 1953.
- [41] Bhise, B. V., Ghatage, A. K., Kulkarni, B. M., Lotka, S. D., and Patil, S. A., "Conduction in Mn substituted Ni-Zn ferrites", *Bulletin of Material Science*, Vol- 19, No. 3, pp 527, 1996.
- [42] Patil, M. G., Mahajan, V. C., Bhise, B. V., Chendke, S. M., and Patil, S. A., "Conduction phenomenon in Mn-substituted NiCd ferrites", *Physica Status Solidi (b)*, Vol-144, pp 415, 1994.
- [43] Tsay, M.J., Tung, M.J., Chen, C.J. and Liu, T.Y. "The Manufacture of High Permeability Mn-Zn Ferrites by Atmospherical Protect" *J; PHYS. IVFRANCE 7 (1997)*
- [44] Ewais, E. M. M., Hessien, M. M., and El-Geassy, A.H. A. "In-Situ Synthesis of Magnetic Mn-Zn Ferrite Ceramic Object by Solid State Reaction" *J. Aust. Ceram. Soc.* 44 [1] 57-62 (2008)
- [45] Syue, M.R., Wei, F.J., Chou, C.S., and Chao-Ming Fu, "Magnetic and electrical properties of Mn-Zn ferrites synthesized by combustion method without subsequent heat treatments" , *J. Appl. Phys.* 109, 07A324 (2011)
- [46] Amarendra K. S., Abhishek K. S., Goelb,T.C., Mendiratta , R.G. "High performance Ni-substituted Mn-Zn ferrites processed by soft chemical technique" *J. Magn.Magn.Mater.*281, 276-280(2004)

Chapter II: Theoretical Background

- [47] Stojanovic,G., Srdic,V. and Maletin,M. “Electrical properties of yttrium-doped Zn and Ni–Zn ferrites” p hys. stat. sol. (a) 205, No. 10, 2464–2468 (2008);
- [48] Ishaque , M. , Islam , M.U., AzharKhan , M., Rahman , I.Z., Genson , A., Hampshire, S. “Structural, electrical and dielectric properties of yttrium substituted nickel ferrites” Physica B 405, 1532–1540(2010)
- [49] Ahmeda, M.A., Okashab, N., Salah, L. “Influence of yttrium ions on the magnetic properties of Ni–Zn ferrites”, J. Magn. Magn. Mater. 264 241–250(2003)

CHAPTER 3

SAMPLE PREPARATION

3.1 Composition of the studied ferrite system

In the present research *Y* substituted Mn-Zn ferrites are synthesized and thoroughly investigated. The ferrites under investigation are:

$Mn_{0.5}Zn_{0.5}Fe_{2-x}Y_xO_4$ (with $x=0.00, 0.05, 0.10, 0.15, 0.20, 0.25$ and 0.30)

3.2 Sample preparation

A common goal to all the ferrites is the formation of the spinel structure. Nowadays, the large majority of ferrite powders are made by the conventional ceramic process or solid state reaction method. Most non-conventional process involves producing the powder by a wet method. Among these methods, some are [1]:

- 1) Co-precipitation
- 2) Organic precursors
- 3) Sol-gel synthesis
- 4) Spray-drying
- 5) Freeze-drying
- 6) Combustion synthesis
- 7) Glass crystallization

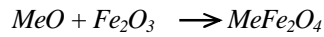
In this chapter, we describe the standard solid state reaction method that is used in this research work.

3.3 Conventional solid state reaction method

In the solid state reaction method, the required composition is usually prepared from the appropriate amount of raw mineral oxides or carbonates by crushing, grinding and milling. The most common type of mill is the ball mill, which consists of a lined pot with hard spheres or rod inside. Milling can be carried out in a wet medium to increase the degree of mixing. This method depends on the solid state inter-diffusion between the raw materials. Solids do not usually react at room temperature over normal time scales. Thus it is necessary to heat them at higher temperatures for the diffusion length $(2Dt)^{1/2}$ to exceed the particle size, where D is the diffusion constant for the fast-diffusing species, and t is the firing time [2]. The ground powders are then

calcined in air or oxygen at a temperature above 850 °C. For some time, this process is continued until the mixture is converted into the correct crystalline phase. The calcined powders are again crushed into fine powders. The pellets or toroid shaped samples are prepared from these calcined powders using die-punch assembly or hydrostatic or isostatic pressure. Sintering is carried out in the solid state, at temperature ranging 1100-1400 °C, for times of typically 1-40 h and in various atmospheres (e.g. Air, O_2 and N_2) [3-6]. Fig. 3.1 shows, diagrammatically, the stages followed in ferrite preparation.

The general solid state reaction leading to a ferrite $MeFe_2O_4$ may be represented as

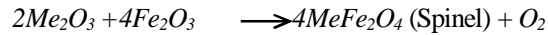
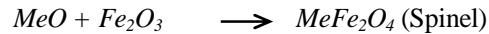


where Me is the divalent ions. There are basically four steps in the preparation of ferrite:

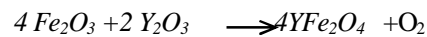
- 1) Preparation of materials to form an intimate mixture with the metal ions in the ratio which they will have in the final product,
- 2) Heating of this mixture to form the ferrite (often called calcining),
- 3) Grinding the calcined powders and pressing the fine powders into the required shape, and
- 4) Sintering to produce a highly densified product.

3.4 Details of calcining, pressing and sintering

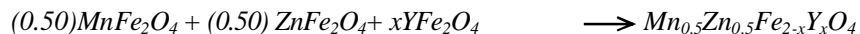
Calcining is defined as the process of obtaining a homogeneous and phase pure composition of mixed powders by heating them for a certain time at a high temperature and then allowing it to cool slowly. During the calcining stage, the reaction of Fe_2O_3 with metal oxide (say, MeO or Me_2O_3) takes place in the solid state to form spinel according to the reactions [7]:



The ZnO , Y_2O_3 and $MnCO_3$ creeps into Fe_2O_3 as below, to form an intermediate phase



And lastly



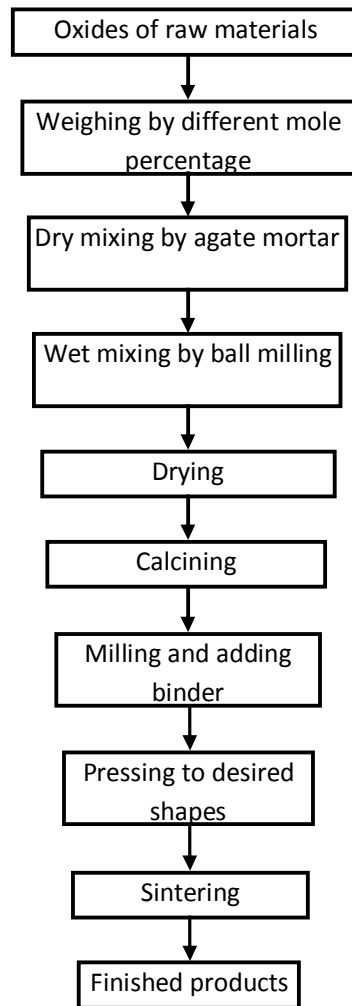


Figure 3.1. Flow chart of the stages in preparation of spinel

The calcining process can be repeated several times to obtain a high degree of homogeneity. The calcined powders are crushed into fine powders. The ideal characteristics of fine powders are [8]:

- 1) Small particle size (sub micron)
- 2) Narrow distribution in particle size
- 3) Dispersed particles
- 4) Equiaxed shape of particles
- 5) High purity
- 6) Homogeneous composition.

A small particle size of the reactant powders provides a high contact surface area for initiation of the solid state reaction; diffusion paths are shortened, leading to more efficient completion of the reaction. Porosity is easily eliminated if the initial pores are very small. A narrow size distribution of spherical particles as well as a dispersed state is important for compaction of the powder during green-body formation. Grain growth during sintering can be better controlled if the initial size is small and uniform.

A binder is usually added prior to compaction, at a concentration lower than 5wt % [8]. Binders are polymers or waxes; the most commonly used binder in ferrite is polyvinyl alcohol. The binder facilitates the particles flow during compacting and increases the bonding between the particles, presumably by forming bonds of the type *particle-binder-particle*. During sintering, binders decompose and are eliminated from the ferrite. Pressures are used for compacting very widely but are commonly several tons per square inch (i. e., up to 10^8 Nm^{-2}).

Sintering is defined as the process of obtaining a dense, tough body by heating a compacted powder for a certain time at a temperature high enough to significantly promote diffusion, but clearly lower than the melting point of the main component. The driving force for sintering is the reduction in surface free energy of the powder. Part of this energy is transferred into interfacial energy (grain boundaries) in the resulting polycrystalline body [8, 9]. The sintering time, temperature and the furnace atmosphere play very important role on the magnetic property of ferrite materials. The purposes of sintering process are:

- 1) To bind the particles together so as to impart sufficient strength to the product,
- 2) To densify the material by eliminating the pores and
- 3) To homogenize the materials by completing the reactions left unfinished in the calcining step.

Sintering of crystalline solids is dealt by Coble and Burke [10] who found the following empirical relationship regarding rate of grain growth:

$$\bar{d} = kt^n$$

where \bar{d} is the mean grain diameter, n is about 1/3, t is sintering time and k is a temperature dependent parameter. Sintering is divided into three stages, Fig. 3.2 [8, 11].

Stage 1. Contact area between particles increases,

Stage 2. Porosity changes from open to closed porosity,

Stage 3. Pore volume decreases; grains grow.

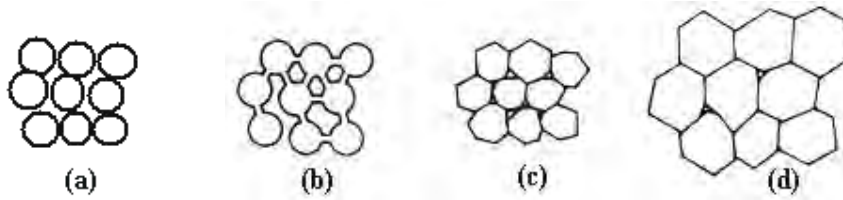


Figure 3.2. Schematic representation of sintering stages: (a) greenbody, (b) initial stage, (c) intermediate stage, and (d) final stage.

In the initial stage, neighbouring particles form a neck by surface diffusion and presumably also at high temperatures by an evaporation-condensation mechanism. Grain growth begins during the intermediate stage of sintering. Since grain boundaries are the sinks for vacancies, grain growth tends to decrease the pore elimination rate due to the increase in distance between pores and grain boundaries, and by decreasing the total grain boundary surface area. In the final stage, the grain growth is considerably enhanced and the remaining pores may become isolated.

3.5 Preparation of the present samples

The $Mn_{0.5}Zn_{0.5}Fe_{2-x}Y_xO_4$ (for $x = 0.00, 0.05, 0.10, 0.15, 0.20, 0.25$ and 0.30) samples were synthesized using the standard solid state reaction technique which is discussed in section 3.3. Powder of $MnCO_3$ (99.9%), ZnO (99.99%), Y_2O_3 (99.99%), Fe_2O_3 (99.5%) were used as raw materials. Stoichiometric amounts of required powders were mixed thoroughly and then calcined at $850\text{ }^\circ\text{C}$ for 5 hours. The calcined powders were again crushed into fine powders by handmilling. Then the fine powder are granulated using Poly Vinyl Alcohol (PVA) [12-15] as a binder and pressed (7000 P.S.I.) into disk and toroid shaped samples shown in Fig. 3.3. The samples were sintered at various temperatures (1100, 1150, 1200, 1250, 1275, 1288, 1300, 1350 and $1400\text{ }^\circ\text{C}$) for 5 hours in air. The temperature ramp was $10\text{ }^\circ\text{C/minute}$ for heating and $5\text{ }^\circ\text{C/minute}$ for cooling.



Figure 3.3. Sample (a) disk shaped, (b) Toroid shaped.

References:

- [1] Goldman, A., "Handbook of Modern Ferromagnetic Materials", Kulwer Acad. Pub, Boston, U.S.A, 1999.
- [2] Janney, M. A., Kimrey, H. D., Allen, W. R. and Kiggans, J. O., "Enhanced diffusion in sapphire during microwave heating", Journal of Materials Science, Vol – 32, No. 5, pp 1347-1355, 1997
- [3] Hossain, A. K. M. Akther, "Investigation of colossal magnetoresistance in bulk and thick film magnetites", Ph. D. Thesis, Imperial College, London, 1998.
- [4] Cullity, B. D., "Introduction to Magnetic Materials", Addison-Wisley Publishing Company, Inc., California, 1972.
- [5] Brook, R. J., "Sintering: An Overview, Concise Encyclopedia of Advanced Ceramic Materials", Pergamon Press, Oxford, pp 438, 1991.
- [6] Reijnen, P., "Science of Ceramics", Academic Press, London, 1967.
- [7] Slick, P. I., "Ferrites for Non-microwave Applications", Vol - 2, North Holland Pub. Co., 1980.
- [8] Valenzuela, R., "Magnetic Ceramics", Cambridge University Press, Cambridge, 1994.
- [9] Kingery, W. D., Bowen, H. K. and Uhlman, D. R., "Introduction to Ceramics", 2nd edition, Wiley Interscience, Newyork, pp 476, 1976.
- [10] Coble, R. L., and Burke, J. E., "4th Int. Symp. On the Reactivity of Solids", Amsterdam, pp 38-51, 1960.
- [11] McColm, I. J., and Clark, N. J., "Forming, Shaping and Working of high Performance Ceramics", Blackie, Glasgow, pp 1-338, 1988.
- [12] Eliassaf, J., "Detection of small quantity of Poly (vinyl alcohol) in poly(vinyl chloride) resins", Polymer Letters, Vol - 16, pp 225-235, 1972.
- [13] El-Kodsi, G. & Schurz, J. "Chemical characterization of high polymers. I. Nitration and Subsequent reactions", Papier (Darmstadt), Vol - 27, pp 253-255, 1973.
- [14] Maslov, V.I., & Kolerko, F.M., "Methods for determination the component of iodopoly(vinylalcohol) in biological media", Lab. Delo, Vol- 5, pp 295-297, 1972.
- [15] Taniguchi, J., & Ohkita, K., "Testing paper for measuring poly (vinyl alcohol) concentration", Japanese Patent, pp 7765, 1977.

CHAPTER 4

EXPERIMENTAL TECHNIQUES

In this chapter we describe basic experimental techniques to measure the lattice parameters, density, surface morphology and frequency dependent AC permeability of ferrite samples.

4.1 X-ray Diffraction

Bragg reflection is a coherent elastic scattering in which the energy of the x-ray is not changed on reflection. If a beam of monochromatic radiation of wavelength λ is incident on a periodic crystal plane at an angle θ and is diffracted at the same angle as shown in Fig. 4.1, the Bragg diffraction condition for x-rays is given by

$$2d \sin\theta = n\lambda \quad (4.1)$$

where d is the distance between crystal planes and n is the positive integer which represents the order of reflection. Equation (4.1) is known as Bragg law. This Bragg law suggests that the diffraction is only possible when $\lambda \leq 2d$ [1]. For this reason we cannot use the visible light to determine the crystal structure of a material. The X-ray diffraction (XRD) provides substantial information on the crystal structure.

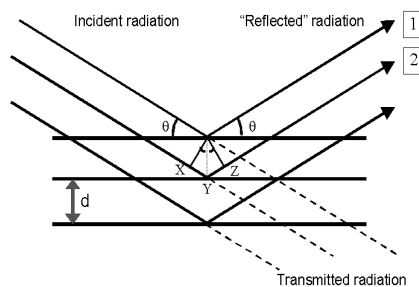


Figure 4.1. Bragg law of diffraction.

X-ray diffraction was carried out with an X-ray diffractometer for the samples $Mn_{0.5}Zn_{0.5}Fe_{2-x}Y_xO_4$ (with $x = 0.00, 0.10, 0.15, 0.20, 0.25,$ and 0.30). The XRD measurements were carried out using D8-Advance Bruker with a Cu-K α X-ray diffractometer ($\lambda = 1.540593 \text{ \AA}$). The lattice parameter for each peak of each sample was calculated by using the formula:

$$a = d\sqrt{h^2 + k^2 + l^2} \quad (4.2)$$

where h , k and l are the indices of the crystal planes. To determine the exact lattice parameter for each sample, Nelson-Riley method was used. The Nelson-Riley function $F(\theta)$ is given as [2]:

$$F(\theta) = \frac{1}{2} \left[\left(\frac{\cos^2 \theta}{\sin \theta} \right) + \left(\frac{\cos^2 \theta}{\theta} \right) \right] \quad (4.3)$$

The values of lattice parameter 'a' of all the peaks for a sample are plotted against $F(\theta)$. Then using a least square fit method exact lattice constant ' a_o ' is determined. The point where the least square fit straight line cut the y-axis (i.e. at $F(\theta) = 0$) is the actual lattice parameter of the sample.

The physical or bulk densities ρ_{exp} of the samples were determined by Archimedes principle with water medium using the following expression [2]:

$$\rho_{exp} = \frac{W}{W - W'} \rho \quad g/cm^3 \quad (4.4)$$

Where W is the weight of the sample in air, W' is the weight of the sample in the water and ρ is the density of water in room temperature.

The theoretical density ρ_{th} was calculated using following expression [3]:

$$\rho_{th} = \frac{8M}{N_A a_o^3} g/cm^3 \quad (4.5)$$

where N_A is Avogadro's number ($6.02 \times 10^{23} \text{ mol}^{-1}$), M is the molecular weight. The porosity was calculated from the relation $P = \{100(\rho_{th} - \rho_B) / \rho_{th}\} \%$, where ρ_B is the bulk density measured by the formula $\rho_{exp} = M/V$ [3].

4.2 Study of Microstructure

The microstructural study was performed in order to have an insight of the grain structures. The samples of different compositions and sintered at different temperatures were chosen for this purpose. The samples were visualized under Scanning Electron Microscope (SEM) and a high-resolution optical microscope (Koehler Illuminator MA 1109,

Swift Instruments, Inc) and then photographed. Average grain sizes (grain diameter) of the samples were determined from optical micrographs by linear intercept technique [4]. To do this, several random horizontal and vertical lines were drawn on the micrographs. Therefore, we counted the number of grains intersected and measured the length of the grains along the line traversed. Finally the average grain size was calculated.

4.3 Complex Permeability Measurement

For high frequency application, the desirable property of a ferrite is high permeability with low loss. One of the most important goals of ferrite research is to fulfill this requirement. The techniques of permeability measurement and frequency characteristics of the present samples are described in sections 4.3.1 and 4.3.2.

4.3.1 Techniques for the Permeability Measurement

Measurements of permeability normally involve the measurements of the change in self-inductance of a coil in presence of the magnetic core. The behaviour of a self-inductance can now be described as follows. We assume an ideal loss less air coil of inductance L_0 . On insertion of a magnetic core with permeability μ , the inductance will be μL_0 . The complex impedance Z of this coil [5] can be expressed as follows:

$$Z = R + jX = j\omega L_0 \mu = j\omega L_0 (\mu' - j\mu'') \quad (4.6)$$

where the resistive part is $R = \omega L_0 \mu''$ (4.7)

and the reactive part is $X = \omega L_0 \mu'$ (4.8)

The RF permeability can be derived from the complex impedance of a coil, Z , given by equation (4.6). The core is taken as toroidal to avoid demagnetizing effects. The quantity L_0 is derived geometrically.

4.3.2 Frequency Characteristics of the present samples

The frequency characteristics of the ferrite samples i.e. the initial permeability spectra were investigated using a Wayne kerr Impedance Analyzer (Model No. 6500B). The complex permeability measurements on toroid shaped specimens were carried out at room temperature on all the samples in the frequency range 100 Hz - 120 MHz. The real part (μ_i') and imaginary part (μ_i'') of the complex permeability were calculated using the following relations [4-5]: $\mu_i' = L_s/L_0$ and $\mu_i'' = \mu_i' \tan \delta$, where L_s is the self-inductance of the sample core and $L_0 = \mu_o N^2 S / \pi \bar{d}$ is derived geometrically. Here L_0 is the inductance of the winding coil without the sample core, N is the number of turns of the coil ($N = 4$), S is the area of cross section of the toroidal sample as given below:

$$S = d \times h,$$

where
$$d = \frac{d_o - d_i}{2},$$

$$d_i = \text{Inner diameter,}$$

$$d_o = \text{Outer diameter,}$$

$$h = \text{Height}$$

and \bar{d} is the mean diameter of the toroidal sample as given below:

$$\bar{d} = \frac{d_i + d_o}{2}$$

The relative quality factor is determined from the ratio $\frac{\mu_i'}{\tan \delta}$.



Photograph: Experimental set up using an Wayne Kerr Impedance Analyzer

(Model No: 6500 B)

References:

- [1] Kittel, C., "Introduction to Solid State Physics", 7th edition, Jhon Wiley & Sons, Inc., Singapore, 1996.
- [2] Rusu, G.I., Prepelita, P., Rusu, R.S., Apetroaie, N., Oniciuc, G. and Amariei, A., "On the structural and optical characteristics of zinc telluride thin films", Journal of Optoelectronics and Advanced Materials, Vol - 8, No. 2, pp 922-926 2006.
- [3] Cullity, B. D., "Introduction to Magnetic Materials", Addison-Wisley Publishing Company, Inc., California, 1972.
- [4] Hossain, A. K. M. Akther, "Investigation of colossal magnetoresistance in bulk and thick film magnetites", Ph. D. Thesis, Imperial College, London, 1998.
- [5] Goldman, A., "Handbook of Modern Ferromagnetic Materials", Kulwer Acad. Pub, Boston, U.S.A, 1999.

CHAPTER 5

RESULTS AND DISCUSSION

The polycrystalline $Mn_{0.5}Zn_{0.5}Fe_{2-x}Y_xO_4$ ($x = 0.00, 0.05, 0.10, 0.15, 0.20, 0.25$ and 0.30), are studied. All ferrite samples are sintered at various temperatures (1100, 1150, 1200, 1250, 1275, 1288, 1300, 1350 and 1400 °C) for five hours in air. Structural and surface morphology are studied by X-ray diffraction and Scanning Electron Microscope (SEM). The magnetic properties of the ferrites are characterized with high frequency (100 Hz-120 MHz) complex initial permeability measurements. The effects of varying Y substitution and sintering temperature on the complex initial permeability of these ferrites are discussed.

5 Investigation of polycrystalline $Mn_{0.5}Zn_{0.5}Fe_{2-x}Y_xO_4$

5.1 X-ray Diffraction analysis

The X-ray diffraction (XRD) patterns for the polycrystalline $Mn_{0.5}Zn_{0.5}Fe_{2-x}Y_xO_4$ compositions are presented in Fig. 5.1. X-ray diffraction patterns were carried out using D8 Advance Bruker gobe mirror with Cu-K α radiation ($\lambda=1.540593\text{\AA}$). The XRD patterns for these compositions confirm the formation of spinel ferrite [1]. All peaks observed in the XRD patterns are identified with their Miller indices.

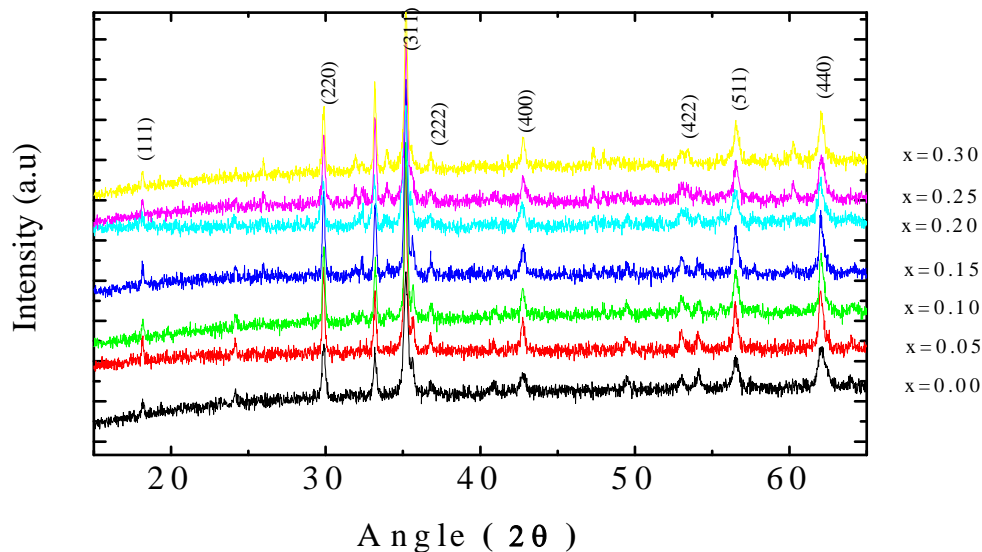


Figure 5.1. The X-ray diffraction pattern of polycrystalline $Mn_{0.5}Zn_{0.5}Fe_{2-x}Y_xO_4$

5.2 Lattice parameters

The values of lattice parameters have been calculated with the help of the Nelson-Riley function [eqⁿ (4.3)]. The value of lattice parameters were estimated from the extrapolation of the line at $F(\theta) = 0$ or $\theta=90^\circ$. The lattice parameter 'a' of $Mn_{0.5}Zn_{0.5}Fe_{2-x}Y_xO_4$ compositions are plotted as a function of $F(\theta)$, as shown in Fig. 5.2(a).

The samples under investigation have the chemical composition $Mn_{0.5}Zn_{0.5}Fe_{2-x}Y_xO_4$. Therefore, the ionic radius of the variant ions for composition can be written as $r_{(\text{variant})} = xr_Y + (2-x)r_{Fe}$ [2], where r_Y is the ionic radius of Y^{3+} ion ($=0.98\text{\AA}$), and r_{Fe} is the ionic radius of Fe^{3+} ion ($=0.73\text{\AA}$). These data are taken from Whittaker and Muntus (1970) [3]. The variation of $r_{(\text{variant})}$ with Y content is shown in Fig 5.2(b), where it increases with the increase of Y ion content.

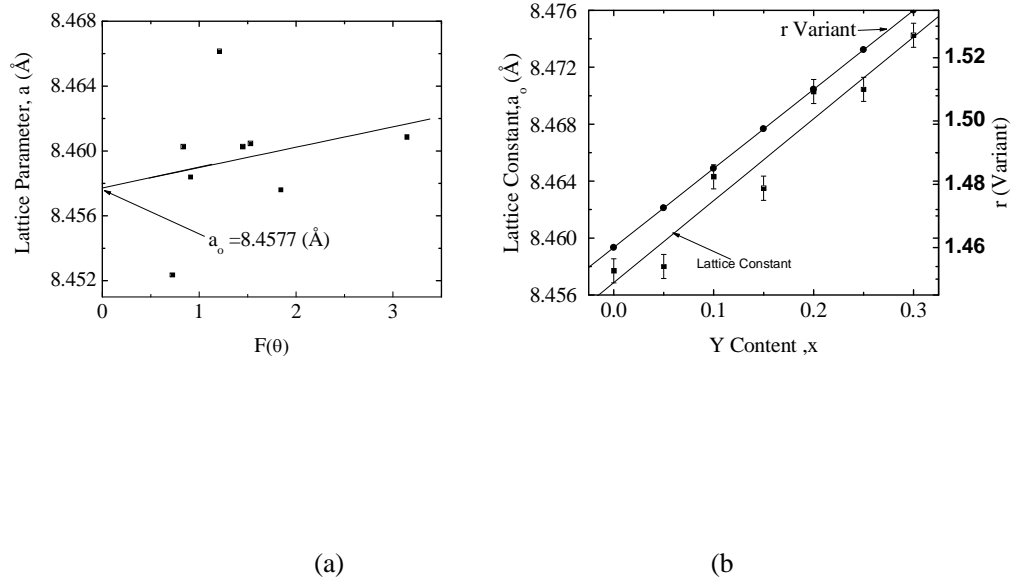


Figure 5.2. (a) Variation of lattice parameter 'a' with $F(\theta)$ and (b) variation of lattice constant with Y content for polycrystalline $Mn_{0.5}Zn_{0.5}Fe_{2-x}Y_xO_4$ sintered 1200°C .

The measured lattice constant, density and porosity for different samples sintered at different temperatures are given in Table 5.1. It is observed that the variation of lattice parameters with Y contents in the $Mn_{0.5}Zn_{0.5}Fe_{2-x}Y_xO_4$ obey Vegard's law in the whole composition range under present investigation. Similar behavior was observed by Bhowmik, *et al* in barium ferrites [4]. Lattice constant increases with increasing of Y content for all compositions. The increase in lattice constant with decreasing Fe content can be explained on the basis of the ionic radii. Since the ionic radius of Y is greater than that of the Fe, increase in lattice constant with the increase in Y substitution is expected.

Table 5.1. The lattice constant, sintering temperature, T_s , density, porosity, average grain size and natural resonance frequency of the $Mn_{0.5}Zn_{0.5}Fe_{2-x}Y_xO_4$ samples sintered at various temperatures with fixed dwell time 5 h.

x	a_o (Å)	T_s (°C)	ρ_{th} (g/cm ³)	ρ_{exp} (g/cm ³)	P (%)	f_r (kHz)	Grain size (μm)	Q_{max}	μ'_i (at 10 kHz)	
0.00	8.4577	1100	5.17802	4.494	13.21	433	4.6	878.11	15.09	
		1150		4.914	5.09			991	15.56	
		1200		4.715	8.94			842	16.72	
		1250		4.637	10.44			1003.05	17.08	
		1300		4.542	12.28			1916.19	207.04	
		1350		4.087	21.07			456	1810.25	211.35
		1400		4.4236	14.56			648	1513.08	184.26
0.05	8.458	1100	5.21373	4.531	13.09	953(1288°C)	3.57	661.12	15.09	
		1150		4.648	10.85			840.89	15.93	
		1200		4.69	10.04			370.181	12.22	
		1250		4.463	14.39			731.34	18.97	
		1300		4.533	13.05			1244.61	124.61	
		1350		4.088	21.59			2048	226.51	
		1400		4.6858	10.12			456	3477.55	347.17
0.10	8.4643	1100	5.23833	4.494	14.20	2820(1288°)	3.81	1600.44	24.34	
		1150		4.627	11.67			549.28	13.30	
		1200		4.686	10.54			606.46	16.91	
		1250		4.633	11.55			463.77	17.1	
		1300		4.435	15.33			752.07	95.44	
		1350		4.089	21.94			648	2106.85	224.84
		1400		4.5288	13.54			920	2011.96	221.06
0.15	8.4635	1100	5.27601	4.547	13.81	3670 2730	4.14	534.59	16.08	
		1150		4.563	13.51			876.87	16.49	
		1200		4.776	9.47			471.56	15.80	
		1250		4.75	9.96			676.79	15.27	
		1300		4.368	17.21			313.81	23.23	
		1350		4.114	22.02			403.79	45.39	
		1400		4.7589	9.80			608.38	98.18	
0.20	8.4703	1100	5.29946	4.625	12.72	637 1860	3.618	1175.12	22.40	
		1150		4.628	12.67			696.71	16.63	
		1200		4.906	7.42			467.18	15.21	
		1250		4.744	10.48			1080.42	20.47	
		1300		4.541	14.31			449.63	16.60	
		1350		4.6189	19.02			520.11	106.25	
		1400		4.6189	12.84			706.03	113.25	
0.25	8.4704	1100	5.33528	4.726	11.41		3.965	610.40	15.90	
		1150		4.803	9.97			840.89	14.72	
		1200		4.894	8.27			495.44	15.24	
		1250		4.815	9.75			717.05	17.21	
		1300		4.499	15.67			503.64	19.63	
		1350		4.253	20.28			538.47	24.69	
		1400		4.732	11.30			308.81	25.75	
0.30	8.4742	1100	5.36419	4.574	14.73		3.51	1693.46	21.84	
		1150		4.901	8.63			696.5	13.31	
		1200		4.895	8.74			560	15.21	
		1250		4.706	12.27			466.63	24.09	
		1300		4.593	14.37			623.36	18.98	
		1350		4.467	16.72			541.17	22.68	
		1400		4.6401	13.49			531.13	27.57	

5.3 Density and Porosity

Density plays a key role in controlling the properties of polycrystalline ferrites. A significant increase in the bulk density is observed with the Y content. A possible explanation may be the formation of solid solution. It is supposed that all Y ions enter into the spinel lattice during sintering and activate the lattice diffusion. This assumption of the formation of solid solution is confirmed by the lattice parameter measurement in which the lattice constant increases with Y content. The increase of the lattice diffusion usually increases the diffusion path, leading to an increase of the rate of cation interdiffusion in the solid solution which is in agreement with the lattice diffusion mechanism proposed by Gupta and Coble [6].

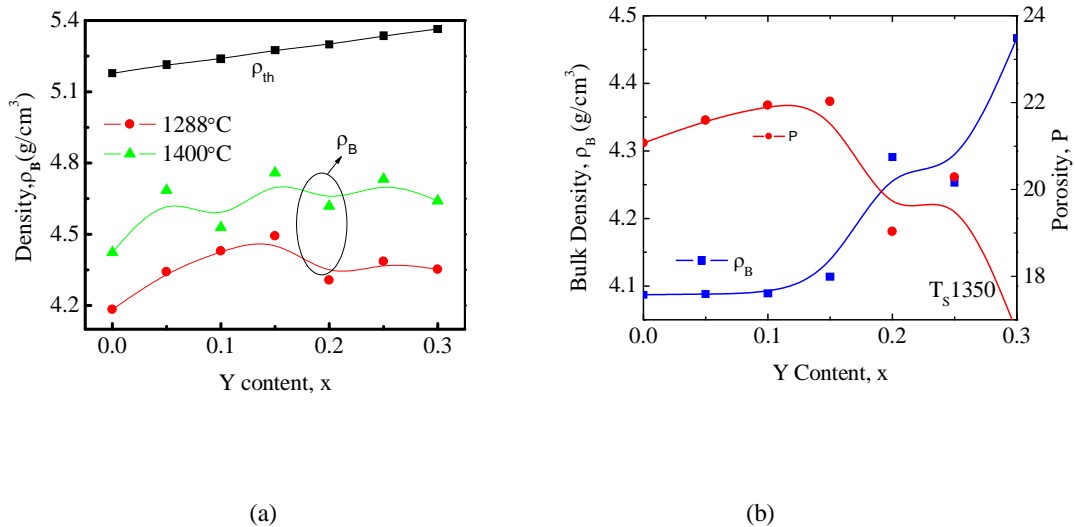
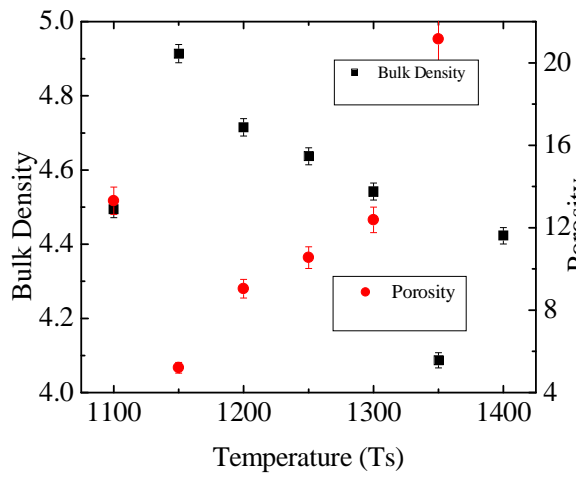
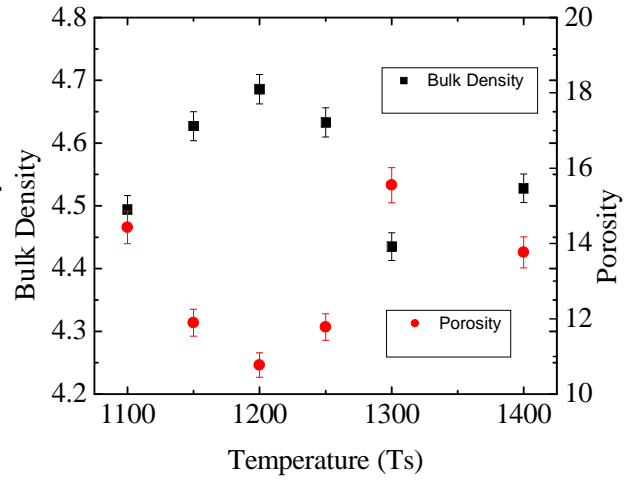


Figure 5.3. (a) Experimental (ρ_B) and theoretical (ρ_{th}) density (b) Density and porosity of the samples of $Mn_{0.5}Zn_{0.5}Fe_{2-x}Y_xO_4$, sintered at 1350 °C

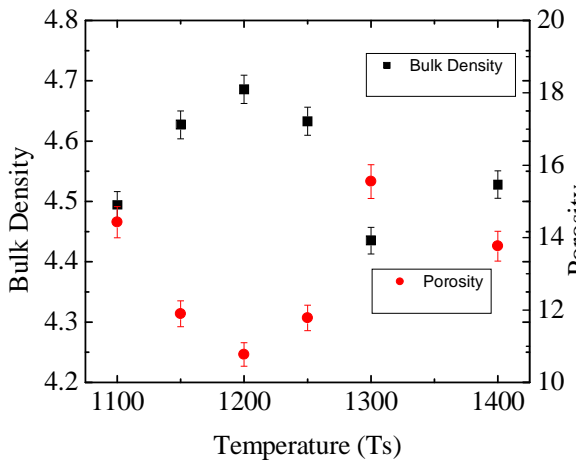
Fig.5.3 (a) shows the experimental and theoretical density (ρ_{exp} and ρ_{th}) of the samples and is observed to be increasing with increasing of Y content. It is observed that the experimental density of the samples increase and the corresponding porosity of the samples decrease with increasing of Y content. This increase in density with increasing Y content can be explained on the basis of the atomic weight. The atomic weight of Y (88.90585amu), and Fe (55.845 amu) [7]. Therefore the density increase in a value is expected.



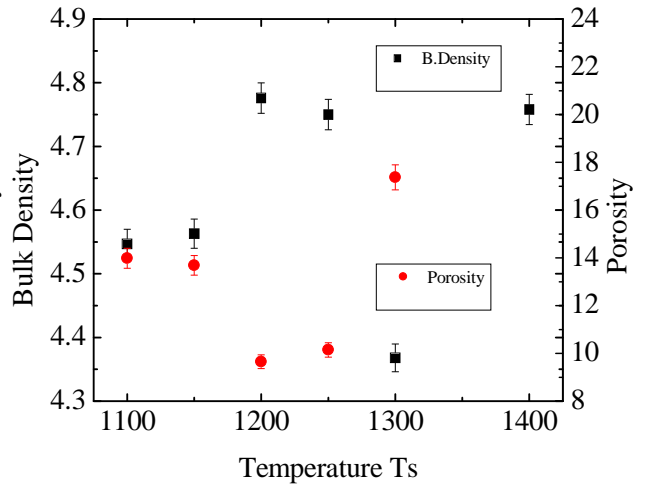
(a)



(b)



(c)



(d)

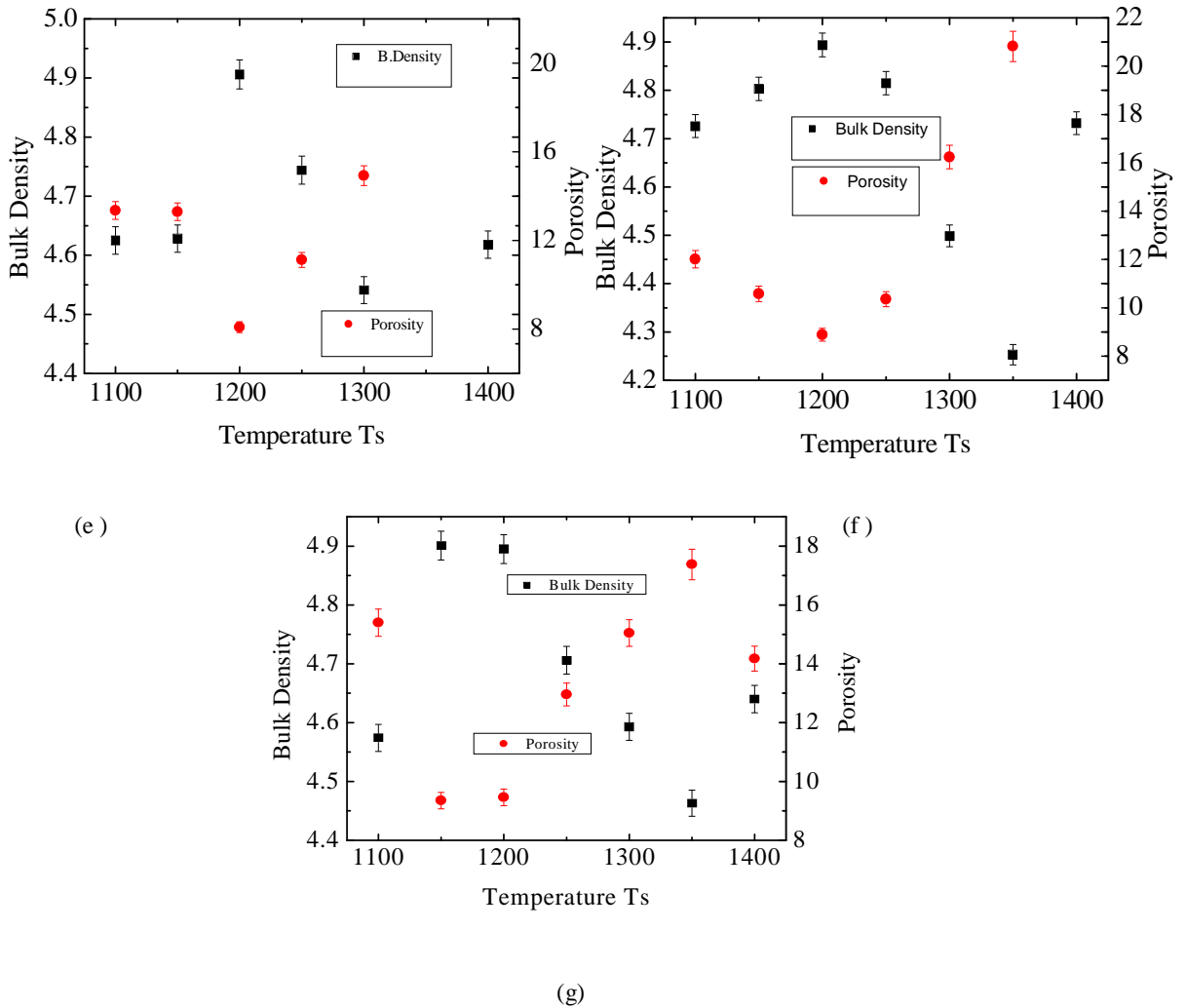
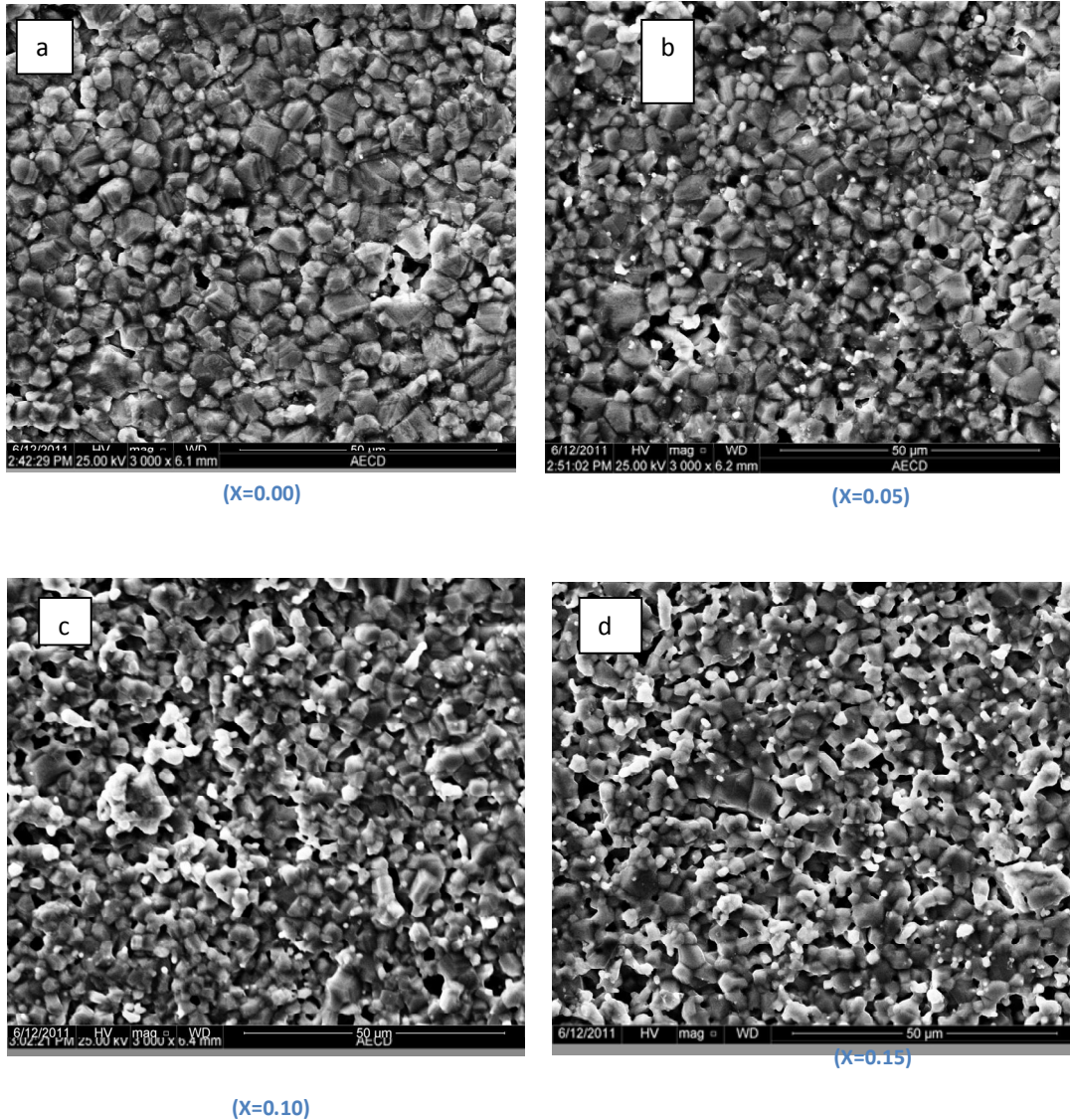


Figure 5.4. The variation of density and porosity for $Mn_{0.5}Zn_{0.5}Fe_{2-x}Y_xO_4$ (a) $x=0.00$, (b) $x=0.05$, (c) $x=0.10$, (d) $x=0.15$, (e) $x=0.20$, (f) $x=0.25$ and (g) $x=0.30$

The density of the $Mn_{0.5}Zn_{0.5}Fe_{2-x}Y_xO_4$ samples increases as the sintering temperature increases from 1050 to 1200 °C. On the other hand, porosity of the sample decreases with increasing sintering temperature up to 1200 °C. The value of density increases and the porosity decreases with increasing sintering temperature T_s , as shown in Table 5.1. During the sintering process, the thermal energy generates a force that drives the grain boundaries to grow over pores, thereby decreasing the pore volume and increasing the density of the material [8]. It is known that the porosity of ceramic samples results from two sources, intragranular porosity and intergranular porosity [8]. Thus the total porosity could be written as $P=P_{intra}+P_{inter}$. The intergranular porosity mainly depends on the grain size [9]. At higher sintering temperatures grain formed uniformly and void reduce as a result density increases.

5.4 Microstructures

The SEM micrographs of various $Mn_{0.5}Zn_{0.5}Fe_{2-x}Y_xO_4$ sintered at 1200 °C are shown in Fig. 5.5. The grain size is significantly dependent on Y substitution. The average grain size decreases with increasing Y substitution. Calculated average grain size of all samples is listed in Table-5.1. It was not possible to find out the average grain size for the samples sintered at 1200 °C because of their lack of clarity. It is found that the average grain size of all samples increases with increasing sintering temperature. $Mn_{0.5}Zn_{0.5}Fe_{2-x}Y_xO_4$ shows the largest grain size among the studied samples sintered at 1200 °C. The SEM micrograph of $Mn_{0.5}Zn_{0.5}Fe_{2-x}Y_xO_4$ samples sintered at 1200, 1250, and 1300 °C are shown in Fig 5.6



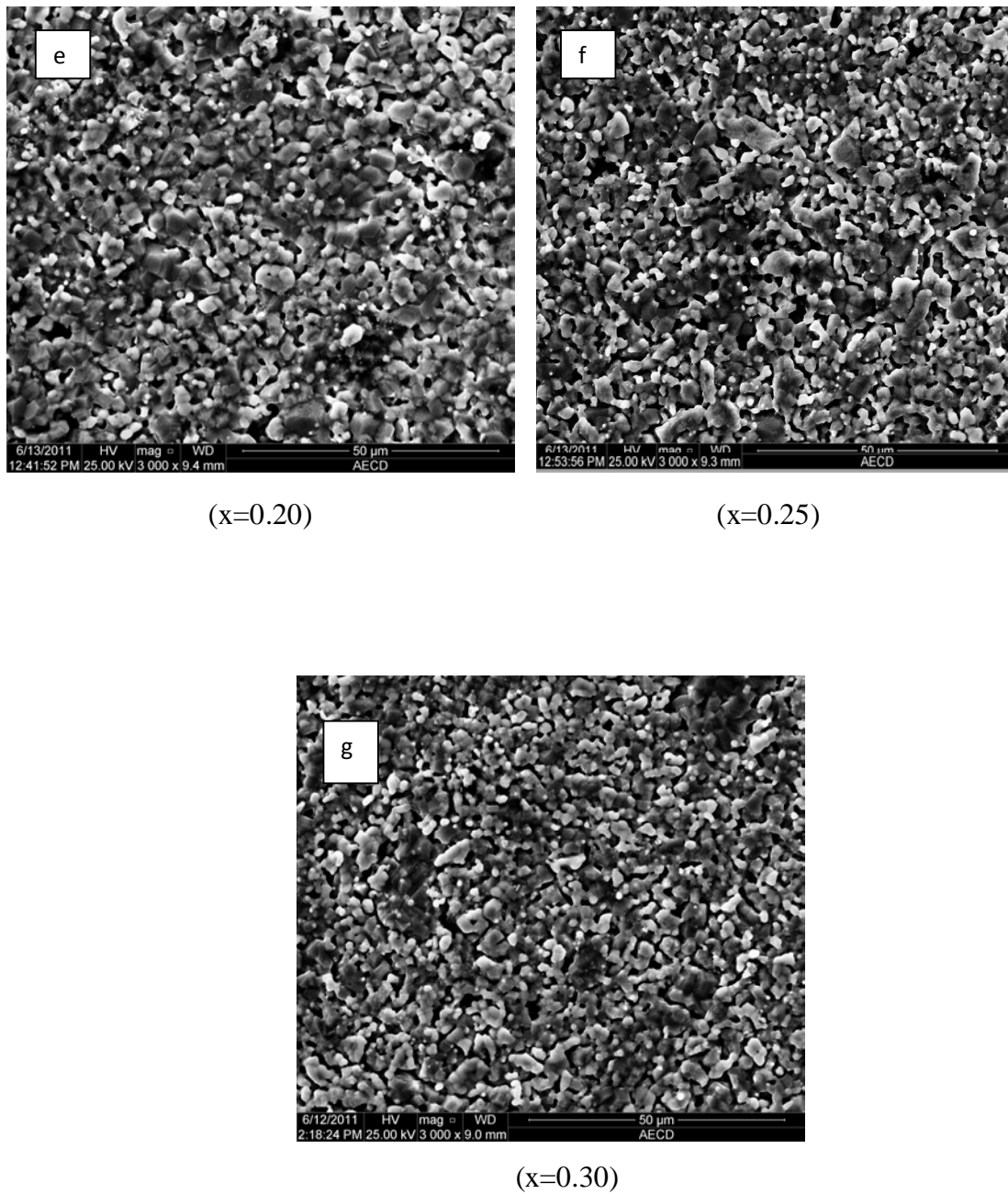


Figure: 5.5 SEM of various compositions of $Mn_{0.5}Zn_{0.5}Fe_{2-x}Y_xO_4$ where, (a) $x=0.00$, (b) $x=0.05$, (c) $x=0.01$, (d) $x=0.15$, (e) $x=0.20$, (f) $x=0.25$, (g) $x=0.30$ at $T_s = 1200^\circ\text{C}$ (magnified 3000 \times).

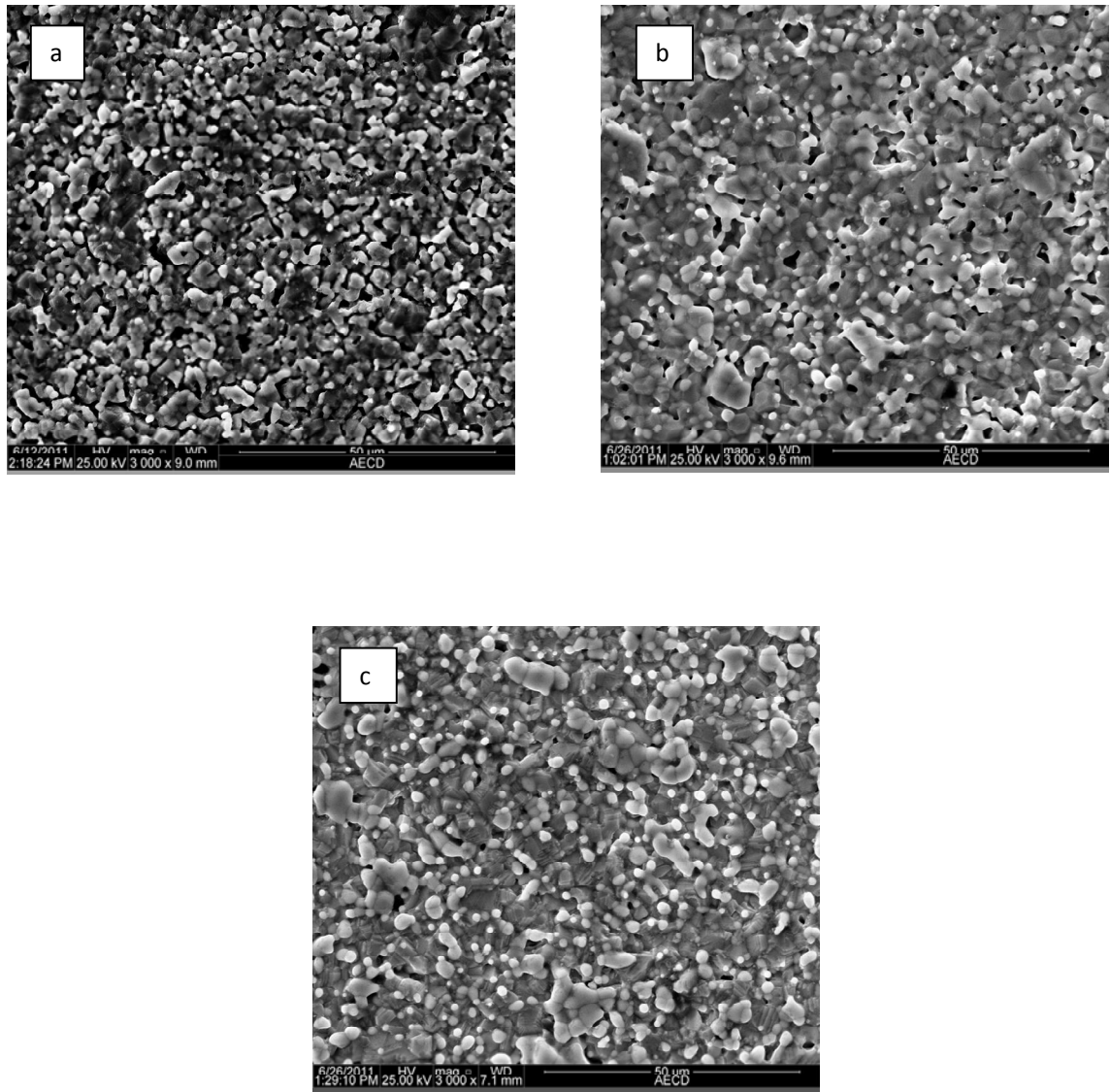


Figure: 5.6 : SEM of $Mn_{0.5}Zn_{0.5}Fe_{1.7}Y_{0.3}O_4$ at various sintering temperatures, where (a) $T_s=1200^\circ\text{C}$, (b) $T_s = 1250^\circ\text{C}$ and (c) $T_s=1300^\circ\text{C}$ (magnified 3000 \times).

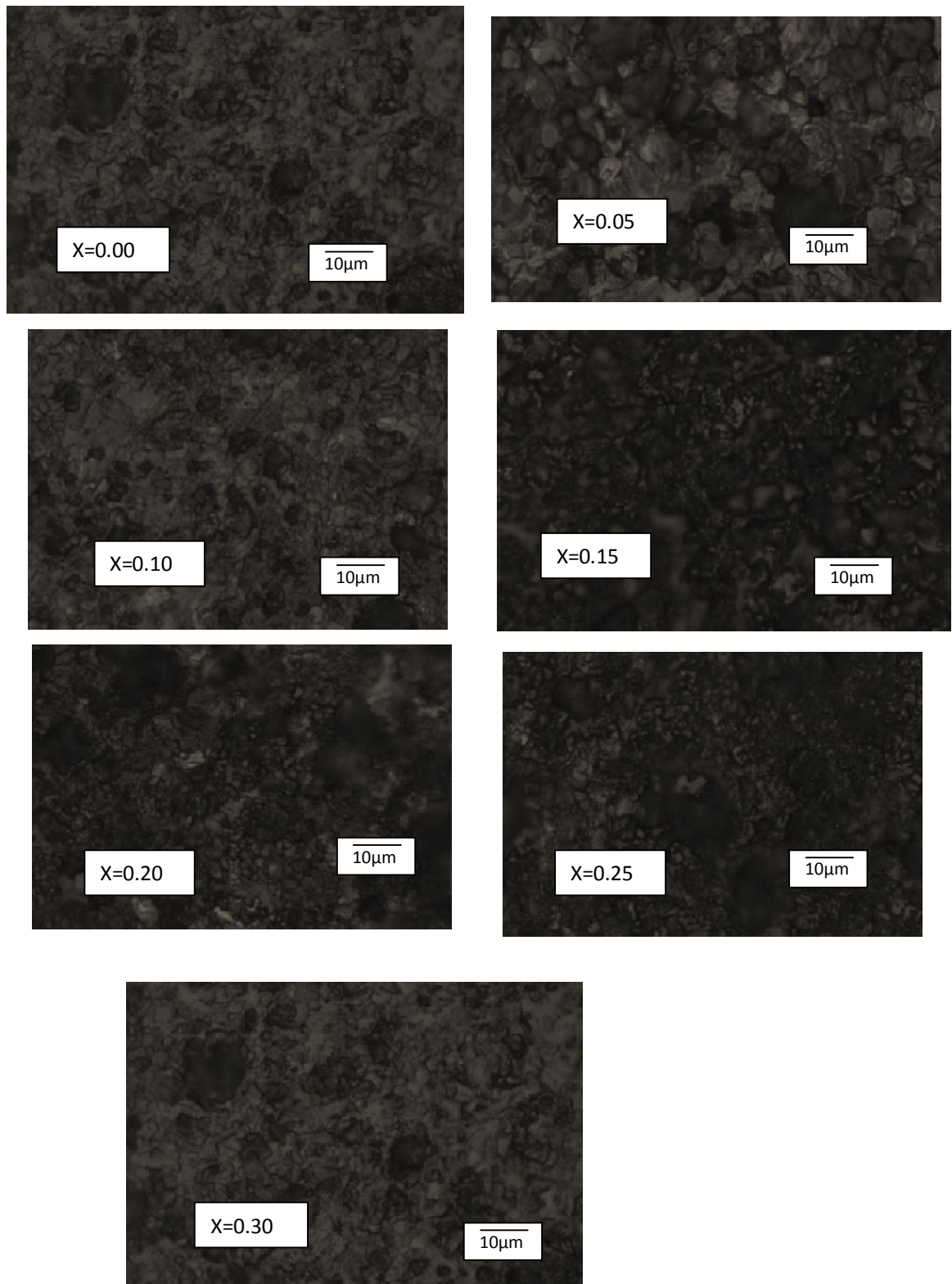


Figure: 5.7: Optical Micrograph of various samples of $Mn_{0.5}Zn_{0.5}Fe_{2-x}Y_xO_4$ sintered at 1288°C

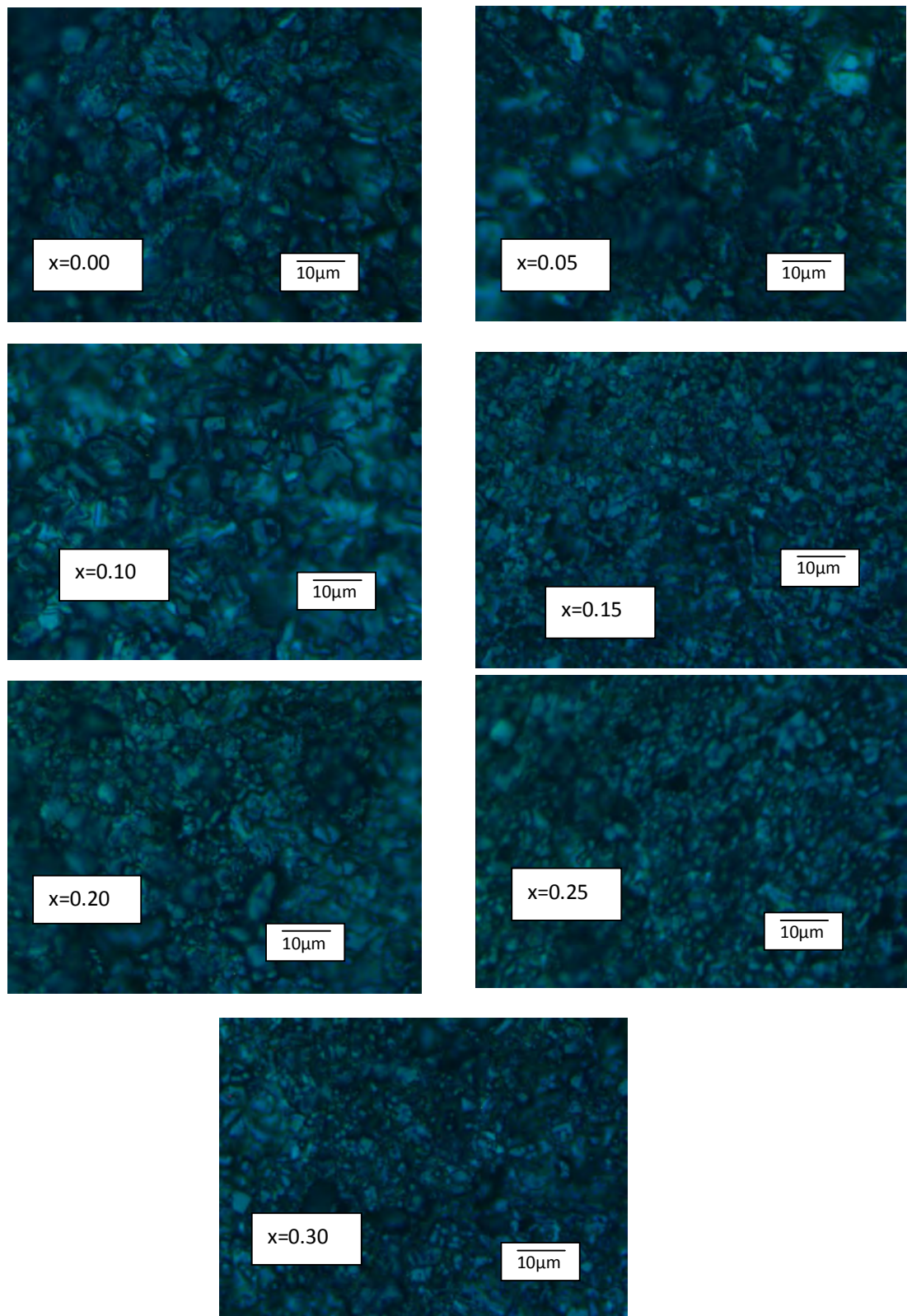


Figure: 5.8: Optical Micrograph of various samples of $Mn_{0.5}Zn_{0.5}Fe_{2-x}Y_xO_4$ sintered at $1300^{\circ}C$

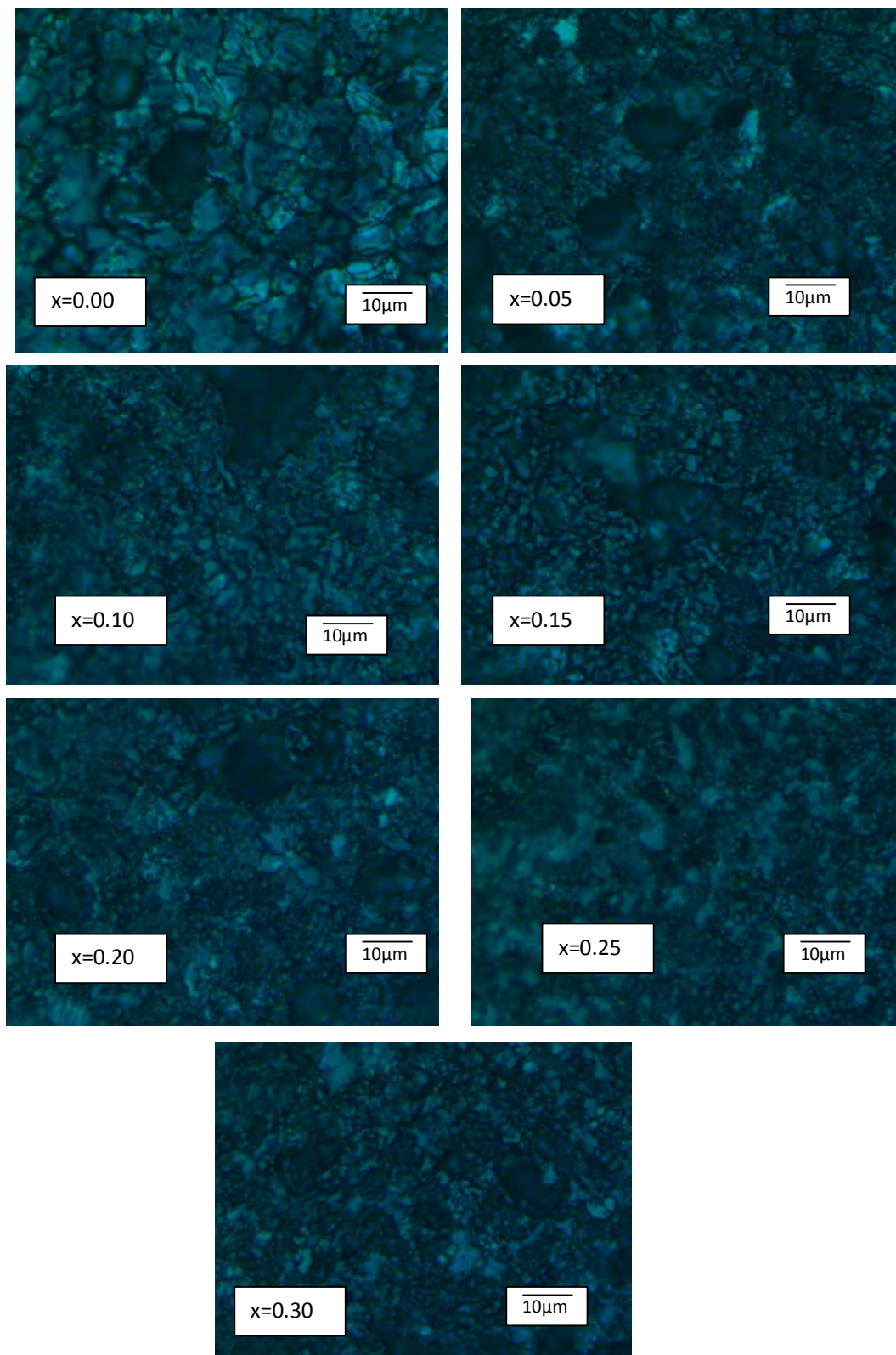


Figure: 5.9: Optical Micrograph of various samples of $Mn_{0.5}Zn_{0.5}Fe_{2-x}Y_xO_4$ sintered at $1350^{\circ}C$

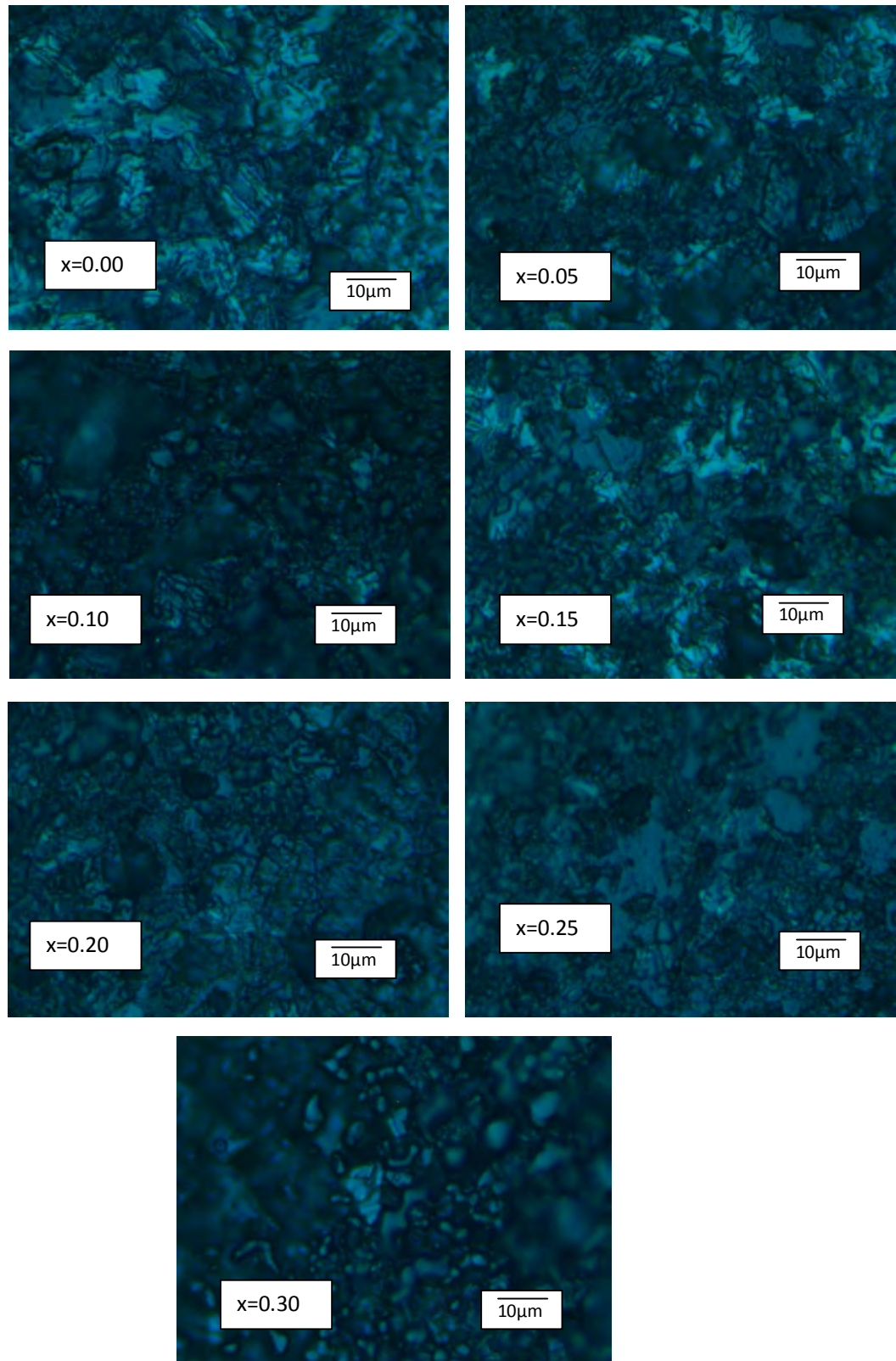


Figure :5.10: Optical Micrograph of various samples of $Mn_{0.5}Zn_{0.5}Fe_{2-x}Y_xO_4$ sintered at $1400^{\circ}C$

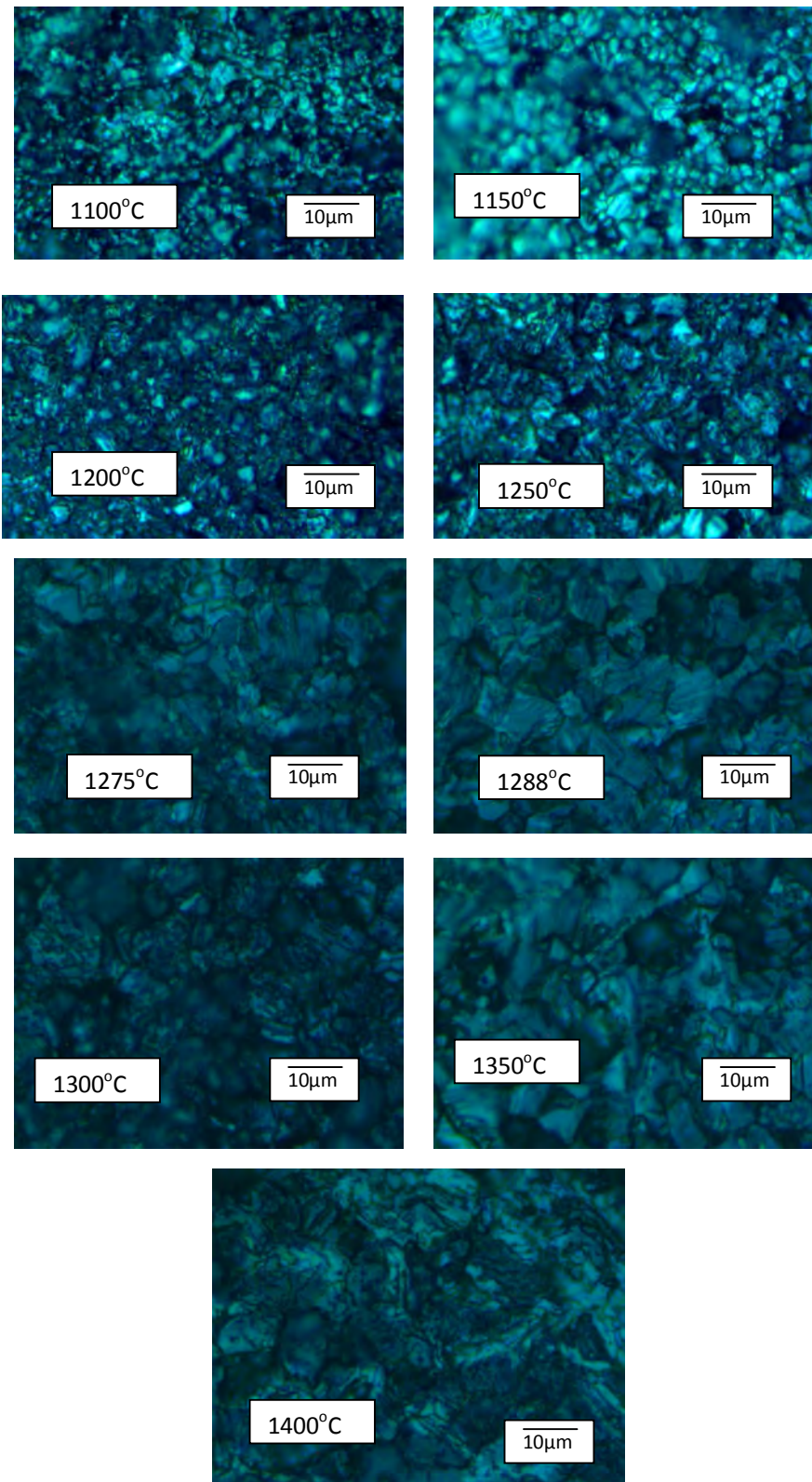


Figure :5.11: Optical Micrograph of $Mn_{0.5}Zn_{0.5}Fe_2O_4$ at various sintering Temperature

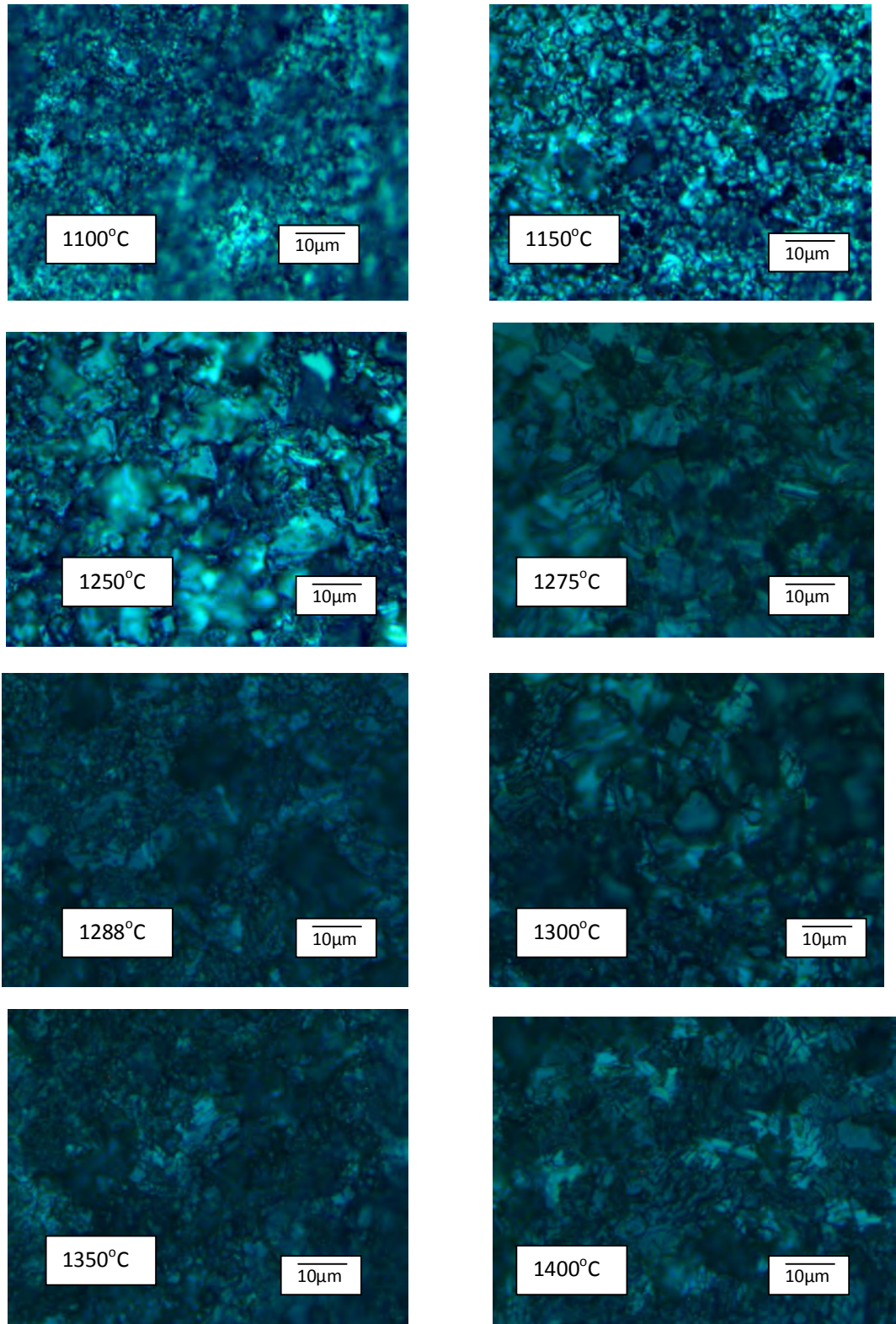


Figure :5.12: Optical Micrograph of $Mn_{0.5}Zn_{0.5}Fe_{1.95}Y_{0.05}O_4$ at various sintering Temperature

5.5 Complex initial Permeability

Figs. 5.13, 5.14, 5.15 and 5.16 show the complex initial permeability spectra for $Mn_{0.5}Zn_{0.5}Fe_{2-x}Y_xO_4$ sintered at 1150, 1200, 1250 and 1300°C respectively. The real (μ'_i) and imaginary (μ''_i) permeability increase with Y substitution from $x=0$ to $x=0.1$ in $Mn_{0.5}Zn_{0.5}Fe_{2-x}Y_xO_4$. The μ'_i increases with the increasing sintering temperatures. This result can be explained with the help of cation redistribution as a result of Y^{3+} substitution. It is known that Y^{3+} , Fe^{3+} and Mn^{2+} ions occupy B sites, although Fe^{3+} and Mn^{2+} ions exist at both A and B sites [10]. The cation distribution of various $Mn_{0.5}Zn_{0.5}Fe_{2-x}Y_xO_4$ ferrite assumed as,

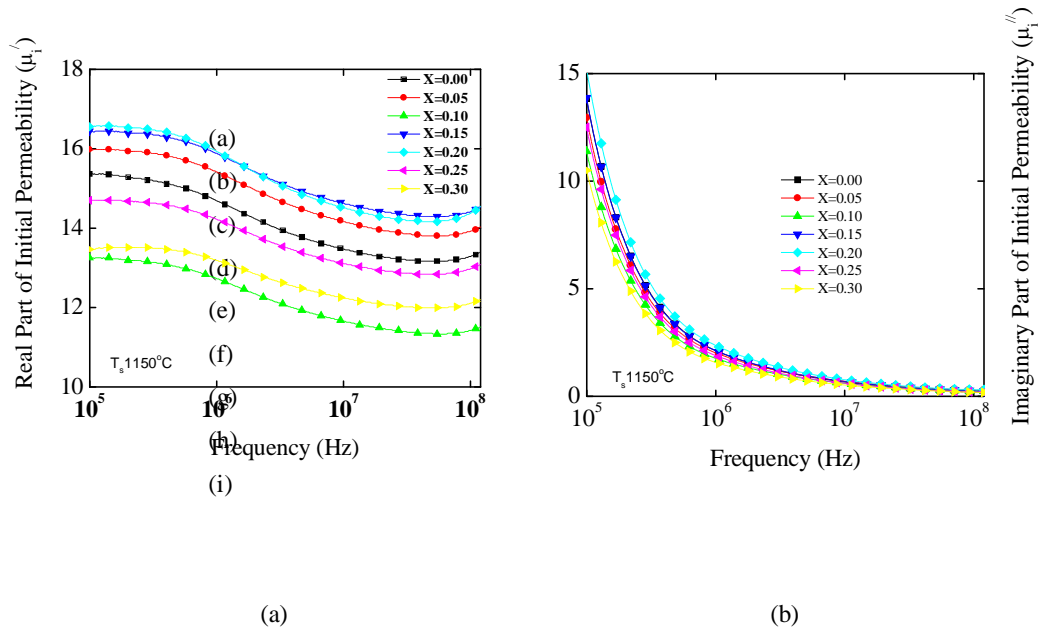
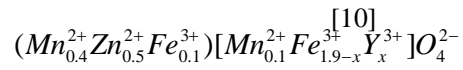


Figure 5.13. (a) The real and (b) imaginary permeability spectra for polycrystalline $Mn_{0.5}Zn_{0.5}Fe_{2-x}Y_xO_4$ samples sintered at 1150 °C for 5 hours.

Where the term within the square bracket indicates the octahedral (B) sites and the first term is tetrahedral (A) sites. When Y^{3+} is introduced at the cost of Mn^{2+} , Fe^{3+} ion concentration at B sites increases. As Y^{3+} and Mn^{2+} are non-magnetic, the magnetic moment of B site will depend on the Fe^{3+} ion. As Y^{3+} content increases in the present ferrites, Fe^{3+} content decreases. As a result, the magnetic moments of B sub-lattice decreases. However, as Y content increases, the magnetic moment of A sub-lattice remains constant. As the net magnetization equals M_B minus M_A , it decreases with increasing Y and Fe concentration. The μ'_i value increases with the

increase of sintering temperature. This is due to the lower porosity for samples sintered at higher sintering temperature. The porosity causes hindrance to the domain wall motion.

As sintering temperature increases, the natural resonance frequency shifted for the $Mn_{0.5}Zn_{0.5}Fe_{2-x}Y_xO_4$ samples. The μ_i' of all samples are found independent of frequency below the resonance frequency. It is also noticed that there are sharp decrease in real part and increase in imaginary part above the resonance frequency (f_r). The initial permeability of polycrystalline ferrite is related to two different magnetizing factors: spin rotation and domain wall motion [11, 12], which can be described as, $\mu_i = 1 + \chi_w + \chi_{spin}$ where χ_w is the domain wall susceptibility, χ_{spin} is intrinsic rotational susceptibility. χ_w and χ_{spin} may be written as: $\chi_w = 3\pi M_s^2 D / 4\gamma$ and $\chi_{spin} = 2\pi M_s^2 / K_u$ with M_s saturation magnetization, K_u the total anisotropy, D the grain diameter, and γ the domain wall energy [13]. Thus, the domain wall motion is affected by the grain size and enhances with the increase of grain size. The initial permeability is therefore a function of grain size. Larger grains tend to consist of a greater number of domain walls. The magnetization caused by domain wall movement requires less energy than that required by domain rotation. As the number of walls increases with the grain sizes, the contribution of wall movement to magnetization is increased.

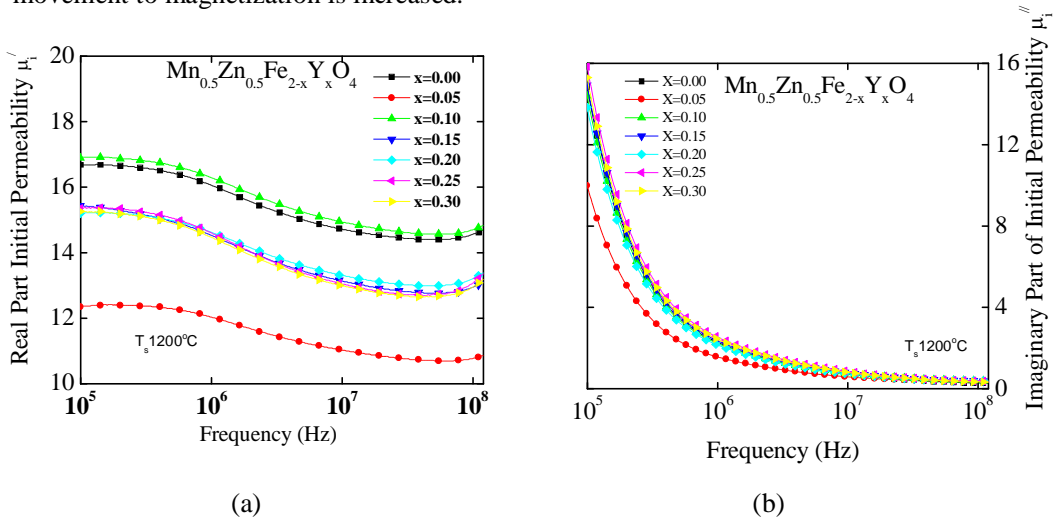


Figure 5.14. (a) The real and (b) imaginary permeability spectra for polycrystalline $Mn_{0.5}Zn_{0.5}Fe_{2-x}Y_xO_4$ samples sintered at $1200^\circ C$ for 5 hours.

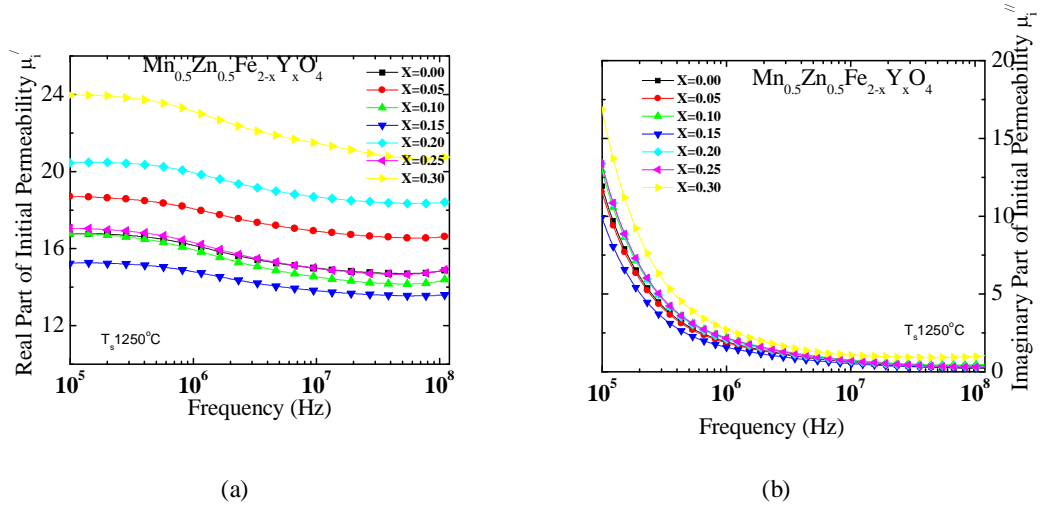
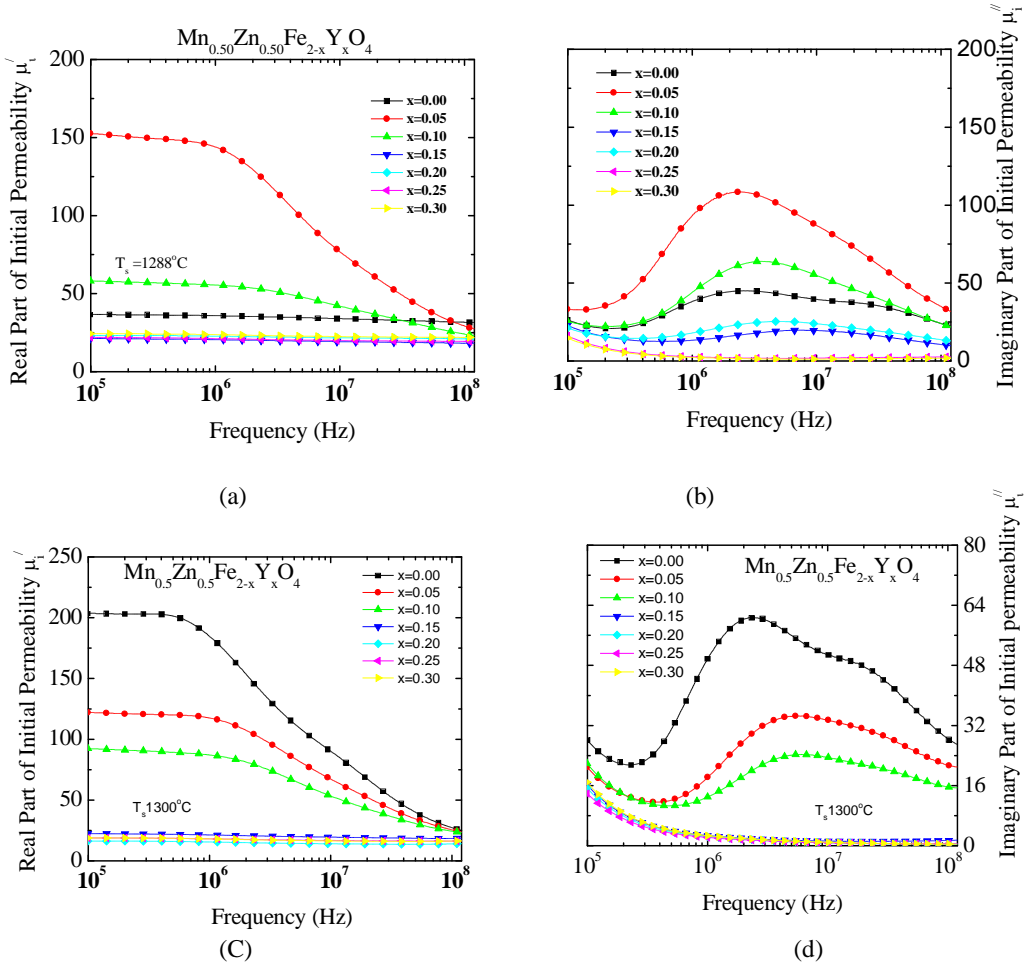


Figure 5.15. (a) The real and (b) imaginary permeability spectra for polycrystalline $Mn_{0.5}Zn_{0.5}Fe_{2-x}Y_xO_4$ samples sintered at 1250 °C for 5 hours.



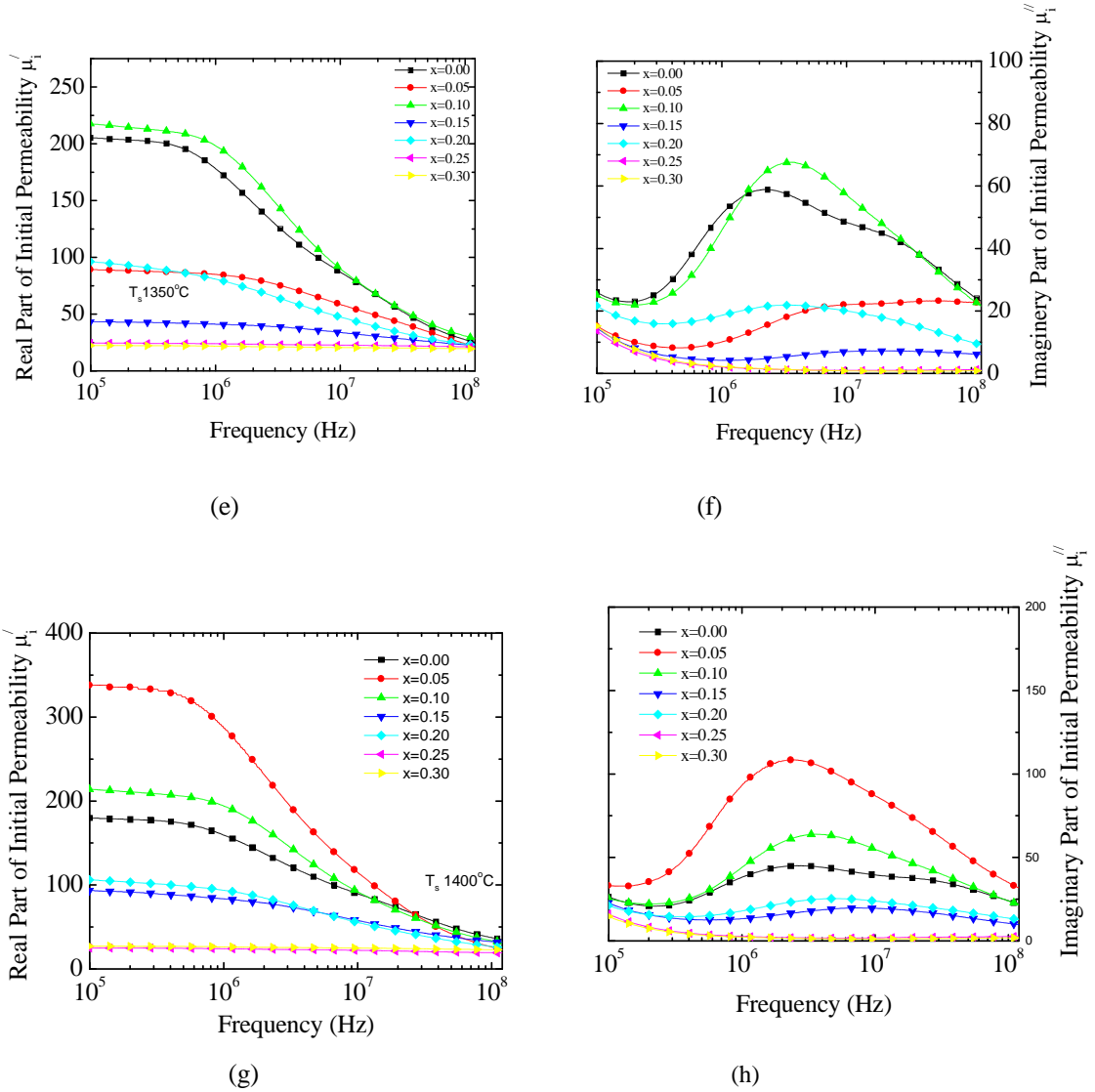
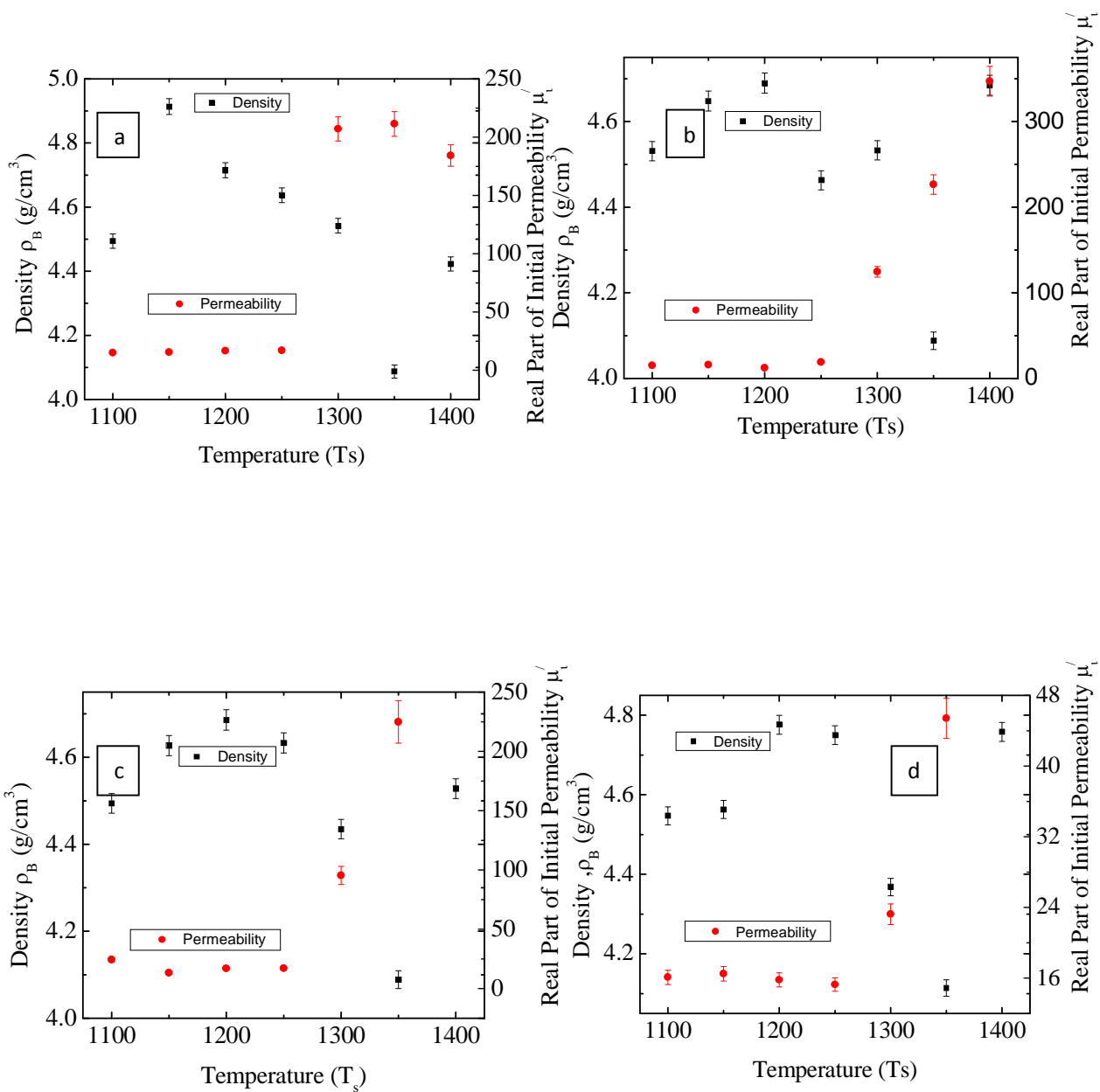


Figure 5.16 (a) , (c), (e), (g) The real and (b), (d), (f), (h) imaginary permeability spectra for polycrystalline $Mn_{0.5}Zn_{0.5}Fe_{2-x}Y_xO_4$ samples sintered at 1288, 1300, 1350 and 1400 °C for 5 hours.

The μ'_i is observed highest for sample sintered at 1400 °C for all compositions because the microstructure is homogeneous with large grain size and a uniform size distribution. All these values are listed in Table 5.1. Fig. 5.17 shows that permeability of all samples depends on the density of the compositions.



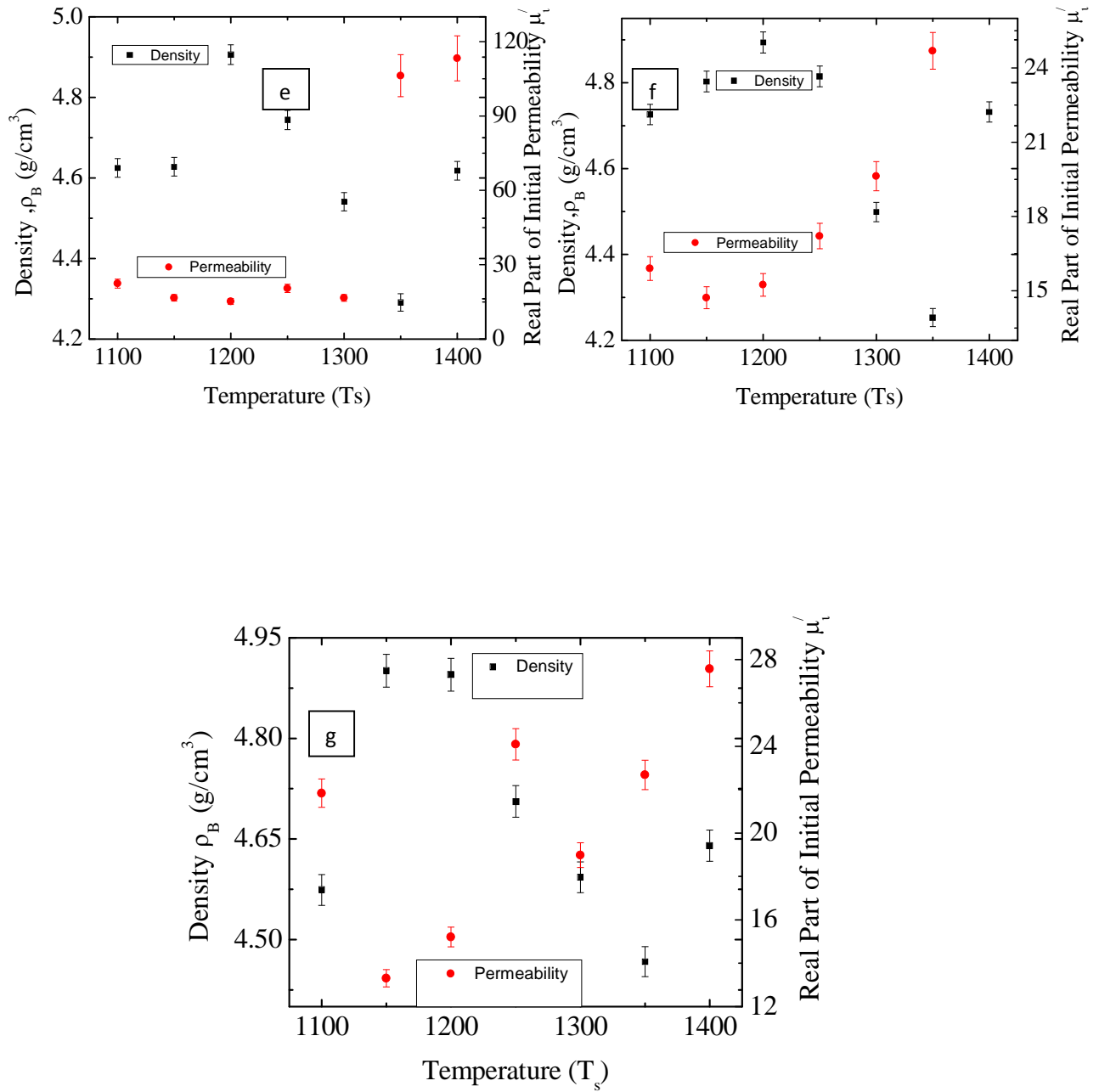


Figure 5.17. The variation of Real Part of Initial Permeability, μ'_i and Bulk Density, ρ_B with T_s for various compositions of $Mn_{0.5}Zn_{0.5}Fe_{2-x}Y_xO_4$ where, (a) $x=0.00$, (b) $x=0.05$, (c) $x=0.01$, (d) $x=0.15$, (e) $x=0.20$, (f) $x=0.25$, (g) $x=0.30$

As the Y content increases in $Mn_{0.5}Zn_{0.5}Fe_{2-x}Y_xO_4$ samples, the f_r for $Mn_{0.5}Zn_{0.5}Fe_{2-x}Y_xO_4$ samples increases up to $x = 0.30$, it increases for a fixed sintering temperature. The f_r values for all samples are tabulated in Table 5.1. There is a normal decrease of μ_i' and increase of the imaginary part, μ_i'' of the initial permeability above the f_r . It is observed that the f_r and the μ_i' are inversely proportional which really confirm Snoek's relation, $f_r \mu_i' = \text{constant}$ [14].

Fig. 5.17 shows the variation of μ_i' and ρ_B with sintering temperature, T_s , for various $Mn_{0.5}Zn_{0.5}Fe_{2-x}Y_xO_4$. It is observed that both μ_i' and ρ_B increase with sintering temperature. Therefore permeability of all samples depends on the density of the compositions.

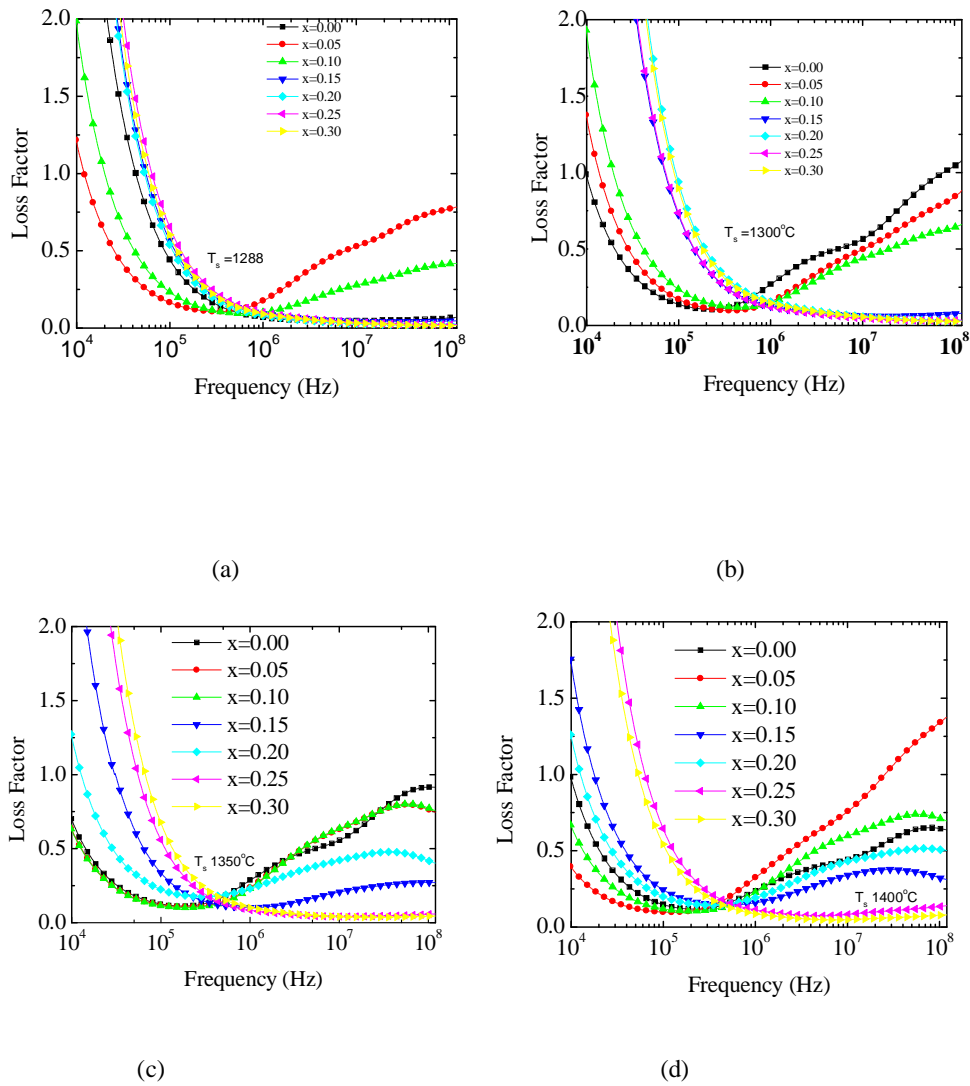


Figure 5.18. The variation of loss factor with frequency for polycrystalline $Mn_{0.5}Zn_{0.5}Fe_{2-x}Y_xO_4$ samples sintered at (a) 1288 °C (b) 1300 °C (c) 1350 °C and (d) 1400 °C temperatures.

The variation of loss $\tan\delta$ with frequency for all samples has been studied. Fig.5.18 shows the variations of loss factors with frequency for $Mn_{0.5}Zn_{0.5}Fe_{2-x}Y_xO_4$ samples sintered at 1250, 1300, 1350 and 1400 °C. At lower frequencies a dispersion in magnetic loss is observed and remains constant up to certain a frequency, this frequency limit depends upon the sintering temperature. The lag of domain wall motion with respect to the applied magnetic field is responsible for magnetic loss and this is accredited to lattice imperfections. [15]

At higher frequencies, a rapid increase in magnetic loss ($\tan\delta$) is observed. A resonance loss peak is shown in this rapid increase of magnetic loss. At the resonance, maximum energy transfer occurs from the applied field to the lattice which results the rapid increases in $\tan\delta$. As it is observed that phase lag between domain rotation and applied field is greater than that between applied field and domain wall displacement, the magnetic losses due to domain rotation overrides those due to domain wall displacement.[16]

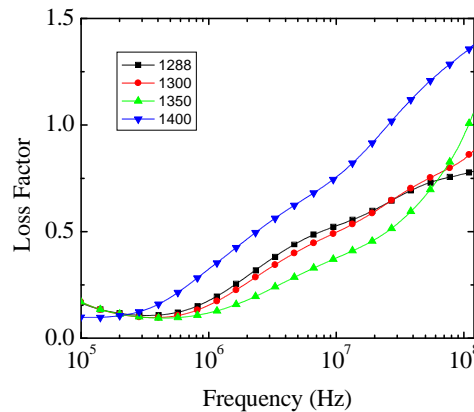
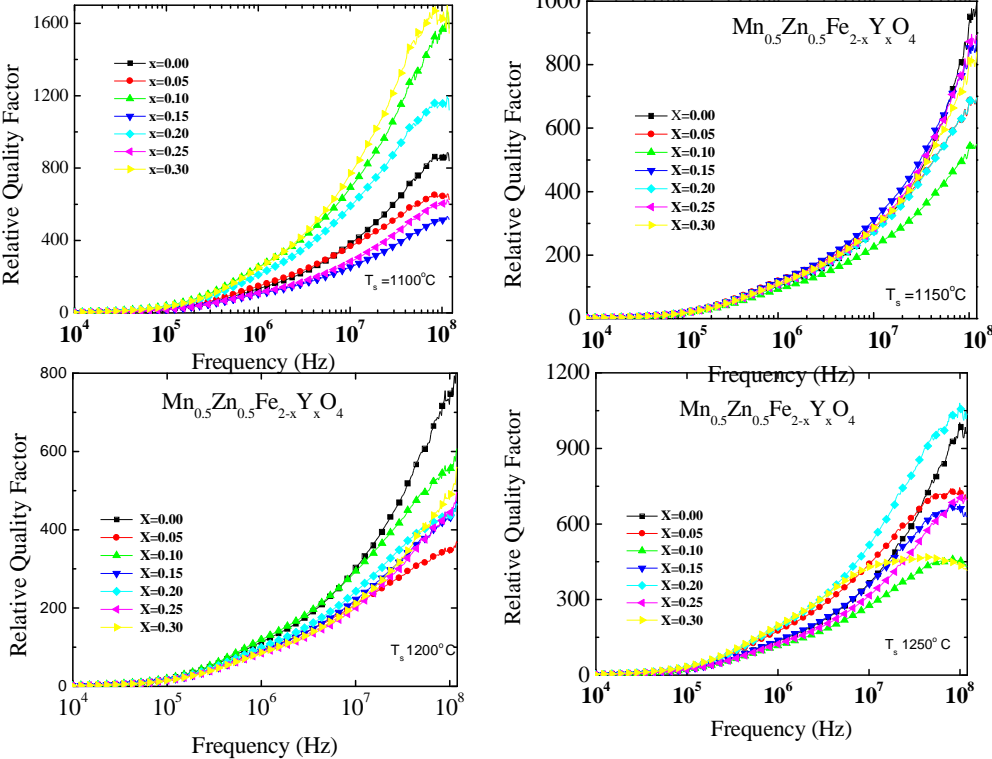


Figure 5.19. The variations of Loss factor with frequency for $Mn_{0.5}Zn_{0.5}Fe_{1.95}Y_{0.05}O_4$ sintered at 1288, 1300, 1350 and 1400 °C.

The $\tan\delta$ is also observed to increase with the increase of sintering temperature. The variation of initial loss with frequency for the sample $Mn_{0.5}Zn_{0.5}Fe_{1.95}Y_{0.05}O_4$ in the sintering temperature range 1288 °C to 1400 °C is shown in Fig. 5.19. The increase in sintering temperature results in increased Y loss in the samples, thereby creating defects in the lattice, which gives rise to magnetic loss.

Energy loss is an extremely important subject in soft ferrimagnetic materials, since the amount of energy wasted on process other than magnetization can prevent the AC applications of a given material. The ratio of μ_i' and μ_i'' representing the losses in the material is a measure of the inefficiency of the magnetic system. Obviously this parameter should be as low as

possible. The magnetic losses, which cause the phase shift, can be split up into three components: hysteresis losses, eddy current losses and residual losses. This gives the formula $\tan \delta_m = \tan \delta_h + \tan \delta_e + \tan \delta_r$. The μ_i is initial permeability which is related to low applied magnetic field. Hysteresis losses vanish at very low field strengths. Thus at low field the remaining magnetic losses are due to eddy current losses and residual losses. Residual losses are independent of frequency. Eddy current losses increase with frequency and are negligible at very low frequency. Eddy current loss can be expressed as $P_e \approx f^2 / \rho$, where P_e is the energy loss per unit volume and ρ is the resistivity [17, 18]. To keep the eddy current losses constant as frequency is increased, the resistivity of the material chosen must increase as the square of frequency. Eddy currents are not problem in the *Mn-Zn* ferrites until higher frequencies are encountered because they have very high resistivity about $10^5 \Omega cm$ to $10^8 \Omega cm$ [19]. The ferrite microstructure is assumed to consist of grains of low resistivity separated by grain boundaries of high resistivity. Thicker grain boundaries are preferred to increase the resistance.



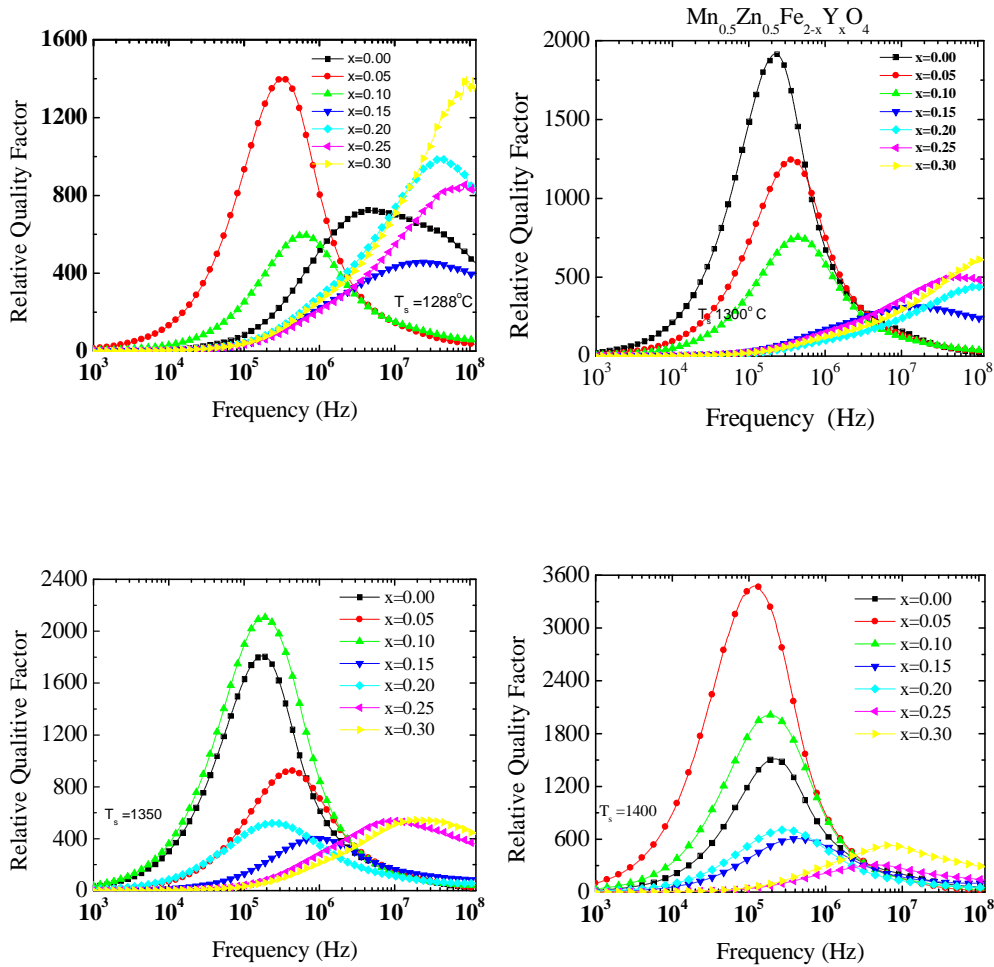


Figure 5.20. The variation of relative quality factors with frequency for polycrystalline $Mn_{0.5}Zn_{0.5}Fe_{2-x}Y_xO_4$ samples sintered at various temperatures.

The variation of relative quality factor, $Q(= \mu_i' / \tan\delta)$, for $Mn_{0.5}Zn_{0.5}Fe_{2-x}Y_xO_4$ sintered at various temperatures and Q_{max} are listed in Table 5.1. It is shown that Q factor increases with increasing Y content up to $x=0.05$ in $Mn_{0.5}Zn_{0.5}Fe_{2-x}Y_xO_4$. It is observed that the sample sintered at 1400 °C is of highest Q value (=3477) for $Mn_{0.5}Zn_{0.5}Fe_{1.95}Y_{0.05}O_4$ samples. This is probably due to the growth of less imperfections and defects in the samples sintered at higher sintering temperature (1400 °C). The Q value increases with increasing sintering temperature which is shown in Table 5.1. For some compositions, there is an abnormal grain growth at higher sintering temperature with trapped pores inside the grain, which causes relatively higher loss factor. It is also observed that maximum quality factor increase with Y content at 1400 °C which is shown in Fig 5.22.

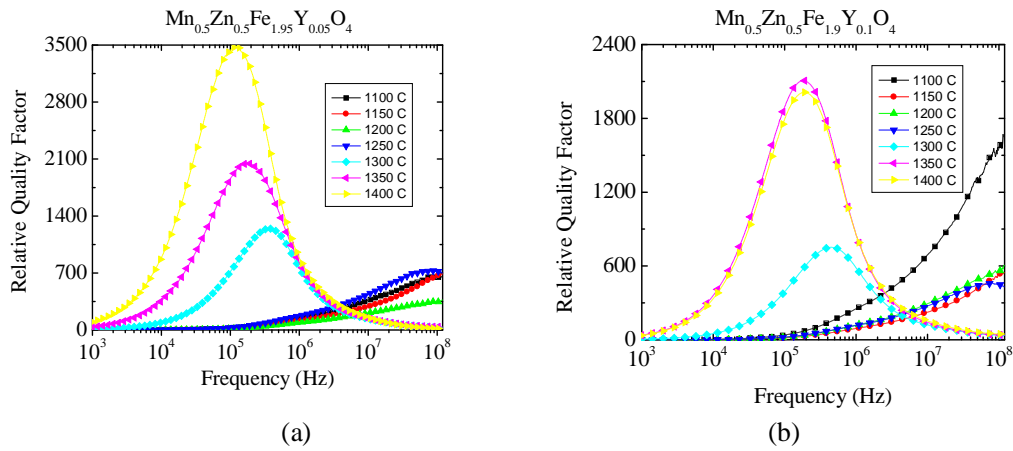


Figure 5.21. Variation of relative quality factor with frequency at different sintering temperature for (a) $Mn_{0.5}Zn_{0.5}Fe_{1.95}Y_{0.05}O_4$ and (b) $Mn_{0.5}Zn_{0.5}Fe_{1.9}Y_{0.1}O_4$

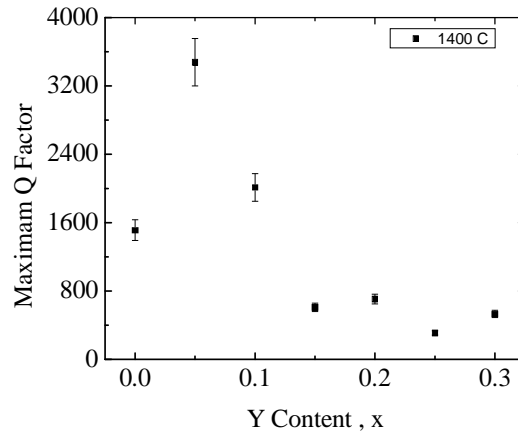


Figure 5.22. Variation of maximum Q factor with Y content for polycrystalline $Mn_{0.5}Zn_{0.5}Fe_{2-x}Y_xO_4$ samples sintered at 1400 °C.

References:

[1] Hossain, A. K. M. A., Seki, M., Kawai, T. and Tabata, H., “Colossal magnetoresistance in spinel type $Zn_{1-x}Ni_xFe_2O_4$ ”, J. App. Phys, Vol - 96, pp 1273, 2004.

[2] Ataa, A.M.A.El, Attiab, S.M., Konya, D. El, and Al-Hammadic, A.H., “Spectral, initial magnetic permeability and transport studies of $Li_{0.5-0.5x}Co_xFe_{2.5-0.5x}O_4$ spinel ferrite”, J.Magn. Magn.Mater, Vol - 295, No. 1, pp 28-36, 2005

[3] Whittaker, E.J.W., & Muntus, R., “Ionic radii for use in geochemistry”, Geochim. Cosmochim. Acta, Vol - 34, No. 9, pp 945-956, 1970.

[4] Hossain, A. K. M. A., Kabir, K. K., Seki, M., Kawai, Tabata, T., H., “Structural, AC, and DC magnetic properties of $Zn_{1-x}Co_xFe_2O_4$ ”, J.Phys. Chem. Solids., Vol - 68, pp 1933–1939, 2007.

- [5] Huhecy, J. E., Keiter, E. A., Keiter, R. L., "Inorganic Chemistry Principles of Structure and Reactivity", 4th Edition.
- [6] Haque, M.M., Huq, M., Hakim, M.A. "Magnetic properties of Mg-Cu-Zn ferrites", J. Magn. Mater., Vol - 320, pp 2292-2799, 2008.
- [7] Winter, M. J., www.webelements.com,©, University of Sheffield, UK, 1995-2006.
- [8] Hossain, A.K.M. Akther, Biswasa, T.S., Mahmuda, S.T., Yanagidab, T., Tanakab, H. and Kawai, T., "Enhancement of initial permeability due to Mn substitution in polycrystalline $\text{Ni}_{0.50-x}\text{Mn}_x\text{Zn}_{0.50}\text{Fe}_2\text{O}_4$ ", J.Magn. Mater., Vol-321, No. 2, pp 81-87, 2009
- [9] Sattar, A. A., El-Sayed, H. M., El-Shokrofy, K. M. and El-Tabey, M. M., "Improvement of the magnetic properties of Mn-Ni-Zn ferrite by the non-magnetic Al^{3+} ion substitution", J.App. Sci., Vol - 5 No. 1,pp 162, 2005.
- [10] Ishaque, M., Islam, M.U., Rahman, I.Z., "Structural, electrical and dielectric properties of yttrium substituted nickel ferrites", Physica B 405 (2010) 1532–1540 .
- [11] Jun, H. and Mi, Y., "Preparation of high permeability Ni-Cu-Zn ferrite", J.Zhejiang University Science, Vol - 6B No. 6, pp 580-583, 2005.
- [12] Tsutaoka, T., Ueshima, M., Tokunaga, T., Nakamura T. and Hatakeyama, K., "Frequency dispersion and temperature variation of complex permeability of Ni-Zn ferrite composite materials", J. Appl. Phys., Vol - 78, No. 6, pp 3983, 1995.
- [13] Hu, J. and Yan, M., "Preparation of high-permeability NiCuZn ferrite", J. Zhejiang University Science, Vol-6, No. 6, pp 580-583, 2005
- [14] Snoek, J. L., "Dispersion and absorption in magnetic ferrites at frequencies above one Mc/s", Physica, Vol - 17, No. 4, pp 207, 1948.
- [15] Rado, G.T., Wright, R.W., Emerson, W. H. and Terris, A., "Ferromagnetism at Very High Frequencies. IV. Temperature Dependence of the Magnetic Spectrum of a Ferrite", Phys. Rev., Vol-88, pp 909-915,1952.
- [16] Chauhan, B. S., Kumar, R., Jadhav, K. M., Singh, M., "Magnetic study of substituted Mg-Mn ferrites Synthesized by citrate precursor method", J. Magn.Magn. Mater. Vol-283, pp 71-81, 2004.
- [17] R. Valenzuela, *Magnetic Ceramics*, Cambridge University Press, Cambridge (1994).
- [18] F. Brailsford, *Physical Principles of Magnetism*, D. Van Nostrand Company Ltd., London (1966).
- [19] B. D. Cullity, *Introduction to Magnetic Materials*, Addison-Wisley Publishing Company, Inc., California (1972).
- [20] Globus, A., Duplex, P., Guyot, M., "IEEE Transactions on Magnetics", Vol - 7, pp 617, 1971.
- [21] Jun, H., Mi, Y., Zhejiang, J., "Preparation of high-permeability NiCuZn ferrite", University Science, Vol - 6B, No. 6, pp 580-583, 2005.

CHAPTER 6

CONCLUSIONS

6.1 Conclusions

The XRD patterns for the polycrystalline $Mn_{0.5}Zn_{0.5}Fe_{2-x}Y_xO_4$ compositions confirm the formation of spinel ferrite. Lattice constant increases with increasing the Y content for all compositions. This increase in lattice constant can be explained on the basis of ionic radius. Since the ionic radius of Y^{3+} (0.98Å) is greater than that of Fe^{3+} (0.73Å), the increase in lattice constant with the increase in Y substitution is expected. The experimental density and the corresponding porosity of the samples respectively increases and decreases with both increasing the Y content and the sintering temperature (T_s) from 1100 to 1400 °C. During the sintering process, the thermal energy generates a force that drives the grain boundaries to grow over pores, thereby decreasing the pore volume and increasing the density of the materials. The surface micrograph study shows that grain size decreases with increasing Y content. The real part of initial permeability μ'_i is observed to increase with increasing Y content, for $x=0.05$ then permeability decrease for further increasing Y content. It is also observed that the μ'_i of the samples increases with increasing sintering temperature from 1100 to 1400 °C because the average grain size increases with increasing sintering temperature. This result can be explained with the help of cation distribution as a result of Y^{3+} and Fe^{3+} substitution. Perhaps, for small content of Y^{3+} substitution it prefers B site and Fe^{3+} prefers both A site and B site, therefore net magnetic moment in B site of the spinel type crystal structure decreases.

The μ'_i values for all samples are found to be independent of frequency below the resonance frequency, f_r , which is found to shift from higher value to lower value as sintering temperature increases for all samples. The maximum value of f_r is 2.82 MHz, as observed for $Mn_{0.5}Zn_{0.5}Fe_{1.9}Y_{0.1}O_4$ which is sintered at 1288 °C.

The loss factor increases with increasing of Y content and sintering temperature. The relative quality factor Q increases with increasing sintered temperature and decreases with increasing Y content except for $x=0.05$. Thus the observed highest Q value determines the appropriate use of this sample in filter application in inductors. It is observed that the sample sintered at 1400 °C shows the highest Q value (3477) for $Mn_{0.5}Zn_{0.5}Fe_{1.95}Y_{0.05}O_4$ sample, probably due to the growth of lesser imperfection in this sample.

6.2 Suggestions for future work

It was found that among the $Mn_{0.5}Zn_{0.5}Fe_{2-x}Y_xO_4$ ferrites $Mn_{0.5}Zn_{0.5}Fe_{1.95}Y_{0.05}O_4$ had the maximum initial permeability μ'_i and maximum Q -factor. So Cu and other Metals which prefers A sublattice to occupy, can be substituted in $Mn_{0.5}Zn_{0.5}Fe_{1.95}Y_{0.05}O_4$ ferrite to enhance the permeability value. Sintering additives like Bi_2O_3 and V_2O_5 can be mixed to promote densification and getting better result in lower sintering temperatures to magnetic materials.